Limitations and Opportunities of Noisy Quantum Devices

Limitations and Opportunities of Noisy Quantum Devices

Master Thesis

in partial fulfilment of the requirements for the degree of

Master of Science
in Applied Physics

at Delft University of Technology

to be defended on Tuesday April 19, 2022 at 13.30h

by

Marios Samiotis

This thesis has been approved by the promoter

Prof. dr. B.M. Terhal

Composition of the thesis committee:

Prof. dr. B.M. Terhal,	Technische Universiteit Delft
Dr. J. Borregaard,	Technische Universiteit Delft
Dr. M. Blaauboer,	Technische Universiteit Delft

Keywords: quantum advantage, relative entropy, master equation, noise

An electronic version of this dissertation is available at
http://repository.tudelft.nl/.

To the memory of my father,
Michalis Samiotis

Contents

Summary

When it comes to a topic in science that has sparked the public's imagination and interest on it, while also contributing just as much to multiple discussions and heated debates amongst the experts, Quantum Computing is definitely at the top of the list. Even though as a concept Quantum Computing has been around since the early 1980s, recent theoretical and experimental developments have brought it back to the spotlight.

Some of the many promises of this new technology include applications in physics, material science, chemistry, biology, pharmacy, finance, machine learning, communications and cryptography. Nations and multinationals all over the world are increasingly investing into what seems to have become a global race for achieving "quantum supremacy". In John Preskill's own words, quantum supremacy is described as the era when "we will be able to perform tasks with controlled quantum systems going beyond what can be achieved with ordinary digital computers" [1].

Whereas all of the above make quantum computing seem like one of the biggest technological accomplishments of humankind, the quantum devices of today are still in their early stage of development. In order to gain a true quantum advantage over classical computational devices, quantum computers would need to be fault-tolerant, that is, resilient to any kind of noise, and operate on millions of *qubits*, short for "quantum bits", the quantum analogue of classical bits. Those two requirements have not been met yet, and reaching either one of them is a formidable task on its own. We are currently living in the *Noisy Intermediate-Scale Quantum* (NISQ) era, during which the quantum devices support only tens of qubits and cannot correct errors that are created by noise processes.

Noise processes can originate from within the devices themselves, due to manufacturing, quantum effects, etc., or caused by external sources, such as control signals generated by laboratory equipment, cosmic rays, etc. Whichever algorithm we choose to run on a given quantum computer, an input quantum state ρ of n qubits gets affected by all the aforementioned noise processes, with the result being that ρ gets corrupted. This corruption affects the coherence of the input state, making its' information less quantum and more classical, stripping away any computational advantage that such a state would have over a classical one.

Correcting these errors and scaling up to millions of qubits constitute the two biggest challenges that quantum scientists are facing today. There are some speculations that both of these challenges might be overcome at the end of this decade [2, 3], but both problems are highly non-trivial and there is no guarantee that they will ever be solved in their entirety.

An important research question in the field is what can be done with the state of the art (noisy) devices that we possess at this moment in time. Could we perhaps demonstrate any quantum advantage for a specific class of problems with a quantum computer consisting of only a few tens of qubits that are not resilient to noise? There have been some recent suggestions for quantum algorithms, such as the Quantum Approximate Optimization Algorithm (QAOA) [4], which is an optimization algorithm designed to tackle quadratic unconstrained

binary optimization (QUBO) problems and is considered by many to be the best algorithm candidate for demonstrating quantum advantage on a NISQ device during this early stage of development. The algorithm seems to be giving non-trivial answers to some QUBO problems even for very shallow circuits [5–7]. *In this work we will focus on analyzing noise and its effects on an input state ρ and assess whether it can overwhelm a quantum computation.*

In **Chapter** 1 we will begin with an introduction to quantum theory and the theory of superconducting qubits. We will lay the foundations for characterizing the quantum state of a system, define the qubit, and introduce the density matrix formalism which will be used throughout this thesis. We end this introductory chapter with a description of the transmon qubit and a brief section on how we will model noise for superconducting qubits.

In **Chapter** 2 we will define the quantum relative entropy $D(\rho\|\sigma)$ between two quantum states, which we will use as a measure of distance between an arbitrary state ρ and a fixed state σ. We will then present a number of propositions that lead to Lemma 2.3.1, which provides a general upper bound of the relative entropy for the discrete time evolution of a general quantum state. Moreover, we will state Theorem 2.4.1 which is an extension of Lemma 2.3.1 for the case of the continuous time evolution of a quantum state. Lastly, we will prove that a dissipative Lindbladian operator describing relaxation and pure dephasing noise satisfies a modified logarithmic Sobolev inequality (MLSI) with constant $\alpha = \kappa$, where κ is the relaxation rate.

In **Chapter** 3 we will introduce Theorem 3.2.1, which is the key tool to declare *when* a quantum computation has lost advantage over a classical computation for optimization problems. We will then briefly analyze the QAOA and focus on its key characteristics. Later on, we will derive two upper bounds for the relative entropy $D(\rho\|\sigma)$ where ρ is the output state of the QAOA and σ is the fixed point of the noise processes that plague a given quantum device. Lastly, we will apply Theorem 3.2.1 for the newly calculated upper bounds and make an assessment over the quality of those bounds.

In **Chapter** 4 we will reformulate the Lindblad Master equation and solve it for the steady state. Then, we will proceed with defining a system consisting of a one-dimensional array of n transmon qubits, on which we act with a chain of coupling cross-resonance drives $Z_i X_{i+1}$ on qubits i and $i+1$, where we impose the boundary condition $X_{i+n} = X_i$. We study the properties of the steady state of this system, by solving exactly the Lindblad Master equation in the case of two or three transmons and then measuring correlations.

Chapter 5 continues with approximating the solution of the Lindblad Master equation for the aforementioned system of coupled transmons. There we analyse two approximation methods: perturbation theory and mean field theory. By perturbation theory, we perturbatively expand the Pauli Transfer matrix in hopes of making its inversion less computationally costly for when we wish to calculate the expectation values of small Pauli strings on a system of n qubits. Then, we introduce the mean field theory and derive the mean field equations for our system of n coupled transmons. Lastly, we compare the results from the approximation methods with the exact solution of the system for two transmon qubits.

We conclude in **Chapter** 6 by summarizing the main results of this thesis and outlining the main issues of the perturbative method (see Chapter 5), for which further research needs to be done. We highlight the need of automating this method, as well as estimating its error and the range for which the method holds.

1

Essentials of Quantum Theory

This chapter is a brief introduction into the theory of Quantum Mechanics and the theory of superconducting qubits and noise. The reader can find a complete and rich exposure to quantum theory in the book "Quantum Mechanics: non-relativistic theory" by Landau and Lifshitz [8] or the book "Modern Quantum Mechanics" by Sakurai [9]. For a modern and comprehensive study of quantum mechanics, the book "Advanced Quantum Mechanics: A Practical Guide" by Nazarov and Danon is recommended [10].

1.1. Introduction to quantum mechanics

Quantum mechanics emerged in the mid 1920s as a new type of physics that could explain phenomena on the atomic scale, for which classical physics proved to be insufficient. The theory went through multiple reformulations and refinements until it developed into its modern form. Here we will introduce quantum mechanics in the Dirac formulation which is widely in use today, and was developed by physicist and mathematician Paul Dirac.

One of the most fundamental concept in all of physics is that of the state of a system. In classical mechanics, the mechanical state of a system of N particles can be determined by having complete knowledge of the $3N$ generalized coordinates q and momenta p [11]. Thus, the mechanical state is determined by a single point in the phase space.

In quantum mechanics, the quantum mechanical state of a system is completely specified by a complex vector $|\psi\rangle$, also called the *state vector*. Therefore, the quantum state of a n-dimensional system is determined by a vector in a n-dimensional Hilbert space.

For a system of N dimensions, one can always choose any orthonormal basis of N vectors $\{|\psi_i\rangle\}$ in the Hilbert space, and write a general state $|\psi\rangle$ as a *superposition* in that basis,

$$|\psi\rangle = \sum_{i=1}^{N} c_i |\psi_i\rangle, \tag{1.1}$$

where c_i are complex constants. Since $|\psi\rangle$ must be normalized,

$$\sum_{i=1}^{N} |c_i|^2 = 1. \tag{1.2}$$

We refer to $|c_i|^2$ as the *probability* of obtaining the state $|\psi_i\rangle$ upon measuring state $|\psi\rangle$ in this particular basis.

Suppose that a system is comprised of two subparts, subsystems A and B. In the case where subsystems A and B are *not* entangled, one can always assign a state vector to each subsystem, i.e. states $|\psi_A\rangle$ and $|\psi_B\rangle$ respectively. Then, the state vector $|\psi\rangle$ for the total system can be written as their tensor product

$$|\psi\rangle = |\psi_A\rangle \otimes |\psi_B\rangle. \tag{1.3}$$

If for a system with state vector $|\psi\rangle$ which is made of two subsystems A and B one cannot assign a state vector to each subsystem, or equivalently, the total system state vector $|\psi\rangle$ cannot be written as a tensor product of two state vectors $|\psi_A\rangle$ and $|\psi_B\rangle$, then we say that subsystems A and B are *entangled*.

1.2. Unitary evolution

The time evolution of the quantum state of a closed system is given by the *Schrödinger* equation,

$$i\hbar \frac{\partial}{\partial t} |\psi(t)\rangle = H|\psi(t)\rangle, \tag{1.4}$$

where H is the Hamiltonian of the system. The Hamiltonian is a Hermitian operator and contains all information about the system's energy. If H is time-independent, the solution of Eq. (1.4) is written as

$$|\psi(t)\rangle = e^{-iHt/\hbar}|\psi(0)\rangle, \tag{1.5}$$

with $|\psi(0)\rangle$ being the initial state of the system at time $t = 0$. By defining

$$U(t) \equiv e^{-iHt/\hbar}, \tag{1.6}$$

we can rewrite Eq. (1.5) as

$$|\psi(t)\rangle = U(t)|\psi(0)\rangle. \tag{1.7}$$

Notice that by definition, operator $U(t)$ is unitary for all t, that is $U^\dagger U = UU^\dagger = \mathbb{I}$. We then say that Eq. (1.7) describes the *unitary evolution* of the initial state $|\psi(0)\rangle$ under the influence of a time-independent Hamiltonian. The notion of a unitary evolution of a system comes hand-in-hand with that of closed system dynamics and one implies the other. A system evolving unitarily in time has also reversible dynamics.

1.3. Measurement

In quantum mechanics, for every observable A in nature there exists a corresponding Hermitian operator $\hat{A}$. The eigenvalues of $\hat{A}$ give all the possible measurement outcomes of

A. It is more apparent now why every observable must be a Hermitian operator: Hermitian operators always have real eigenvalues.

Let us now choose a basis $\{|\psi_i\rangle\}$ where $\hat{A}$ is diagonal. Then,

$$\hat{A}|\psi_i\rangle = a_i|\psi_i\rangle, \tag{1.8}$$

where a_i are the eigenvalues of $\hat{A}$ and $|\psi_i\rangle$ are the corresponding eigenstates. If we write a general state $|\psi\rangle$ as a superposition in the eigenbasis of $\hat{A}$, then

$$\hat{A}|\psi\rangle = \sum_{i=1}^{N} c_i a_i |\psi_i\rangle. \tag{1.9}$$

If we want to measure the value of A of system with state vector $|\psi\rangle$, then the measurement outcome is

$$\langle A\rangle = \langle\psi|\hat{A}|\psi\rangle = \sum_{i=1}^{N} |c_i|^2 a_i, \tag{1.10}$$

where $|c_i|^2$ is the probability of measuring a_i. The act of measurement collapses the state vector $|\psi\rangle$ into one of the eigenstates of $\hat{A}$. As a process, measurement is a non-unitary operation on the state $|\psi\rangle$, and is thus *irreversible*.

1.4. The qubit

A qubit is the simplest quantum system; a two-level system. Usually the ground state is denoted as $|0\rangle$ while the excited state is $|1\rangle$. A general qubit state $|\psi\rangle$ can be written as a superposition of those two states,

$$|\psi\rangle = a|0\rangle + b|1\rangle, \tag{1.11}$$

where a and b are complex constants that need to satisfy $|a|^2 + |b|^2 = 1$ due to normalization of $|\psi\rangle$. The basis $\{|0\rangle, |1\rangle\}$ is often called the *computational basis*.

The qubit constitutes the basic unit of quantum information, hence its name "quantum-bit", and is the basic block of quantum computation. We control qubits by acting on them with unitary operations U, which are now called *unitary gates* (a direct influence from computer science nomenclature). Due to their unitarity, all gates in quantum computation must be reversible, a unique characteristic that is not true in classical computation.

Many physical systems in nature can be utilized in order to manufacture a stable qubit. Qubits have already been made using non-linear superconducting oscillators [12], trapped-ions [13], optical photons [14], nitrogen-vacancy centers in diamond [15] and quantum dots in semiconductor materials [16].

1.5. Density matrix formalism

Alongside the state vector formulation of quantum mechanics, there exists an equivalent definition for the state of a quantum system, which is given by the *density matrix* ρ. For a pure state $|\psi\rangle$, the density matrix equals

$$\rho = |\psi\rangle\langle\psi|. \tag{1.12}$$

The motivation behind using the density matrix formalism is that it can describe a wider spectrum of possible physical systems that the state vector $|\psi\rangle$ cannot. More specifically, the density matrix ρ can also define a statistical ensemble of quantum states, and can be used to describe open system dynamics (more on this at the end of this chapter).

If density matrix ρ evolves in time according to the *von Neumann* equation

$$i\hbar\frac{\partial\rho}{\partial t} = [H, \rho], \tag{1.13}$$

where H is the Hamiltonian of the system and $[.,.]$ denotes the commutator. Eq. (1.13) describes the unitary evolution of the state ρ, and therefore guarantees the reversibility of the dynamics in time.

A statistical ensemble of quantum states can be written as

$$\rho = \sum_{i=1}^{N} p_i |\psi_i\rangle\langle\psi_i|, \tag{1.14}$$

where $|\psi_i\rangle$ are orthonormal state vectors, and $p_i \geq 0$, $\sum_i p_i = 1$ for p_i being the probability of picking state $|\psi_i\rangle$ from the ensemble. If $\rho^2 = \rho$, then we say that ρ is a pure quantum state, otherwise we say that ρ is a mixed state. We can see from Eq. (1.14) that a density matrix ρ is pure if and only if $p_i = 1$ and $p_j = 0$ for all $j \neq i$.

1.6. Noise in superconducting transmon devices

1.6.1. The transmon qubit

We will now analyse how we can manufacture a qubit using superconducting materials. As previously mentioned, any physical system that has a number of discrete energy levels can be used to make a qubit: the ground state will be the $|0\rangle$ state while the first-excited state will be the $|1\rangle$ state. A simple and well studied system for our purposes is the *quantum harmonic oscillator*.

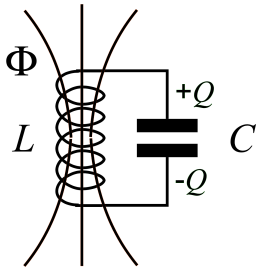

Figure 1.1: A simple LC circuit with one inductor and a capacitor, characterised by the inductance L and capacitance C respectively. The total charge of the capacitor is Q, while Φ is the magnetic flux that pierces through the inductor.

We begin with a simple LC oscillator circuit, where L is its inductance and C its capacitance. The total energy of this system is given by the sum of its charging and inductive energies,

$$H_{\text{LC}} = \frac{Q^2}{2C} + \frac{\Phi^2}{2L}, \tag{1.15}$$

where Q is the charge of the capacitor and Φ is the magnetic flux piercing through the inductor. The angular frequency of the oscillator is $\omega_r = 1/\sqrt{LC}$, and so we can rewrite Eq. (1.15) as

$$H_{\mathrm{LC}} = \frac{Q^2}{2C} + \frac{1}{2}C\omega_r^2\Phi^2. \tag{1.16}$$

By quantizing the charge Q and the magnetic flux Φ, they satisfy the following commutation relation

$$[\hat{\Phi}, \hat{Q}] = i\hbar. \tag{1.17}$$

Having in our mind the quantum harmonic oscillator, we define

$$\hat{\Phi} = \sqrt{\frac{\hbar}{2\omega_r C}}(\hat{a}^\dagger + \hat{a}) \quad \text{and} \quad \hat{Q} = i\sqrt{\frac{\hbar\omega_r C}{2}}(\hat{a}^\dagger - \hat{a}), \tag{1.18}$$

where $\hat{a}^\dagger$ and $\hat{a}$ are the creation and annihilation operators respectively [12]. The definitions of Eq. (1.18) transform the Hamiltonian of Eq. (1.16) into

$$\hat{H}_{\mathrm{LC}} = \hbar\omega_r(\hat{a}^\dagger\hat{a} + 1/2), \tag{1.19}$$

where $\hat{a}^\dagger\hat{a}|n\rangle = n|n\rangle$ for $n = 0, 1, 2, \ldots$. Below we see the energy spectrum for the quantized Hamiltonian of the LC circuit

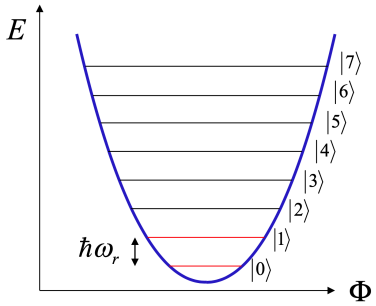

Figure 1.2: The energy spectrum of the quantum harmonic oscillator. Every energy level is equidistant, providing an ill-platform to manufacture qubits on.

One could now ask, is this energy spectrum good enough to make a stable qubit? If we are able to restrict ourselves to the subspace $\{|0\rangle, |1\rangle\}$ then that should be enough. Unfortunately, this is not the case for our simple LC circuit. The transitions between all quantum levels are degenerate for linear circuits. If we try to drive the transition $|0\rangle \leftrightarrow |1\rangle$ on an energy spectrum like the one in Fig. 1.2, then we run the risk of escaping the $\{|0\rangle, |1\rangle\}$ subspace.

We solve the degeneracy issue by introducing a superconducting non-linear inductor $L(\Phi)$ called the Josephson junction, which is a superconductor-insulator-superconductor tunnel junction. The non-linear inductor changes the spacing between the different energy levels (see Fig. 1.3), thus making possible the manufacturing of a stable qubit. By using a

superconducting non-linear inductor, we also minimize the dissipation in the system caused by resistance and heat.

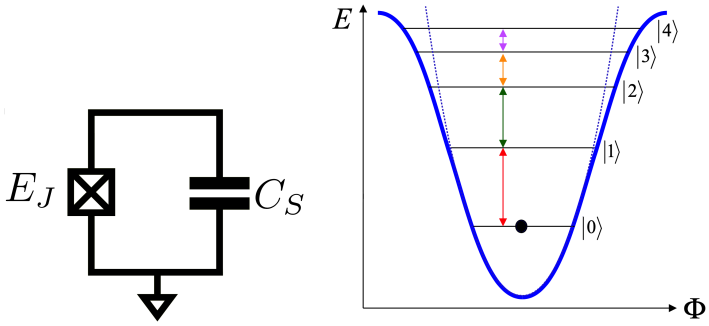

Figure 1.3: Left: A transmon qubit of fixed frequency. The Josephson junction of energy E_J is depicted by a square with a cross inside.
Right: Energy spectrum of a transmon qubit. Here the energy levels are not equidistant, and the very first two levels can be used to manufacture a stable qubit.

1.6.2. Modeling noise

The density matrix of a single qubit may be written as

$$\rho = \frac{1}{2}(\mathbb{I} + \vec{r}\cdot\vec{\sigma}) = \frac{1}{2}(\mathbb{I} + r_x X + r_y Y + r_z Z), \tag{1.20}$$

where $\vec{\sigma} = (X, Y, Z)^{\mathrm{T}}$ is a vector consisting of the three Pauli matrices, and $\vec{r} \in \mathbb{R}^3$ is a real vector where $|\vec{r}| \leq 1$. Usually all qubits undergo corruption by noise during their time evolution, due to the unavoidable interactions with their environment and errors that occur during their operation. Such effects cannot be described by unitary operations and therefore the Von Neumann equation of motion is not sufficient to describe the dynamics of state ρ anymore.

For this purpose, we introduce the Lindblad Master Equation

$$\frac{\partial\rho}{\partial t} = -\frac{i}{\hbar}[H,\rho] + \sum_k \left(L_k \rho L_k^\dagger - \frac{1}{2}\{L_k^\dagger L_k, \rho\} \right), \tag{1.21}$$

which is similar to the Von Neumann Eq. (1.13), but now also includes the *quantum jump operators* L_k which describe the dissipation (non-unitary dynamics) of the system.

Within the standard Bloch-Redfield model of decoherence [17, 18], we can distinguish two main noise processes that affect transmon qubits: longitudinal relaxation and transverse relaxation. Longitudinal relaxation, or else energy relaxation, is caused by energy exchange between the transmon and its environment, which in general leads to relaxation transitions $|1\rangle \to |0\rangle$ or excitation transitions $|0\rangle \to |1\rangle$. We can model the energy relaxation by using two quantum jump operators, $L_1 = \sqrt{\kappa p}\sigma_-$ and $L_2 = \sqrt{\kappa(1-p)}\sigma_+$ accounting for the relaxation and excitation transitions respectively. Here κ is the energy relaxation rate, where $\kappa = 1/T_1$ for T_1 being the energy relaxation time, and $\sigma_- = |0\rangle\langle 1|$, $\sigma_+ = |1\rangle\langle 0|$ being

the spin-down and spin-up operators respectively. The relaxation (or damping) probability p satisfies a Boltzmann distribution, i.e.

$$p = \frac{1}{1 + e^{-h\omega_0/k_B\mathcal{T}}}, \tag{1.22}$$

where ω_0 is the transition frequency between the states $|0\rangle$ and $|1\rangle$. Even though the qubits can spontaneously lose energy to their cold environment, it is very difficult for their environment to introduce any qubit excitations. Because of its nature, energy relaxation is a *non-reversible* process [19].

Longitudinal relaxation also causes stochastic shifts in the qubit's frequency, which can be modeled by pure dephasing. We do this by using a third quantum jump operator $L_3 = \sqrt{\chi}Z$, where χ is the pure dephasing rate, or else $\chi = 1/T_\varphi$ where T_φ is the pure dephasing time, and Z is the Pauli matrix. Longitudinal relaxation along with pure dephasing give rise to transverse relaxation which describes the loss of quantum coherence on the qubit state ρ (off-diagonal elements of the density matrix decay). The transverse relaxation time T_2 is given by

$$\frac{1}{T_2} = \frac{1}{2T_1} + \frac{1}{T_\varphi}. \tag{1.23}$$

Throughout this thesis we will be using the aforementioned quantum jump operators L_1,L_2 and L_3 to model superconducting qubit noise.

2

Bounding the Relative Entropy

2.1. Introduction

With the emergence of advanced communication systems in the mid-20th century, the physical substance of information started becoming more apparent, and there were made numerous efforts in order to describe it in the language of mathematics. Shannon in 1948 was the first to define and use entropy as a measure of information [20]. A few years later, in 1951 Kullback and Leibler introduced the relative entropy [21], which is a statistical distance that measures how two probability distributions differ from each other.

In quantum information theory an important question that arises is the following, how do two finite quantum states differ from each other? The quantum relative entropy, which is the quantum analogue of the relative entropy, is a well fitting quantity to give an answer. Since the relative entropy for two general probability distributions of arbitrary size is near impossible to compute analytically, one can estimate it by bounding it. Petz in 1988 derived a variational expression for the relative entropy [22] which establishes an upper bound, while much later Berta *et al.* derived variational expressions which upper bound the quantum relative entropy [23].

In the framework of open quantum dynamics, a dissipative quantum system evolving under the Markovian approximation obeys the Lindblad Master Equation [24]. In 1996 Diaconis and Saloff-Coste used logarithmic Sobolev inequalities to bound the rates of convergence of Markov chains on finite distributions to their stationary states [25]. Kastoryano and Temme [26] extended the use of logarithmic Sobolev inequalities [27, 28] to finite quantum dissipative systems that evolve under the Markovian approximation. Their work effectively established an upper bound on the quantum relative entropy between a finite quantum state that evolves according to the Lindblad Master Equation and the steady state of this evolution.

Since then, there have been numerous recent studies of log-Sobolev inequalities on classical and quantum lattice spin systems [29–31]. Recently, França and Garcia-Patron

[32] were the first to establish two upper bounds for the quantum relative entropy for a general dissipation process. More specifically, the two bounds are derived for the cases of a general discrete evolution of a quantum state under the influence of an error channel $\mathcal{E}$ and for the continuous time evolution of a dissipative quantum system obeying the Lindblad Master Equation for a general Hamiltonian and dissipator.

Up to now, all studies on log-Sogolev inequalities have focused only on the use of a global depolarizing channel as the main and only source of noise. Motivated by recent experimental efforts made on superconducting hardware, we are interested in using log-Sobolev inequalities in order to establish upper bounds for the quantum relative entropy for relaxation and pure dephasing, which model the noise processes that superconducting transmon qubits suffer from. In what follows, we bound the quantum relative entropy for relaxation noise with the addition of pure dephasing. The results show that the bounds are only dependent on the relaxation rate κ, which implies that the convergence rate of the upper bounds is optimal only for the case $\chi \ll 1$, where χ is the pure dephasing rate.

2.2. The quantum relative entropy

Definition 2.2.1. *Let ρ and σ be two arbitrary quantum states of n qubits. The quantum relative entropy $D(\rho\|\sigma)$ (also called Kullback–Leibler divergence) between the states ρ and σ is defined as*

$$D(\rho\|\sigma) = Tr[\rho(\log(\rho) - \log(\sigma))]. \tag{2.1}$$

For the rest of this work, we will always refer to ρ as an arbitrary output state of a given quantum circuit, and to σ as the fixed point of the noise model that describes the noise processes in that circuit. For a general noise channel $\mathcal{E}$, a state σ is its fixed point if it satisfies $\mathcal{E}(\sigma) = \sigma$. For the analysis in [32] to apply, σ needs to be a full-rank state, and therefore, our method will refrain from those noise models where σ is a state that cannot be inverted. An example of such a noise model is the Amplitude Damping Channel for temperature $\mathcal{T} = 0$, where in the case of n qubits $\sigma = |0\rangle\langle 0|^{\otimes n}$, which is not a full-rank state.

Let us now understand why it is useful to think of the states ρ and σ in a manner as is described above. The relative entropy measures *how* the state ρ differs from the state σ. In the case where it becomes zero, then $\rho = \sigma$ and the two states are identical. Therefore, we can see that the relative entropy can be thought of as a measure between the two states ρ and σ (even though it is *not* a proper distance metric by definition). If the state ρ_0 describes a pure input state of a quantum circuit, that is $\rho_0^2 = \rho_0$, by keeping the state σ fixed, we can then examine whether the noise processes along with the action of the circuit brings the output state ρ closer to σ.

For the simplest and most widely in use noise models, such as depolarization, relaxation and pure dephasing, the fixed point of noise σ is diagonal in the computational basis, which corresponds to a probability distribution of classical states. Since a pure quantum state can also have non-zero elements on the off-diagonal of its matrix representation, which represent the coherent quantum information of the system (superposition and entanglement are encoded into the off-diagonal elements of ρ), a decreasing relative entropy with respect to the circuit size for the aforementioned noise models would mean that the off-diagonal elements of ρ start to vanish as the system evolves. Consequently, quantum coherence is

gradually being lost and the output state of the circuit resembles more a classical state than a quantum one. What is of importance in this case is to determine *how fast* this decrease happens during a computation, since it can serve as a measure of how rapidly an input quantum state degenerates into a classical output state under the influence of noise.

Assuming that the state ρ of n qubits is known, and that the fixed point of noise σ is a full-rank state of n qubits, then the relative entropy can be directly computed using Eq. (2.1). Suppose now that for an input state ρ_0, ρ is the output of a quantum circuit, i.e. $\rho = \mathcal{S}(\rho_0)$, where $\mathcal{S}$ is a general quantum channel (which includes noise) acting non-trivially on the state ρ. Since noise processes are interfering with the manipulation of ρ_0 inside the circuit, in general, it is impossible to obtain an exact expression for $\mathcal{S}(\rho_0)$. In this case, the relative entropy cannot be computed and therefore we need to resort to estimations rather than exact computations.

Luckily, there exist methods with which one can upper bound $D(\rho\|\sigma) = D(\mathcal{S}(\rho_0)\|\sigma)$ in two distinct cases. First, for when we describe $\mathcal{S}$ as a series of discrete unitary quantum channels $\mathcal{U}$ interspersed by some noise channels $\mathcal{E}$ acting on n qubits for a circuit of depth D. Second, for when we describe the action of the circuit along with that of the noise as a quantum channel $\mathcal{S}_t$, where $\rho(t) = \mathcal{S}_t(\rho_0)$ is the continuous time evolution of an input state $\rho_0 = \rho(0)$ under the influence of a Lindbladian operator $\mathcal{L}$, where $\mathcal{S}_t = e^{t\mathcal{L}}$ for $t > 0$. The rest of this chapter is devoted to calculating such upper bounds.

2.3. Upper bounds for the relative entropy

Perhaps the most important property of the relative entropy for a quantum channel $\mathcal{S}$ which acts on two quantum states ρ and σ is the contraction property, that is, the relative entropy satisfies a data-processing inequality:

Proposition 2.3.1. *Let ρ and σ be two arbitrary quantum states of n qubits, and let $\mathcal{S} : \mathcal{M}_{2^n} \to \mathcal{M}_{2^n}$ be a quantum channel which acts non-trivially on both states. Thereupon, it holds that*

$$D(\mathcal{S}(\rho)\|\mathcal{S}(\sigma)) \leq D(\rho\|\sigma). \tag{2.2}$$

If for a quantum channel $\mathcal{S}$ we choose σ to be its fixed point, i.e. $\mathcal{S}(\sigma) = \sigma$, then from Proposition 2.3.1 it follows that

$$D(\mathcal{S}(\rho)\|\sigma) \leq D(\rho\|\sigma). \tag{2.3}$$

Eq. (2.3) justifies our reasoning for fixing the state σ while studying the behavior of the relative entropy. It is now clear that for a state that satisfies $\mathcal{S}(\sigma) = \sigma$, our attention can be concentrated only upon the quantity $\mathcal{S}(\rho)$.

Even though the relative entropy is not a proper distance metric, as has already been mentioned, it satisfies a data-processed triangle inequality for a general quantum channel $\mathcal{S}$ (Theorem 3.1, [33]):

Proposition 2.3.2. *Let ρ be an arbitrary quantum state of n qubits and σ, σ' be full-rank quantum states of n qubits, and let $\mathcal{S} : \mathcal{M}_{2^n} \to \mathcal{M}_{2^n}$ be a quantum channel which acts non-trivially on the states ρ and σ'. The relative entropy $D(\mathcal{S}(\rho)\|\sigma)$ then satisfies a data-processed triangle inequality*

$$D(\mathcal{S}(\rho)\|\sigma) \leq D(\rho\|\sigma') + D_\infty(\mathcal{S}(\sigma')\|\sigma), \tag{2.4}$$

where $D_\infty(\rho\|\sigma)$ is the max-relative entropy defined as

$$D_\infty(\rho\|\sigma) = \ln(\|\sigma^{-\frac{1}{2}}\rho\sigma^{-\frac{1}{2}}\|). \tag{2.5}$$

2

In Proposition 2.3.2 we introduced a new quantity, the max-relative entropy $D_\infty(\rho\|\sigma)$. For an arbitrary n qubit state ρ and full-rank state σ, it holds that [34]

$$D(\rho\|\sigma) \leq D_\infty(\rho\|\sigma). \tag{2.6}$$

We are now in the position to upper bound the quantum relative entropy for a discrete quantum circuit. Let a quantum circuit be comprised of D layers of unitary channels $\mathcal{U}_1, \mathcal{U}_2, ..., \mathcal{U}_D$ which act on n qubits, and let $\rho = |0\rangle\langle 0|^{\otimes n}$ be the input quantum state of n qubits. Due to the presence of noise in the circuit, we will assume that each unitary layer $\mathcal{U}_i$ is preceded and succeeded by a layer of a noise channel $\mathcal{E}$ which acts on n qubits and describes the effects of noise inside the circuit (see Fig. 2.1). We will assume that the noise channel $\mathcal{E}$ acts locally and uniformly on each qubit, an assumption that is valid for the noise models that are considered throughout this thesis. It is important to comment here that this model of noise *does not take into account the propagation of errors* through the quantum circuit.

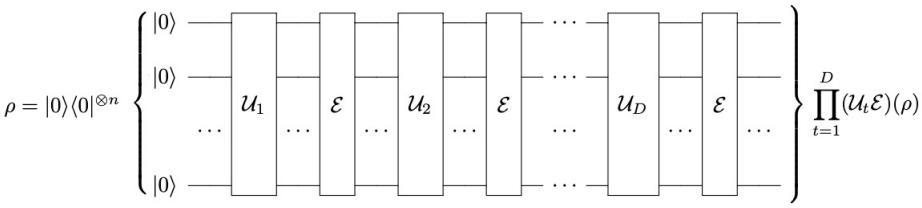

Figure 2.1: A quantum circuit of D unitary layers $\mathcal{U}_1, \mathcal{U}_2, ..., \mathcal{U}_D$, interspersed by D layers of noise channels $\mathcal{E}$ which act locally and uniformly on n qubits.

Lemma 2.3.1. *Let $\mathcal{E} : \mathcal{M}_{2^n} \to \mathcal{M}_{2^n}$ be a quantum channel with a fixed point σ that satisfies a strong data-processing inequality with constant $\alpha > 0$. That is,*

$$D(\mathcal{E}(\rho)\|\sigma) \leq (1-\alpha)D(\rho\|\sigma) \tag{2.7}$$

for all quantum states ρ. Then for any other quantum channels $\mathcal{U}_1, ..., \mathcal{U}_D : \mathcal{M}_{2^n} \to \mathcal{M}_{2^n}$ we have:

$$D\left(\prod_{t=1}^{D}(\mathcal{U}_t\mathcal{E})(\rho)\|\sigma\right) \leq (1-\alpha)^D D(\rho\|\sigma) + \sum_{t=1}^{D}(1-\alpha)^{D-t} D_\infty(\mathcal{U}_t(\sigma)\|\sigma). \tag{2.8}$$

The reader can find a proof for the above lemma in [32]. Eq. (2.8) is the main result of a general upper bound on the relative entropy for a noisy quantum circuit of circuit depth D as illustrated on Fig. 2.1. For all practical purposes, α is the error probability of quantum channel $\mathcal{E}$. We can see that the first term on the r.h.s. (right-hand side) of Eq. (2.8) always contracts as the circuit depth increases and eventually converges to zero at large D. Consequently, the second term on the r.h.s. of Eq. (2.8) is the term which controls the

contraction of the relative entropy: if the max-relative entropy term does not converge to zero at large D, then the upper bound diverges and does not provide any useful information about the exact value of the relative entropy.

This is problematic since we expect any input quantum state after a certain circuit depth to converge to a fixed point due to the unavoidable effects of decoherence, when the noise effects are the dominant driving force during the evolution of the system. This would mean that the relative entropy must converge to zero at a very large circuit depth. Another important point to consider here is that we cannot make any concrete arguments about the *quality* of the upper bound itself. Furthermore, the convergence speed of the exact value of the relative entropy could differ from that of its upper bound, if the later one does converge at all.

Lemma 2.3.1 gives us an upper bound for the relative entropy that converges with respect to the circuit depth D on the following two individually sufficient conditions:

1. The fixed point of noise is the maximally mixed state, i.e. $\sigma = \mathbb{I}/2^n$

2. The max-relative entropy term converges to zero at very large circuit depths

For the first condition we would need to consider those noise models, such as the symmetric depolarizing channel, which drive any input quantum state ρ to the maximally mixed state $\sigma = \mathbb{I}/2^n$. Such an analysis is being done in [32], and therefore it will not be the focus of this study, rather it will only serve as a reference point in the results section.

For the second condition to be satisfied, we would need to consider those quantum algorithms where the max-relative entropy term converges to zero at large circuit depths. Luckily, there exist such algorithms, and for them we can use Lemma 2.3.1 to gain some insight for the evolution and coherence of an input quantum state $\rho = |0\rangle\langle 0|^{\otimes n}$. In this work we will use Lemma 2.3.1 with a focus on the second condition being satisfied, which restricts our choices of algorithms but nonetheless lets us study the evolution of a system under the influence of relaxation and pure dephasing noise.

2.4. Dissipative Lindbladian operators and relative entropy inequalities

Let $\rho(t)$ be an arbitrary quantum state of n qubits and of time t. The time evolution of the state $\rho(t)$ is described by the Lindblad Master Equation,

$$\frac{\partial \rho(t)}{\partial t} = -i[\rho(t), H] + \mathcal{L}_{\text{dissip}}(\rho) \equiv \mathcal{L}(\rho(t)), \tag{2.9}$$

where $[.,.]$ is the commutator, $H = H(t)$ is the time-dependent Hamiltonian of the system and $\mathcal{L}_{\text{dissip}}$ is the Lindbladian describing the dissipation due to noise in the system. The formal solution of Eq. (2.9) is

$$\rho(t) = e^{t\mathcal{L}}(\rho_0), \tag{2.10}$$

where $\rho_0 = \rho(0)$ is the initial state of the system.

Suppose that we can describe the action of a quantum circuit along with its noise processes by a quantum channel $\mathcal{S}_t = e^{t\mathcal{L}}$. We wish to define a contraction property of the

relative entropy $D(\mathcal{S}_t(\rho_0)\|\sigma)$ for the continuous time evolution of an input quantum state ρ_0.

There exists a continuous time version of Lemma 2.3.1 that gives an upper bound for the relative entropy $D(\mathcal{S}_t(\rho_0)\|\sigma) = D(\rho(t)\|\sigma)$. We present this result below as a theorem:

Theorem 2.4.1. *Let $\rho(t)$ be an arbitrary quantum state of n qubits and of time t, and let $\mathcal{L}_{dissip} : \mathcal{M}_{2^n} \to \mathcal{M}_{2^n}$ be a Lindbladian that describes the dissipation of the system with a full-rank fixed point σ, i.e. $\mathcal{L}_{dissip}(\sigma) = 0$, satisfying a modified logarithmic Sobolev inequality (MLSI) with constant $\alpha > 0$. Moreover, let $\mathcal{H}_t : \mathcal{M}_{2^n} \to \mathcal{M}_{2^n}$ be given by $\mathcal{H}_t(X) = -i[X, H_t]$ for some time-dependent Hamiltonian $H_t = H(t)$. Furthermore, let $\mathcal{T}_t$ be the time evolution at time t of the system under the Lindbladian $\mathcal{S}_t = \mathcal{H}_t + \mathcal{L}_{dissip}$, given by*

$$\mathcal{T}_t = \lim_{m\to\infty} \prod_{l=1}^{n} e^{\frac{t}{m}\mathcal{S}_{t_l}}, \tag{2.11}$$

with $t_l = tl/m$. Then for all states ρ and times $t > 0$:

$$D(\mathcal{T}_t(\rho(0))\|\sigma) \leq e^{-\alpha t} D(\rho(0)\|\sigma) + X(t, H_t, \sigma), \tag{2.12}$$

where

$$X(t, H_t, \sigma) = \int_0^t d\tau e^{-\alpha(t-\tau)} \|\sigma^{-\frac{1}{2}}[\sigma, H_\tau]\sigma^{-\frac{1}{2}}\|, \tag{2.13}$$

and $\rho(0)$ is the initial state of the system.

The reader can find a detailed proof of the above theorem in [32]. The proof follows from Lemma 2.3.1, and therefore, all the characteristics and limitations of Lemma 2.3.1 naturally transfer to Theorem 2.4.1.

The first term on the r.h.s. of Eq. (2.12) describes solely the effect of the dissipative Lindbladian $\mathcal{L}_{\text{dissip}}$ on the contraction of the relative entropy, while the second term describes only the effect of the Hamiltonian $H_t = H(t)$. For Theorem 2.4.1 to hold, $\mathcal{L}_{\text{dissip}}$ needs to satisfy a MLSI with constant $\alpha > 0$. This is similar to the discrete case where we previously stated that Lemma 2.3.1 holds for a noisy quantum channel $\mathcal{S} : \mathcal{M}_{2^n} \to \mathcal{M}_{2^n}$ which satisfies a strong data-processing inequality with constant $\alpha > 0$.

In the following, we will examine the different types of dissipative Lindbladians that satisfy a MLSI with constant $\alpha > 0$. In the spirit of [35], we will begin by finding an upper bound of the time derivative $\partial_t D(\rho(t)\|\sigma)$ for a Lindbladian $\mathcal{L} = \alpha\mathcal{L}_\sigma$, where $\mathcal{L}_\sigma(\rho(t)) = \text{Tr}(\rho(t))\sigma - \rho(t)$ and α is a positive constant. It turns out that any dissipative Lindbladian that can be brought into the form $\mathcal{L} = \alpha\mathcal{L}_\sigma$ or $\mathcal{L} = \alpha\mathcal{L}_\sigma + \mathcal{L}'$, with $\mathcal{L}'$ being an arbitrary Lindbladian s.t. $\mathcal{L}'(\sigma) = 0$, satisfies a MLSI with constant α. We will finish this chapter by computing constant α for the relaxation and pure dephasing noise processes described by a dissipative Lindbladian $\mathcal{L}_{\text{dissip}}$ that will be used throughout this thesis.

Proposition 2.4.1. *Let $\rho(t)$ be an arbitrary quantum state of time t and $\mathcal{L} = \alpha\mathcal{L}_\sigma$ be a dissipative Lindbladian with a full-rank fixed point σ, with $\mathcal{L}_\sigma(\rho(t)) = Tr(\rho(t))\sigma - \rho(t)$ and α being a positive constant, where the relative entropy between the states $\rho(t)$ and σ is defined as $D(\rho(t)\|\sigma) = Tr(\rho(t)(\log(\rho(t)) - \log(\sigma)))$. For $\partial_t(\rho(t)) = \mathcal{L}(\rho(t))$, the following inequality holds*

$$\frac{\partial}{\partial t} D(\rho(t)\|\sigma) \leq -2\alpha D(\rho(t)\|\sigma). \tag{2.14}$$

Proof. By taking the derivative of $D(\rho(t)\|\sigma)$ with respect to time t we compute

$$\begin{aligned}\partial_t D(\rho(t)\|\sigma) &= \partial_t(\mathrm{Tr}(\rho(t)(\log(\rho(t)) - \log(\sigma)))) = \mathrm{Tr}[\partial_t(\rho(t)(\log(\rho(t)) - \log(\sigma)))] \\ &= \mathrm{Tr}\left[\log(\rho(t))\partial_t(\rho(t)) + \rho(t)\partial_t(\log(\rho(t))) - \log(\sigma)\partial_t(\rho(t)) - \rho(t)\partial_t(\log(\sigma))\right] \end{aligned} \tag{2.15}$$

For $\mathcal{L} = \alpha\mathcal{L}_\sigma$ and $\mathcal{L}_\sigma(\rho(t)) = \mathrm{Tr}(\rho(t))\sigma - \rho(t)$, one can easily verify that

$$\rho(t)\partial_t(\log(\rho(t))) = \alpha(\mathrm{Tr}[\log(\rho(t))]\rho(t)\sigma - \rho(t)\log(\rho(t)), \tag{2.16}$$

$$\rho(t)\partial_t(\log(\sigma)) = \alpha(\mathrm{Tr}[\log(\sigma)]\rho(t)\sigma - \rho(t)\log(\sigma)). \tag{2.17}$$

Using the above relations for $\rho(t)\partial_t(\log(\rho(t)))$ and $\rho(t)\partial_t(\log(\sigma))$, we compute

$$\begin{aligned}\partial_t D(\rho(t)\|\sigma) &= \mathrm{Tr}[\log(\rho(t))\partial_t(\rho(t)) - \log(\sigma)\partial_t(\rho(t))] + \mathrm{Tr}[\rho(t)\partial_t(\log(\rho(t))) - \rho(t)\partial_t(\log(\sigma))] \\ &= \mathrm{Tr}[\mathcal{L}(\rho(t))(\log(\rho(t)) - \log(\sigma))] - \alpha D(\rho(t)\|\sigma). \end{aligned} \tag{2.18}$$

By substituting $\mathcal{L}(\rho(t)) = \alpha\mathcal{L}_\sigma(\rho(t)) = \alpha(\mathrm{Tr}(\rho(t))\sigma - \rho(t))$ into Eq. (2.18), we obtain

$$\begin{aligned}\partial_t D(\rho(t)\|\sigma) =& \mathrm{Tr}[\alpha(\mathrm{Tr}(\rho(t))\sigma - \rho(t))(\log(\rho(t)) - \log(\sigma))] - \alpha D(\rho(t)\|\sigma) \\ =& \alpha\mathrm{Tr}[\mathrm{Tr}(\rho(t))\sigma\log(\rho(t)) - \mathrm{Tr}(\rho(t))\sigma\log(\sigma) - \rho(t)\log(\rho(t)) + \rho(t)\log(\sigma)] \\ & - \alpha D(\rho(t)\|\sigma) \\ =& \alpha[-\mathrm{Tr}[\rho(t)(\log(\rho(t)) - \log(\sigma))] - \mathrm{Tr}(\rho(t))\mathrm{Tr}[\sigma(\log(\sigma) - \log(\rho(t)))]] \\ & - \alpha D(\rho(t)\|\sigma) \\ =& -2\alpha D(\rho(t)\|\sigma) - \alpha\mathrm{Tr}(\rho(t))D(\sigma\|\rho(t)). \end{aligned}$$

Since $\mathrm{Tr}(\rho(t)) = 1$ and $D(\sigma\|\rho(t)) \geq 0$ holds for an arbitrary state $\rho(t)$, we finally get

$$\frac{\partial}{\partial t}D(\rho(t)\|\sigma) \leq -2\alpha D(\rho(t)\|\sigma),$$

which concludes the proof. □

In Proposition 2.4.1 we proved that for a dissipative Lindbladian that can be brought into the form $\mathcal{L} = \alpha\mathcal{L}_\sigma$ with $\mathcal{L}_\sigma(\rho(t)) = \mathrm{Tr}(\rho(t))\sigma - \rho(t)$ for two quantum states $\rho(t)$ and σ with $\alpha > 0$, Eq. (2.14) is satisfied. We will now make a more general statement, by proving that for a dissipative Lindbladian that can be brought into the form $\mathcal{L} = \alpha\mathcal{L}_\sigma + \mathcal{L}'$, with $\mathcal{L}'$ being an arbitrary Lindbladian s.t. $\mathcal{L}'(\sigma) = 0$, then Eq. (2.14) is still being satisfied.

Proposition 2.4.2. *Let $\rho(t)$ be an arbitrary quantum state of time t and $\mathcal{L} = \alpha\mathcal{L}_\sigma + \mathcal{L}'$ be a dissipative Lindbladian with a full-rank fixed point σ, with $\mathcal{L}_\sigma(\rho(t)) = Tr(\rho(t))\sigma - \rho(t)$, α being a positive constant and $\mathcal{L}'$ an arbitrary Lindbladian s.t. $\mathcal{L}'(\sigma) = 0$, where the relative entropy between the states $\rho(t)$ and σ is defined as $D(\rho(t)\|\sigma) = Tr[\rho(t)(\log(\rho(t)) - \log(\sigma))]$. For $\partial_t(\rho(t)) = \mathcal{L}(\rho(t))$, the inequality given by Eq. (2.14) holds.*

Proof. By substituting $\mathcal{L}(\rho(t)) = \alpha\mathcal{L}_\sigma(\rho(t)) + \mathcal{L}'(\rho(t)) = \alpha(\mathrm{Tr}(\rho(t)) - \sigma) + \mathcal{L}'(\rho(t))$ into Eq. (2.15), we obtain

$$\begin{aligned}\partial_t D(\rho(t)\|\sigma) =& \alpha\mathrm{Tr}[\mathcal{L}_\sigma(\rho(t))(\log(\rho(t)) - \log(\sigma))] + \mathrm{Tr}[\mathcal{L}'(\rho(t))(\log(\rho(t)) - \log(\sigma))] \\ & - \alpha D(\rho(t)\|\sigma) + \mathrm{Tr}[\rho(t)\mathcal{L}'(\log(\rho(t)) - \log(\sigma))], \end{aligned} \tag{2.19}$$

while taking into consideration that $\mathcal{L}'$ is a linear operator.

The reader can verify that the second and fourth term on the r.h.s. of Eq. (2.19) gives

$$\begin{aligned}\mathrm{Tr}[\mathcal{L}'(\rho(t))(\log(\rho(t)) - \log(\sigma))] + \mathrm{Tr}[\rho(t)\mathcal{L}'(\log(\rho(t)) - \log(\sigma))] \\ = \mathrm{Tr}[\mathcal{L}'(\rho(t)(\log(\rho(t)) - \log(\sigma)))]\end{aligned} \tag{2.20}$$

Let us define a quantum state of time t as $\rho'(t) \equiv \rho(t)(\log(\rho(t)) - \log(\sigma))$. If we write $\mathcal{L}'(\rho'(t))$ by using its quantum jump operators (see Eq. (1.21)), then due to the cyclic property of the trace, $\mathrm{Tr}[\mathcal{L}'(\rho'(t))] = 0$.

Consequently, Eq. (2.19) becomes

$$\partial_t D(\rho(t)\|\sigma) = -2\alpha D(\rho(t)\|\sigma) - \alpha D(\sigma\|\rho(t)) \Rightarrow$$

$$\Rightarrow \frac{\partial}{\partial t} D(\rho(t)\|\sigma) \leq -2\alpha D(\rho(t)\|\sigma), \tag{2.21}$$

which concludes the proof.

□

We will now integrate Eq. (2.21) in order to upper bound $D(\rho(t)\|\sigma)$ for a Lindbladian $\mathcal{L}(\rho(t)) = \alpha\mathcal{L}_\sigma(\rho(t)) + \mathcal{L}'(\rho(t))$.

Theorem 2.4.2. *Let $\rho(t)$ be an arbitrary quantum state of time t and $\mathcal{L} = \alpha\mathcal{L}_\sigma + \mathcal{L}'$ be a Lindbladian with a full-rank fixed point σ, with $\mathcal{L}_\sigma(\rho(t)) = Tr(\rho(t))\sigma - \rho(t)$, α a positive constant and $\mathcal{L}'$ an arbitrary Lindbladian s.t. $\mathcal{L}'(\sigma) = 0$, where the relative entropy between the states $\rho(t)$ and σ is defined as $D(\rho(t)\|\sigma) = Tr[\rho(t)(\log(\rho(t)) - \log(\sigma))]$. If $\partial_t(\rho(t)) = \mathcal{L}(\rho(t))$ holds, then the Lindbladian $\mathcal{L}$ satisfies a modified logarithmic Sobolev inequality (MLSI) with constant $\alpha > 0$, which implies that $\mathcal{L}$ satisfies*

$$D(e^{t\mathcal{L}}(\rho_0)\|\sigma) \leq e^{-2\alpha t} D(\rho_0\|\sigma), \tag{2.22}$$

where $\rho_0 = \rho(0)$ is the initial state of the system.

Proof. Following from Proposition 2.4.2, since $D(\rho(t)\|\sigma) \geq 0$ for every state $\rho(t)$, we can divide both sides of Eq. (2.21) with $D(\rho(t)\|\sigma)$ without a change of sign,

$$\frac{\partial}{\partial t} D(\rho(t)\|\sigma) \leq -2\alpha D(\rho(t)\|\sigma) \Rightarrow \frac{dD(\rho(t)\|\sigma)}{D(\rho(t)\|\sigma)} \leq -2\alpha dt.$$

We then proceed to integrate both sides,

$$\int_0^{t'} \frac{dD(\rho(t)\|\sigma)}{D(\rho(t)\|\sigma)} \leq -2\alpha \int_0^{t'} dt \Rightarrow \log|D(\rho(t)\|\sigma)| - \log|D(\rho_0\|\sigma)| \leq -2\alpha t' \Rightarrow$$

$$\Rightarrow \log(D(\rho(t)\|\sigma)) \leq -2\alpha t' + \log(D(\rho_0\|\sigma)). \tag{2.23}$$

By exponentiating both sides of Eq. (2.23) and making the change $t' \to t$, we get

$$D(\rho(t)\|\sigma) \leq e^{-2\alpha t} D(\rho_0\|\sigma), \tag{2.24}$$

where $\rho_0 = \rho(0)$ is the initial state of the system. □

In the following proposition, we will prove that a dissipative Lindbladian $\mathcal{L}_{\text{dissip}}$ describing relaxation with pure dephasing can be brought into the form $\alpha\mathcal{L}_\sigma + \mathcal{L}'$, and therefore by Theorem 2.4.2, $\mathcal{L}_{\text{dissip}}$ will satisfy a MLSI with constant α. In this case, we will be able to use Theorem 2.4.1 and bound the relative entropy for the aforementioned dissipative Lindbladian.

Proposition 2.4.3. *Let $\rho(t)$ be an arbitrary quantum state of n qubits and of time t, where the time evolution of the system is given by the Lindblad Master Equation (2.9), and $\mathcal{L}_{dissip} : \mathcal{M}_{2^n} \to \mathcal{M}_{2^n}$ describes the dissipation of the system caused by relaxation and pure dephasing noise. Then, the dissipative Lindbladian $\mathcal{L}_{dissip}$ satisfies a MLSI with constant $\alpha = \kappa$, where κ is the spin relaxation rate $\kappa = 1/T_1$ with T_1 being the relaxation time.*

Proof. Let $\mathcal{L}^{(i)}$ be a dissipative Lindbladian that acts on an arbitrary qubit i given as $\rho(t)$, and which describes relaxation and pure dephasing noise with quantum jump operators $L_1 = \sqrt{\kappa p}\sigma_-$, $L_2 = \sqrt{\kappa(1-p)}\sigma_+$ and $L_3 = \sqrt{\chi}Z$, where $\sigma_- = |0\rangle\langle 1|$ and $\sigma_+ = |1\rangle\langle 0|$ are the lowering and raising operators respectively, Z is the Pauli-Z matrix, κ is the spin relaxation rate and χ is the pure dephasing rate. The fixed point σ of $\mathcal{L}^{(i)}$ is given by

$$\sigma = \begin{pmatrix} p & 0 \\ 0 & 1-p \end{pmatrix}, \tag{2.25}$$

where the relaxation probability p is given by Eq. (1.22).

The Lindbladian $\mathcal{L}^{(i)}$ can then be written as

$$\mathcal{L}^{(i)}(\rho) = \kappa p\sigma_-\rho\sigma_+ + \kappa(1-p)\sigma_+\rho\sigma_- + \chi Z\rho Z - \frac{1}{2}\kappa p\{\sigma_+\sigma_-, \rho\} - \frac{1}{2}\kappa(1-p)\{\sigma_-\sigma_+, \rho\} - \chi\rho. \tag{2.26}$$

An arbitrary qubit state $\rho(t)$ is given by

$$\rho(t) = \begin{pmatrix} a(t) & b(t) \\ b^*(t) & 1-a(t) \end{pmatrix}, \tag{2.27}$$

where $a(t) \in \mathbb{R}$ and $b(t) \in \mathbb{C}$. For our convenience, we will assign $c(t) \equiv b^*(t)$ and $d(t) \equiv 1 - a(t)$. We then compute,

$$\mathcal{L}^{(i)}(\rho) = \begin{pmatrix} \kappa pd - \kappa(1-p)a & -\frac{1}{2}\kappa b - 2\chi b \\ -\frac{1}{2}\kappa c - 2\chi c & \kappa(1-p)a - \kappa pd \end{pmatrix} \tag{2.28}$$

Let $\mathcal{L}_\sigma^{(i)}$ be a Lindbladian that acts on an arbitrary qubit i given as $\rho(t)$ s.t. $\mathcal{L}_\sigma^{(i)}(\rho(t)) = \text{Tr}(\rho(t))\sigma - \rho(t)$. By applying $\mathcal{L}_\sigma^{(i)}$ on the state $\rho(t)$ given by Eq. (2.27) (with $c \equiv b^*$ and $d \equiv 1 - a$), we obtain

$$\mathcal{L}_\sigma^{(i)}(\rho) = \begin{pmatrix} pa + pd - a & -b \\ -c & a - pa - pd \end{pmatrix}.$$

We can write Eq. (2.28) as

$$\mathcal{L}^{(i)}(\rho(t)) = \kappa\mathcal{L}_\sigma^{(i)}(\rho(t)) + \begin{pmatrix} 0 & \frac{1}{2}\kappa b - 2\chi b \\ \frac{1}{2}\kappa c - 2\chi c & 0 \end{pmatrix}. \tag{2.29}$$

By defining

$$\mathcal{L}'^{(i)}(\rho(t)) := \begin{pmatrix} 0 & \frac{1}{2}\kappa b - 2\chi b \\ \frac{1}{2}\kappa c - 2\chi c & 0 \end{pmatrix}, \tag{2.30}$$

for the fixed point σ given by Eq. (2.25), $\mathcal{L}'^{(i)}(\sigma) = 0$ since $b = c = 0$, and so we have proven that the Lindbladian $\mathcal{L}^{(i)}$ given by Eq. (2.26) can be brought into the form $\mathcal{L}^{(i)}(\rho(t)) = \kappa\mathcal{L}_{\sigma}^{(i)}(\rho(t)) + \mathcal{L}'^{(i)}(\rho(t))$, with $\mathcal{L}_{\sigma}^{(i)}(\rho(t)) = \mathrm{Tr}(\rho(t))\sigma - \rho(t)$ and $\mathcal{L}'^{(i)}(\sigma) = 0$. Therefore, according to Theorem 2.4.2, $\mathcal{L}^{(i)}$ satisfies a MLSI with constant $\alpha = \kappa$ for every qubit i.

For an arbitrary quantum state $\rho(t)$ of n qubits and of time t, where the time evolution of the system is given by Eq. (2.9), for relaxation and pure dephasing noise both of which act individually and uniformly on n qubits, it holds that $\mathcal{L}_{\text{dissip}} = \sum_{i=1}^{n} \mathcal{L}^{(i)}$, where $\mathcal{L}^{(i)}$ is given by Eq. (2.26). In that case, Theorem 19 of [36] guarantees that since $\mathcal{L}^{(i)}$ satisfies a MLSI with constant $\alpha = \kappa$ for every qubit i, then the Lindbladian $\mathcal{L}_{\text{dissip}}$ satisfies a MLSI with constant $\alpha = \kappa$, which concludes the proof. □

It is worth mentioning here that constant α does not depend on the pure dephasing rate χ, and therefore the effects of dephasing are being ignored. This implies that the convergence rate of the upper bound given by Eq. (2.24) is optimal only for $\chi \ll 1$.

3

Certifying Quantum Advantage for the QAOA

3.1. Introduction

Recent theoretical and experimental efforts on quantum computing are focused on achieving quantum advantage on a NISQ device of tens, or even a few hundreds of qubits. On the experimental forefront, in 2019 Google's research team published a paper claiming the first demonstration of quantum advantage [37], where their superconducting 53-qubit processor (Google Sycamore) completed succesfully a benchmark task in about 200 seconds, whereas an equivalent task carried out by a state-of-the-art classical supercomputer would take approximately 10,000 years to complete. IBM was quick to dispute those claims [38], stating in their research blog that the term quantum supremacy "was to describe the point where quantum computers can do things that classical computers can't, this threshold has not been met" [39].

Just about a year later after Google's publication, Zhong *et al.* demonstrated quantum advantage on a photonic quantum processor performing a boson sampling task [40], while in 2021 Wu *et al.* [41] used a superconducting 66-qubit processor to perform a much harder benchmarking task than the one previously carried out on the Google Sycamore processor. Even though those results are indicative of the potential of these early-development systems, it still remains to be shown if NISQ devices are capable of demonstrating a strong advantage over their classical counterparts for problems of practical interest.

Early 2021, Harrigan *et al.* ran a promising variational algorithm [5], the Quantum Approximate Optimization Algorithm (QAOA), on the Google Sycamore processor. Their results were poor and suggested that it will be a real challenge to gain an advantage by implementing the QAOA on NISQ hardware in the near future. In parallel to the experimental implementations, theorists strive to answer the question, could some of the proposed variational algorithms be fundamentally limited by the effects of noise when executed on a NISQ device? Some notable early work on this topic comes from Brandao *et al.* [42] and Wang *et al.* [43].

França and Garcia-Patron have proposed the use of quantum relative entropy bounds in order to compare the performance of a quantum algorithm to that of a classical, when both are used to solve the same problem [32]. In their paper, they claim that when a quantum state evolves under the influence of a global depolarizing channel, the QAOA implemented on current NISQ devices cannot achieve a quantum advantage for some graph problems.

In this chapter we will use their methods for the case of the QAOA running on a planar superconducting chip, by assuming relaxation as the dominant and only source of noise. This is an analysis which is much closer to the hardware of superconducting transmon qubits rather than assuming depolarizing noise, and demonstrates how one could accurately use these techniques to obtain results on any other quantum computing platform. We will show that the choice of a noise model greatly affects the results, and one can disprove the conclusions that have been made in [32] for a different noise model than depolarization.

3.2. Declaring the loss of quantum advantage

We can always describe any quantum algorithm as the evolution of an input quantum state ρ_0 to an output state $\mathcal{S}(\rho_0) = \rho$. Here $\mathcal{S}$ is a general quantum channel describing the algorithm, or equivalently, the action of the quantum circuit, along with the effects of decoherence due to its implementation on a noisy quantum device. The evolution $\mathcal{S}(\rho_0)$ of an input state ρ_0 can be either the application of a series of unitary layers $\mathcal{U}$ in the presence of an error quantum channel $\mathcal{E}$ (see Fig. 2.1), or either the dynamics induced by a Lindblad Master Equation (Eq. (1.21)), where a dissipative Lindbladian operator $\mathcal{L}_{\text{dissip}}$ influences the evolution of the system for the total runtime T of the algorithm.

For the fixed point of noise σ, i.e. $\mathcal{S}(\sigma) = 0$ when we remove the unitary layers from $\mathcal{S}$ and leave only the noise, then the relative entropy of an output state $\mathcal{S}(\rho_0) = \rho$, given by $D(\rho(T)\|\sigma)$, indicates the corruption that the input state ρ_0 has suffered due to the effects of noise at time T. It is clear by now that under such considerations, the smaller $D(\rho\|\sigma)$ becomes, the closer the output state ρ is to σ, which is undesirable but inevitable altogether. In Section 2 we introduced some general upper bounds for the relative entropy $D(\rho\|\sigma)$, which can give us a good estimation over the quality of the output state ρ of a general quantum circuit.

There exists a class of classical problems called the *Quadratic Unconstrained Binary Optimization* problems, or QUBO for short, where their solution involves finding a bitstring $z = z^*$, with $z \in \{0,1\}^n$, which minimizes a quadratic objective function

$$\min_{z\in\{0,1\}^n} z^{\mathrm{T}} Q z + c^{\mathrm{T}} z \tag{3.1}$$

under no variable constraints, for given $c \in \mathbb{R}^n$ and $Q \in \mathbb{R}^{n\times n}$ [44]. By defining

$$C(z) \equiv z^{\mathrm{T}} Q z + c^{\mathrm{T}} z \tag{3.2}$$

as the problem-specific cost function $C(z)$, the solution to a QUBO problem can then be restated as finding the bitstring z^* which solves

$$\min_{z\in\{0,1\}^n} C(z). \tag{3.3}$$

QUBO problems are generically hard (NP-complete), also when $z^{\mathrm{T}} Q z + c^{\mathrm{T}} z$ has the connectivity of a planar graph. For QUBO problems there exist families of classical

optimization algorithms, such as Monte Carlo sampling, that can find an approximate solution to a particular problem by estimating the partition function $\mathcal{Z}_{\beta_\mathcal{T}} = \mathrm{Tr}(e^{-\beta_\mathcal{T} H})$ of a classical Gibbs state $\sigma_{\beta_\mathcal{T}} = e^{-\beta_\mathcal{T} H}/\mathcal{Z}_{\beta_\mathcal{T}}$ at an inverse temperature $\beta_\mathcal{T} = 1/\mathcal{T}$. Such an algorithm is considered to be efficient if for a specific range of values $\beta_\mathcal{T} \in [0, \beta_C]$, a conventional computer can find an optimal solution to the problem in polynomial time $O(n)$, with β_C being an inverse temperature where we can sample from σ_{β_C} *efficiently*.

We can solve QUBO problems using a quantum computer by encoding the cost function $C(z)$ into a problem Hamiltonian H_C, such that

$$H_C|z\rangle = C(z)|z\rangle, \tag{3.4}$$

and therefore finding the solution bitstring z^* which minimizes the cost function $C(z)$ now means finding the quantum state $\rho^* = |z^*\rangle\langle z^*|$ which minimizes the output energy $E(\rho) = \mathrm{Tr}(\rho H_C)$.

We have already established that the effects of relaxation and pure dephasing noise (without the application of unitary layers) erase the off-diagonal elements of any input quantum state ρ_0 as a function of the circuit depth D, thus transforming ρ_0 into a classical probabilistic state (see Eq. (2.14). It is reasonable to assume that after a certain amount of corruption, the output state ρ of a quantum circuit after a total runtime T cannot retain any computational advantage over a classical optimization algorithm which estimates a partition function $\mathcal{Z}_{\beta_\mathcal{T}}$ for a sufficient range of $\beta_\mathcal{T}$. Along these lines, the output energies $\mathrm{Tr}(\rho(T)H_C)$ and $\mathrm{Tr}(\sigma_{\beta_\mathcal{T}} H_C)$ are expected to be very close for some $\beta_\mathcal{T} \in [0, \beta'_\mathcal{T}]$. The above observation is formulated concretely into the following theorem:

Theorem 3.2.1. *Let $\mathcal{S}(\rho_0)$ be the output of a noisy quantum device and for some full-rank state $\sigma > 0$ let $V = -\log(\sigma)$ and $D(\mathcal{S}(\rho_0)\|\sigma) = Tr(\mathcal{S}(\rho_0)(\log(\mathcal{S}(\rho_0)) - \log(\sigma)))$ be their relative entropy. Then for any Hamiltonian H there is a $\beta_\mathcal{T} \in [0, \frac{4D(\mathcal{S}(\rho_0)\|\sigma)}{\epsilon\|H\|}]$ such that the state $\sigma_{V,\beta_\mathcal{T}}$ defined as*

$$\sigma_{V,\beta_\mathcal{T}} = exp(-V - \beta_\mathcal{T} H)/\mathcal{Z}_{\beta_\mathcal{T}} \tag{3.5}$$

satisfies:

$$Tr(\mathcal{S}(\rho_0)H) \geq Tr(\sigma_{V,\beta_\mathcal{T}} H) - \epsilon\|H\|, \tag{3.6}$$

for some given error parameter $\epsilon > 0$.

The reader can find the proof of the above theorem on [32]. It is important to understand that Theorem 3.2.1 holds even if for the range $\beta_\mathcal{T} \in \left[0, \frac{4D(\mathcal{S}(\rho_0)\|\sigma)}{\epsilon\|H\|}\right]$ a classical optimization algorithm cannot sample *efficiently* from the Gibbs state $\sigma_{V,\beta_\mathcal{T}}$.

For this reason, it becomes obvious that Theorem 3.2.1 is useful only in the case where the relative entropy $D(\mathcal{S}(\rho_0)\|\sigma)$ is sufficiently small so that a classical optimization algorithm can sample in polynomial time $O(n)$ from a Gibbs state $\sigma_{V,\beta_\mathcal{T}}$ at inverse temperatures $\beta_\mathcal{T} \leq \beta_C$. Since we have already derived upper bounds for the relative entropy $D(\mathcal{S}(\rho_0)\|\sigma)$, the key idea is that *when* the upper bound reaches the value $\epsilon\|H\|\beta_C/4$, because of Theorem 3.2.1, we can guarantee that the output energy $E = \mathrm{Tr}(\mathcal{S}(\rho_0)H)$ is close to that of $\mathrm{Tr}(\sigma_{V,\beta_\mathcal{T}} H)$, where the latter can be efficiently computed. Thus, quantum computational advantage has been lost.

3.3. The quantum approximate optimization algorithm in a nutshell

The *Quantum Approximate Optimization Algorithm* [4], or in short QAOA, is a hybrid quantum-classical algorithm that belongs to the algorithmic family of Variational Quantum Eigensolvers (VQEs). It is intended to be used for solving QUBO problems, where the cost function C of a given problem can be recast into a problem Hamiltonian H_C, which is diagonal in the computational basis (as in Eq. (3.4)).

Every QAOA algorithm begins with a variational quantum circuit that parametrizes an input state $|\psi_0\rangle = |+\rangle^{\otimes n}$ as $|\psi(\gamma,\beta)\rangle = U(\gamma,\beta)|\psi_0\rangle$, where $U(\gamma,\beta)$ is called the variational form and γ,β belong to the parameter vector spaces $\gamma = (\gamma_1,\gamma_2,\gamma_3,...)$ and $\beta = (\beta_1,\beta_2,\beta_3,...)$ respectively. The main objective of QAOA is to solve

$$\min_{\gamma,\beta}\langle\psi(\gamma,\beta)|H_C|\psi(\gamma,\beta)\rangle, \tag{3.7}$$

for a given problem Hamiltonian H_C which can be then recast back into the cost function C. This way, if we are able to solve Eq. (3.7) then we can also solve for $C_{\min}$.

The quantum part of the algorithm creates the trial wave functions $|\psi(\gamma,\beta)\rangle$, while the classical part of the algorithm is an optimization procedure, usually a SPSA (Simultaneous perturbation stochastic approximation) optimizer, that updates the parameters γ,β in such a way that the expectation value $\langle\psi(\gamma,\beta)|H|\psi(\gamma,\beta)\rangle$ approximates the global minimum after a number of P repetitions. In general, the performance of the QAOA can only improve with increasing P [4], while it applies adiabatic evolution for $P\to\infty$ [44]. For our analysis, we will focus on the quantum part of the QAOA, more specifically, the variational form $U(\gamma,\beta)$.

Below we present a general circuit describing the QAOA algorithm:

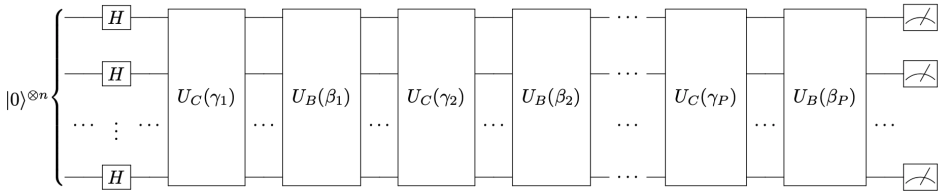

Figure 3.1: The QAOA algorithm for a number of P repetitions.

First, we create an equal superposition of all states $|\psi_0\rangle = |+\rangle^{\otimes n}$ and then proceed with parametrizing it. Parametrization is achieved by using two unitaries, first the *cost layer* $U_C(\gamma)$, also called the problem unitary, and then the *mixer layer* $U_B(\beta)$, also called the driver unitary.

For a problem Hamiltonian H_C given by

$$H_C = \sum_{i=1}^{n} c_i Z_i + \sum_{i,j=1}^{n} Q_{ij} Z_i \otimes Z_j, \tag{3.8}$$

the two unitaries can be expressed as [44]

$$U_C(\gamma) = e^{-i\gamma H_C} = e^{-i\gamma\left(\sum_{i=1}^{n} c_i Z_i + \sum_{i,j=1}^{n} Q_{ij} Z_i \otimes Z_j\right)}, \tag{3.9}$$

and

$$U_B(\beta) = e^{-i\beta \sum_{i=1}^{n} X_i}, \tag{3.10}$$

with Z_i and X_i denoting the Pauli Z-matrix and Pauli X-matrix respectively acting on the i^{th} qubit, while c_i and Q_{ij} are the given QUBO vector and matrix respectively that appear on Eq. (3.1).

The unitary $U_C(\gamma)$ is problem specific since it encodes the cost function $C(z)$, and it creates entanglement between all qubits in such a way that there is a change in phase for the states that comprise the bitstrings which most likely approximate the solution (or *are* the solution) of the QUBO problem at hand (see more on [44]). This assists the classical optimizer with the search for the most optimal set of parameters γ, β that can solve Eq. (3.7).

The unitary $U_B(\beta)$ is the same for every problem that we want to solve using the QAOA and its purpose is to mix all the parameters γ and β in such a way that the complexity of the superposition of states in $|\psi(\gamma, \beta)\rangle$ increases. By doing this, we can search for the solution in multiple directions in the Hilbert space at the same time, thus assisting the classical optimizer in finding the most optimal solution.

We will now go in more depth discussing some of the important characteristics of both unitary layers $U_C(\gamma)$ and $U_B(\beta)$.

3.3.1. The cost layer $U_C(\gamma)$

The cost layer $U_C(\gamma)$ is problem specific and thus there exists no generic decomposition for it. For QUBO problems that can be depicted as graphs, there exist three main problem categories of interest [5, 32], namely the *Hardware grid* problems, the *Three-regular MaxCut* problems and the fully connected *Sherrington-Kirkpatrick model* (SK model). While the Hardware grid problems match the topology of the quantum device of choice and they do not require qubit routing, the MaxCut problem defined on a three-regular graph as well as the SK model are high connectivity problems and require routing, with the latter having a Hamiltonian with all-to-all connectivity which is the most taxing for routing.

The cost layer $U_C(\gamma)$ can be decomposed into a number of single-qubit and two-qubit gates, accounting for single-qubit rotations of the form $e^{-i\gamma c_i Z_i}$ and the nearest-neighbour interactions $e^{-i\gamma Q_{ij} Z_i Z_j}$ respectively. For problems with high connectivity, the number of layers that the decomposition of a single cost layer $U_C(\gamma)$ amounts to is proportional to the system size n [5, 32]. This can affect significantly the runtime Δt of a single repetition of the QAOA. For our analysis, we will consider the cost layer $U_C(\gamma)$ as a big unitary block that can be decomposed into a number m of single unitary layers, which act on n qubits and are diagonal in the computational basis.

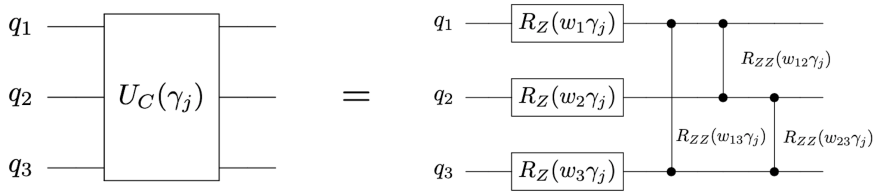

Figure 3.2: A possible decomposition of the cost layer $U_C(\gamma_j)$ acting on $n = 3$ qubits into a series of single-qubit and two-qubit gates accounting for the $e^{-i\gamma c_i Z_i}$ and $e^{-i\gamma Q_{ij} Z_i Z_j}$ interactions respectively, for a repetition j of the QAOA for an instance of the MaxCut problem. Notice how due to the high connectivity, the number of layers of this decomposition exceeds the number of qubits of the system. The individual weights w_k and w_{kl} correspond to the values of c_k and Q_{kl} of the problem Hamiltonian (Eq. (3.8)) for qubits k and l.

3.3.2. The mixer layer $U_B(\beta)$

The mixer layer, as it is described by Eq. (3.10), can be decomposed into n single-qubit rotations as follows:

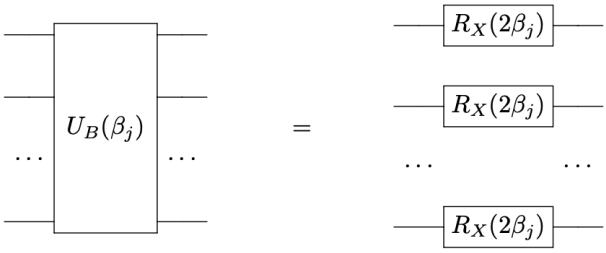

Figure 3.3: Decomposition of the mixer layer $U_B(\beta_j)$ into n single-qubit rotations $R_X(2\beta_j)$ for a repetition j of the QAOA. The above decomposition remains the same for every repetition j and is not problem dependent.

If we set

$$\beta_j = A_j \tau_{1,j}, \tag{3.11}$$

with A_j being the interaction strength with units $[A_j] = s^{-1}$ and $\tau_{1,j}$ being the single-qubit duration of an individual $R_X(2\beta_j)$ gate of units $[\tau_{1,j}] = s$, then the Hamiltonian describing the mixer layer for a repetition j of the QAOA is given by

$$H_B^j = A_j \sum_{i=1}^{n} X_i. \tag{3.12}$$

Notice how for a given repetition j, on every qubit $i = 1, ..., n$ we apply the same rotation $R_X(2\beta_j)$ (rotation over the X-axis by an angle $2\beta_j$). By using Eq. (3.11) we can rewrite Eq. (3.12) as

$$H_B^j = \frac{\beta_j}{\tau_{1,j}} \sum_{i=1}^{n} X_i. \tag{3.13}$$

3.3.3. OPTIMIZING THE PERFORMANCE OF THE QAOA

The QAOA is a general-purpose algorithm which for some problems, even for $P = 1$ number of repetitions, it produces non-trivial results which outperform random guessing [45]. That being said, little is known about the performance of the algorithm for $P > 1$ repetitions, and exploring the regime $1 < P < \infty$ is part of an active research in the quantum computing community.

Until now, we have defined the two parameter vector spaces γ and β which are being optimized by a classical optimizer at the end of the QAOA circuit, only to be fed back to it once the parameters are being updated. It would seem that for any QAOA algorithm of P repetitions, there is no intelligent initial guess that one can make for the parameters γ_1 and β_1, which complicates the optimization process. Nonetheless, there have been recent studies which suggest that *when* the performance of the QAOA algorithm is optimized for a number of problems such as instances of the MaxCut problem [6, 46] and the SK model [45], the variational parameters γ and β display an optimization pattern.

Upon examining the results in all of the above cases, the variational parameter γ increases monotonically with P while the variational parameter β decreases monotonically with P when the performance of the QAOA is optimized. For the variational parameters β_j of Eq. (3.13), we apply a polynomial fit to the data sets provided by [45] and we find the following function for the values of $\beta(j)$,

$$\beta(j) = 0.781433 - 1.44634j + 2.24229j^2 - 1.57737j^3. \tag{3.14}$$

For $P = 16$ repetitions of the QAOA, we plot the variational parameters $\beta(j)$ that we sampled from Eq. (3.14) as a function of the repetitions j:

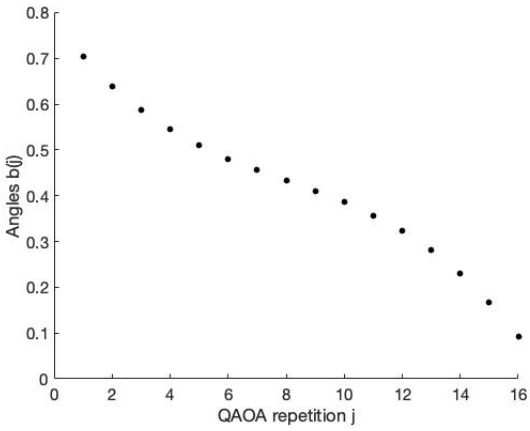

Figure 3.4: Generated values of the optimized variational parameters $\beta(j)$ for $P = 16$ repetitions of the QAOA. We recognise the same monotonal decrease pattern that the parameters $\beta(j)$ show on [6, 45, 46].

We can see that the values of $\beta(j)$ sampled from Eq. (3.14) display the same pattern as those observed at [6, 45, 46]. We will use Eq. (3.14) in order to generate approximate values of $\beta(j)$ for any number of repetitions P, that optimize the performance of the QAOA.

The reader should keep in mind that this is a necessary approximation, since we will need a generator of β parameter values for our numerical simulations at the end of this chapter.

3.4. Discrete time evolution of an input state

Let $\rho_0 = |+\rangle\langle+|^{\otimes n}$ be an input quantum state of n qubits and let $\mathcal{E}^{(1)} : \mathcal{M}_2 \to \mathcal{M}_2$ be the Relaxation Channel (RC) acting on one qubit for positive temperatures $\mathcal{T} > 0$ with Kraus operators

$$E_0 = \sqrt{p}\begin{pmatrix} 1 & 0 \\ 0 & \sqrt{1-\gamma} \end{pmatrix}, \; E_1 = \sqrt{p}\begin{pmatrix} 0 & \sqrt{\gamma} \\ 0 & 0 \end{pmatrix}, \tag{3.15}$$

$$E_2 = \sqrt{1-p}\begin{pmatrix} \sqrt{1-\gamma} & 0 \\ 0 & 1 \end{pmatrix}, \; E_3 = \sqrt{1-p}\begin{pmatrix} 0 & 0 \\ \sqrt{\gamma} & 0 \end{pmatrix}, \tag{3.16}$$

where the relaxation probabilities p for the states $|0\rangle$ and $|1\rangle$ follow the Boltzmann distribution given by Eq. (1.22), and γ is the decay probability, thus $0 \leq \gamma \leq 1$.

The fixed point of the Relaxation Channel $\mathcal{E}^{(1)}$ is

$$\sigma_0 = \begin{pmatrix} p & 0 \\ 0 & 1-p \end{pmatrix}, \tag{3.17}$$

which is a full-rank state for $p \neq 1$. Let us now define the Relaxation Channel $\mathcal{E} : \mathcal{M}_{2^n} \to \mathcal{M}_{2^n}$ as the composition of individual one-qubit Relaxation Channels $\mathcal{E}^{(1)}$ as can be seen on Fig. 3.5 below:

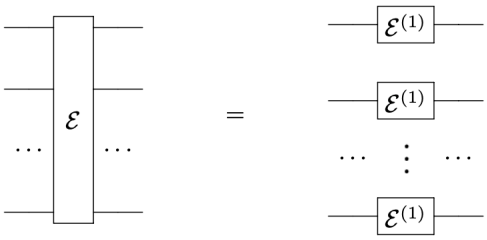

Figure 3.5: In our model for relaxation along with dephasing noise we assume an error layer channel $\mathcal{E}$ acting on n qubits that is comprised of individual Relaxation Channels $\mathcal{E}^{(1)}$ acting on single qubits uniformly.

The Relaxation Channel $\mathcal{E}$ acting on n qubits has a full-rank fixed point $\mathcal{E}(\sigma) = \sigma$ given by

$$\sigma = \begin{pmatrix} p & 0 \\ 0 & 1-p \end{pmatrix}^{\otimes n}. \tag{3.18}$$

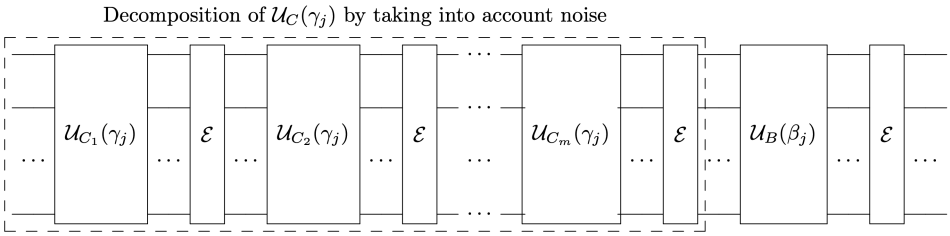

Figure 3.6: A single repetition j of the QAOA, where the Relaxation Channel $\mathcal{E}$ acts uniformly and individually on n qubits. Here, we assume that the cost layer $\mathcal{U}_C(\gamma_j)$ decomposes into m single unitary layers that are all diagonal in the computational basis (see Section 3.3.1).

Since the Relaxation Channel $\mathcal{E}$ satisfies a strong data-processing inequality with constant $\alpha > 0$ (error probability) [47, 48], we apply Lemma 2.3.1 for a noisy quantum circuit, which implements P repetitions of QAOA on n qubits for a total of D layers, and get the following upper bound on the relative entropy:

$$D(\rho\|\sigma) \leq (1-\alpha)^D D(\rho_0\|\sigma) + \sum_{t=1}^{D}(1-\alpha)^{D-t} D_\infty(\mathcal{U}_t(\sigma)\|\sigma), \tag{3.19}$$

where the unitary channels $\mathcal{U}_t$ act on an arbitrary n-qubit state ρ as $\mathcal{U}_t(\rho) = U_t \rho U_t^\dagger$, for all repetitions $j \in \{1, 2, ..., P\}$.

Here we assume that for a general repetition j of the algorithm, a cost layer $\mathcal{U}_C(\gamma_j)$ decomposes into m single unitary layers $\mathcal{U}_{C_k}(\gamma_j)$ (as in Fig. 3.6), with $1 \leq k \leq m$. Since all single unitary layers $\mathcal{U}_{C_k}(\gamma_j)$ are diagonal in the computational basis (see Section 3.3.1), we have

$$D_\infty(\mathcal{U}_{C_k}(\gamma_j)(\sigma)\|\sigma) = D_\infty(\sigma\|\sigma) = 0, \tag{3.20}$$

for any single unitary layer k of the decomposition of a single cost layer $\mathcal{U}_C(\gamma_j)$ and for any repetition j of the algorithm. Since the QAOA has P repetitions, by taking into account the decomposition of the cost layer, the total circuit depth will be $D = (m+1)P$, hence we can rewrite Eq. (3.19) as

$$D(\rho\|\sigma) \leq (1-\alpha)^{(m+1)P} D(\rho_0\|\sigma) + \sum_{j=1}^{P}(1-\alpha)^{(m+1)(P-j)} D_\infty(\mathcal{U}_B(\beta_j)(\sigma)\|\sigma). \tag{3.21}$$

By carrying out all of the necessary calculations (see Appendix A.1), we find that

$$D(\rho\|\sigma) \leq n\left[-\frac{(1-\alpha)^{(m+1)P}}{2}(\log(p) + \log(1-p)) + \sum_{j=1}^{P}(1-\alpha)^{(m+1)(P-j)}\log(\|A(j)\|)\right] \tag{3.22}$$

where the matrix $A(j)$ is given by

$$A(j) \equiv \begin{pmatrix} \cos^2(\beta_j) + \frac{1-p}{p}\sin^2(\beta_j) & i\sin(\beta_j)\cos(\beta_j)\frac{1-2p}{\sqrt{p(1-p)}} \\ i\sin(\beta_j)\cos(\beta_j)\frac{2p-1}{\sqrt{p(1-p)}} & \cos^2(\beta_j) - \frac{p}{1-p}\sin^2(\beta_j) \end{pmatrix}. \tag{3.23}$$

Equation (3.22) constitutes the relative entropy upper bound for the QAOA of P repetitions running on a quantum device of n qubits, with α being the error probability of the RC and p being the damping probability with which a single qubit goes from the excited state $|1\rangle$ to the ground state $|0\rangle$ due to relaxation.

3.5. Continuous time evolution of an input state

3.5.1. Prerequisites

Let $\rho_0 = \rho(0)$ be an arbitrary input quantum state of n qubits and $\mathcal{L}_{\text{dissip}}(\rho_0) = \sum_{i=1}^{3} L_i \rho_0 L_i^\dagger - \frac{1}{2}\{L_i^\dagger L_i, \rho_0\}$ be a Lindbladian operator which describes the dissipation of the system caused by relaxation noise along with pure dephasing noise, with quantum jump operators $L_1 = \sqrt{\kappa p}\sigma_-$, $L_2 = \sqrt{\kappa(1-p)}\sigma_+$ and $L_3 = \sqrt{\chi}Z$. By Proposition 2.4.3, the dissipator $\mathcal{L}_{\text{dissip}}$ satisfies a MLSI with constant $\alpha = \kappa$.

Thus, for an output quantum state of n qubits that satisfies the Lindblad Master Equation (2.9) with the solution given by Eq. (2.10) for a time-dependent Hamiltonian $H = H(t)$ and a quantum channel $S_t = e^{t\mathcal{L}}$, Theorem 2.4.1 states that for all times $T > 0$, the output state $\rho(t) = S_t(\rho_0)$ satisfies

$$D(\rho(t)\|\sigma) \leq e^{-\kappa T} D(\rho_0\|\sigma) + X(T, H, \sigma), \tag{3.24}$$

where

$$X(T, H, \sigma) = \int_0^T d\tau e^{-\kappa(T-\tau)} \|\sigma^{-\frac{1}{2}}[H, \sigma]\sigma^{-\frac{1}{2}}\|. \tag{3.25}$$

Our task is to compute the bound of Eq. (3.24) for the case of the QAQA running on a quantum device of n qubits for a total runtime T of the algorithm. We have already computed the term $D(\rho_0\|\sigma)$ in Appendix A.1, and so using Eq. (A.6) we can rewrite Eq. (3.24) as

$$D(\rho(t)\|\sigma) \leq -\frac{ne^{-\kappa T}}{2}(\log(p) + \log(1-p)) + X(T, H, \sigma). \tag{3.26}$$

What remains now is to compute the integral term $X(T, H, \sigma)$, which we will do in the following.

3.5.2. CALCULATING THE INTEGRAL TERM

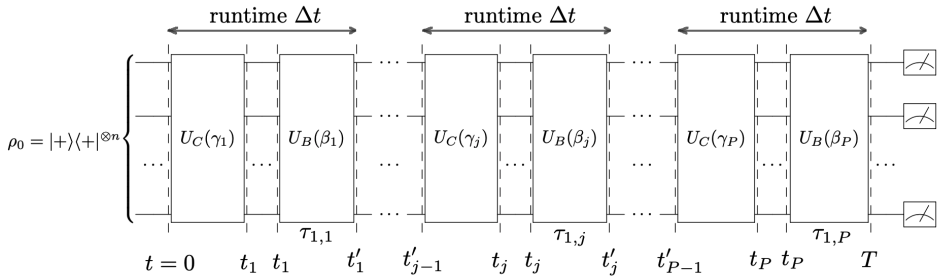

Figure 3.7: The QAOA algorithm for a number of P repetitions. Here we assume that every repetition has the same runtime Δt, with the total runtime of the algorithm being $T = P\Delta t$. We can see in the figure the different times for when the switching Hamiltonian $H(t)$ of Eq. (3.27) acts accordingly. Each mixer layer $U_B(\beta_j)$ has a duration $\tau_{1,j} = t'_j - t_j$ for a repetition j. It is assumed that no time elapses after the application of a cost layer until the application of the following mixer layer.

In order to compute the integral term $X(T, H, \sigma)$ we first need to properly define the Hamiltonian $H = H(t)$ for the QAOA. Following Fig. 3.7, we define a switching Hamiltonian $H(t)$ as follows:

$$H(t) = \begin{cases} H_C^1, & 0 \le t < t_1, \\ H_B^1, & t_1 \le t < t'_1, \\ \vdots & \vdots \\ H_C^j, & t'_{j-1} \le t < t_j, \\ H_B^j, & t_j \le t < t'_j, \\ \vdots & \vdots \\ H_C^P, & t'_{P-1} \le t < t_P, \\ H_B^P, & t_P \le t < T. \end{cases} \tag{3.27}$$

By Eq. (3.8), the Hamiltonian H_C is comprised only of Pauli-Z matrices and their tensor products, which are all diagonal in the computational basis. Consequently, for the fixed point $\sigma = \sigma_0^{\otimes n}$ with σ_0 given by Eq. (3.17), it is easy to verify that $[H_C, \sigma] = 0$ for any problem unitary $U_C(\gamma)$.

Therefore, the only non-zero terms in Eq. (3.25) are the ones that are computed at times t_j to t'_j with $j \in \{1, 2, ..., P\}$, that is, *only* when the mixer layers $U_B(\beta_j)$ are applied, and so

$$X(T, H, \sigma) = \int_0^T d\tau e^{-\kappa(T-\tau)} \|\sigma^{-\frac{1}{2}}[H, \sigma]\sigma^{-\frac{1}{2}}\| = \sum_{j=1}^{P} \int_{t_j}^{t'_j} d\tau e^{-\kappa(T-\tau)} \|\sigma^{-\frac{1}{2}}[H_B^j, \sigma]\sigma^{-\frac{1}{2}}\|. \tag{3.28}$$

Given that H_B^j can be expressed as a sum of Pauli-X terms (Eq. (3.13)), by using the triangle

inequality we get

$$\|\sigma^{-\frac{1}{2}}[H_B^j,\sigma]\sigma^{-\frac{1}{2}}\| \leq \frac{|\beta_j|}{\tau_{1,j}} \sum_{i=1}^{n} \|\sigma^{-\frac{1}{2}}[X_i,\sigma]\sigma^{-\frac{1}{2}}\|. \tag{3.29}$$

Hence, using the result of Eq. (3.29) we can rewrite Eq. (3.28) as

$$X(T,H,\sigma) \leq \frac{1}{\tau_{1,j}} \sum_{i=1}^{n} \|\sigma^{-\frac{1}{2}}[X_i,\sigma]\sigma^{-\frac{1}{2}}\| \sum_{j=1}^{P} |\beta_j| \int_{t_j}^{t_j'} d\tau e^{-\kappa(T-\tau)} \tag{3.30}$$

We can easily compute now the integral term as follows:

$$\int_{t_j}^{t_j'} d\tau e^{-\kappa(T-\tau)} = \frac{e^{-\kappa T}}{\kappa}\left(e^{\kappa t_j'} - e^{\kappa t_j}\right) = \frac{e^{-\kappa T}}{\kappa}\left(e^{\kappa(t_j'-t_j)} - 1\right)e^{\kappa t_j} = \frac{e^{-\kappa T}}{\kappa}\left(e^{\kappa\tau_{1,j}} - 1\right)e^{\kappa t_j}, \tag{3.31}$$

where we used $\tau_{1,j} = t_j' - t_j$ (see Fig. 3.7).

For all $j \in \{1,2,...,P\}$, the single-qubit gate duration $\tau_{1,j}$ in all current superconducting devices is typically of the tens of ns in value [49]. Since $\kappa = 1/T_1$, where T_1 is of the order of μs for all current superconducting devices [49], the exponential term $e^{\kappa\tau_{1,j}}$ in Eq. (3.31) will approximately have the same value for all j. Accordingly, we can make the approximation $\tau_{1,j} \approx \tau_1$ for all j, where τ_1 is the typical single-qubit gate duration of all rotations for a given quantum device.

By applying this approximation, Eq. (3.30) becomes

$$X(T,H,\sigma) \leq \frac{e^{-T/T_1}\left(e^{\tau/T_1} - 1\right)T_1}{\tau_1} \sum_{i=1}^{n} \|\sigma^{-\frac{1}{2}}[X_i,\sigma]\sigma^{-\frac{1}{2}}\| \sum_{j=1}^{P} e^{t_j/T_1}|\beta_j|. \tag{3.32}$$

By Fig. 3.7, the total runtime T of the algorithm can be expressed as $T = P\Delta t$, where Δt is the runtime of a single repetition of the QAOA, and $t_j = j\Delta t - \tau_1$ for every $j \in \{1,2,...,P\}$. Therefore,

$$X(T,H,\sigma) \leq \frac{\left(1 - e^{-\tau_1/T_1}\right)T_1}{\tau_1} \sum_{i=1}^{n} \|\sigma^{-\frac{1}{2}}[X_i,\sigma]\sigma^{-\frac{1}{2}}\| \sum_{j=1}^{P} e^{-(P-j)\Delta t/T_1}|\beta_j|. \tag{3.33}$$

By computing the term $\|\sigma^{-\frac{1}{2}}[X_i,\sigma]\sigma^{-\frac{1}{2}}\|$ (see Appendix A.2), we finally obtain

$$D(\rho(t)\|\sigma) \leq n\Bigg[-e^{-P\Delta t/T_1}\frac{\log(p)+\log(1-p)}{2} + \\ + \frac{|2p-1|}{\sqrt{p(1-p)}}\frac{\left(1-e^{\tau_1/T_1}\right)T_1}{\tau_1}\sum_{j=1}^{P} e^{-(P-j)\Delta t/T_1}|\beta_j|\Bigg]. \tag{3.34}$$

3.6. Results and Discussion

By having two upper bounds for the relative entropy given by Eqs. (3.22) and (3.34), we can now compare the performance between a quantum computer and a classical computer

when both are solving an optimization problem of the form of Eq. (3.1). We choose to compare the performance of QAOA running on a planar superconducting chip with the performance of a classical optimization algorithm which estimates the partition function $\mathcal{Z}_{\beta_\mathcal{T}}$ of a classical Gibbs state $\sigma_{\beta_\mathcal{T}}$ efficiently for inverse temperatures $\beta_\mathcal{T} \leq \beta_C$.

For Ising Hamiltonians given by Eq. (3.8), Theorem 11 of [50] guarantees that when

$$\beta\|Q\| < \frac{1}{2}, \tag{3.35}$$

where $(Q)_{i,j} = Q_{ij}$ is the QUBO matrix with $Q \in \mathbb{R}^{n\times n}$, a Gibbs state σ_β can be sampled from efficiently in $O(n\log(n))$ time. By Theorem 3.2.1, we know that there exists a Gibbs state $\sigma_{V,\beta_\mathcal{T}}$ of inverse temperature $\beta_\mathcal{T} \in \left[0, \frac{4D(\rho\|\sigma)}{\epsilon\|H_C\|}\right]$ that satisfies Eq. (3.6). When Eq. (3.35) is satisfied, as long as

$$\frac{4D(\rho\|\sigma)}{\epsilon\|H_C\|} \leq \frac{1}{2\|Q\|}, \tag{3.36}$$

then we can estimate the partition function of $\sigma_{V,\beta_\mathcal{T}}$ efficiently in $O(n\log(n))$ time, and hence, *we can declare that we have lost quantum advantage*.

The authors of [32] claim that for planar graph problems, it generally holds that

$$\|Q\|\|H_C\|^{-1}n \approx 1, \tag{3.37}$$

where n is the number of qubits of the system. By dividing both sides of Eq. (3.36) with n and making use of Eq. (3.37), we obtain

$$\frac{D(\rho\|\sigma)}{n} \leq \frac{\epsilon}{8}, \tag{3.38}$$

where ρ is the output state of the quantum circuit. By numerically simulating the upper bounds of the relative entropy $D(\rho\|\sigma)$ given by Eqs. (3.22) and (3.34), we can find the repetition P of the QAOA for which Eq. (3.38) is satisfied and therefore declare a loss of quantum advantage.

It is apparent that the value of ϵ directly influences our results. The authors of [32] claim that the range $\epsilon = 10^{-2} - 10^{-1}$ "corresponds to a conservative estimate as to when advantage is lost", with advantage already being lost reportedly for the SK model and random 3-regular graphs at the value $\epsilon = 0.7$ for a problem size of 1000 spins and 10 repetitions of the QAOA (see Fig. 3 of [32]). Here, we will use three values for ϵ, more specifically $\epsilon = 1$, $\epsilon = 0.1$ and $\epsilon = 0.01$ in order to make a more general assessment of our methods.

The runtime Δt of a single repetition of the algorithm depends on the decomposition of the cost layer $U_C(\gamma)$, and so, Δt depends on the complexity and size of the given problem. Here, we will study how the upper bounds of the relative entropy behave when we run the QAOA to solve the SK model. For n number of qubits, a scaling of $3n$ two-qubit gates per QAOA repetition is reported in [32]. Here, we disregard the parallel application of gates in a single unitary layer $\mathcal{U}_{C_k}(\gamma_j)$ for simplicity, and assume that a single cost layer $\mathcal{U}_C$ decomposes into $m = n$ number of single unitary layers $\mathcal{U}_{C_k}$, and so $m = n$. Therefore, we can approximate the runtime of a single repetition as $\Delta t = n\tau_2$, where τ_2 is the two-qubit gate duration. Let us assume $n = 1000$ qubits, then for a two-qubit gate duration of $\tau_2 = 50ns$ we get $\Delta t = 50\mu s$ as the time duration of a single repetition of the QAOA.

Planar Superconducting QPU of tens of qubits		
Analysis	Discrete evolution	Continuous evolution
Error layer $\mathcal{E}$ probability	$\alpha = 0.05$	
Damping probability	$p = 0.9985$	$p = 0.9985$
Single-qubit gate duration		$\tau_1 = 20ns$
Two-qubit gate duration		$\tau_2 = 50ns$
Single repetition duration		$\Delta t = 50\mu s$
Relaxation time		$T_1 = 30\mu s$

Table 3.1: Specifications of a state of the art superconducting processor that we will use for our simulations [51]. We make the distinction between the values that are necessary for the discrete and continuous time evolution of an input state ρ_0, corresponding to the two upper bounds given by equations (3.22) and (3.34) respectively. We assume that our device has $n = 1000$ qubits, and that the cost layer $\mathcal{U}_C$ decomposes into $m = 1000$ single unitary layers $\mathcal{U}_{C_k}$.

The table above sums up the device specifications that we will use for our simulations:

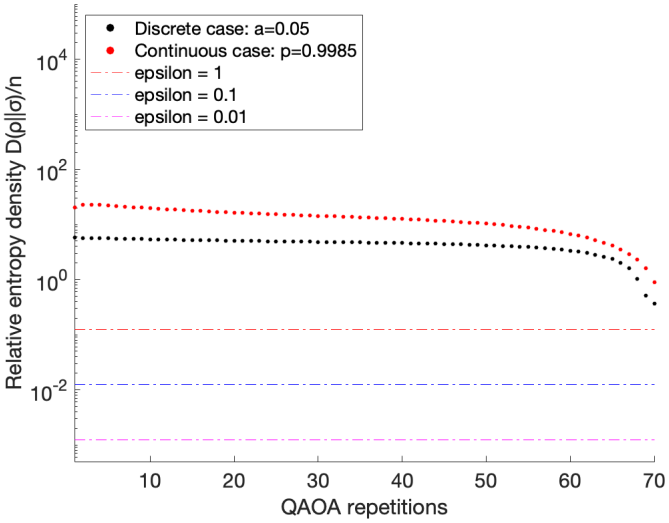

Figure 3.8: Simulation of the relative entropy upper bound density given by Eqs. (3.22) and (3.34), as a function of the QAOA repetitions P, for the device specification values that are listed on Table 3.1. The plot points indicated by black are those of Eq. (3.22) for the discrete evolution while the plot points indicated by red are those of Eq. (3.34) for the continuous evolution of an input state. The colored horizontal lines indicate the different values of ϵ for which if the value of the relative entropy density reaches one can claim loss of quantum advantage, according to the bound of Eq. (3.38). We see here that none of the plots reach any of those ϵ values for a large number of repetitions P, indicating a poor convergence rate of the bounds. Even at 70 repetitions of the QAOA, none of the upper bounds reaches the value $\epsilon = 0.7$ which was reported in [32] for just 10 repetitions of the QAOA for a device of 1000 qubits.

We present the simulation results in Fig. 3.8. Both of the upper bounds that we have

derived display a very low convergence rate, even at a very large number of repetitions P of the QAOA. Naturally, we would expect otherwise for the current noise rates of the state of the art superconducting processors, at a large number of repetitions such as $P = 70$, when the quality of the state would have significantly dropped. Our results seem to indicate that, (1) the QAOA is quite resilient to relaxation noise, (2) the methods of [32] are not adequate to declare the loss of quantum advantage for planar graph problems.

This is largely a consequence of the max-relative term that appears on Eq. (2.8) of Lemma 2.3.1. In order to gain a tight bound from Lemma 2.3.1, the max-relative terms should in general be very small, with a near negligible effect on the upper bound value, and rapidly decay to zero as a function of the circuit depth t. In our case, as we can see from Eq. (3.21), the max-relative term has a dependency on the values of the variational parameters β_j. As we have shown in Section 3.3, when the performance of QAOA is optimized, the variational parameters β_j decay polynomially with respect to the circuit depth (see Eq. (3.14)), which is not enough to make the upper bound given by Eq. (3.22) tight. The issue becomes more clear if we look at the upper bound of Eq. (3.34), where there is a linear dependence on the variational parameters β_j which, due to their nature and importance in the algorithm, take non-negligible values, and as a result, slow down decisively the convergence rate of the upper bound.

Lastly, it needs to be stressed that even though we included pure dephasing in our noise model, the pure dephasing rate does not influence the convergence rates of both upper bounds. This could be problematic, since after the application of each unitary layer, we could be artificially amping up the effects of pure dephasing, messing up considerably the coherence of our input state from the early evolution, and that would still not affect the convergence rates of our bounds. This puts into question the universality of the methods that are being used in [32]. In conclusion, we have proven that the question of whether the QAOA can achieve a quantum advantage on a NISQ device remains open.

4

Exact Solution of the Master Equation

4.1. Introduction

Due to the multiple advancements on quantum technologies over the past decade, there is a renewed interest in the systematic study of dissipative quantum systems. The main equation to study such systems is the Lindblad Master equation, which expands traditional quantum mechanics so that it also includes open system dynamics.

A dissipative system evolving under the influence of a Hamiltonian might reach a steady state, depending on how the strength of the Hamiltonian compares to that of the dissipation. In the previous chapters, we saw that the choice of the fixed point σ for a continuous time evolution of a state $\rho(t)$ directly influenced the upper bounds of the relative entropy $D(\rho(t)\|\sigma)$. More specifically, in Chapter 3 we studied the convergence rate of such bounds for long-time dynamics, where we found that the choice of the noise model for some dynamics can change significantly our results. It is reasonable to ask, how would the fixed point of the dissipator of some dynamics change if we would include a steady Hamiltonian drive, i.e. $H(t) = H$. Our main objective in this chapter is to study the steady state of the Lindblad Master equation for such nontrivial long-time dynamics, and explore its' properties. Is there perhaps a specific Hamiltonian for which the steady state is entangled? If yes, under which conditions could this happen?

There have been a number of recent studies on the phase transitions of many-body driven-dissipative systems [52–56], where most of them focus on the Ising model. In the next two chapters, we will study the steady state of a driven-dissipative system for a one-dimensional chain of transmon qubits which is coupled by a chain of cross-resonance ZX drives. This specific drive is native to superconducting qubits and can be easily implemented in an experimental setup [57]. In this chapter, we will solve this system exactly for the steady state, for the cases of two and three qubits.

4.2. Fixed point of the Lindblad Master equation

Let us re-introduce the Lindblad Master Equation in the following form,

$$\frac{\partial \rho}{\partial t} = -i[\mathcal{H}, \rho] + \sum_k \mathcal{D}[L_k](\rho) \equiv \mathcal{L}(\rho), \tag{4.1}$$

with ρ being a quantum state of n qubits, $\mathcal{H}$ being the Hamiltonian of the system, and

$$\mathcal{D}[L_k](\rho) = L_k \rho L_k^\dagger - \frac{1}{2}\{L_k^\dagger L_k, \rho\}, \tag{4.2}$$

with L_k being the quantum jump operators describing the noise processes of the system, and

$$\mathcal{L}_{\text{dissip}}(\rho) \equiv \sum_k \mathcal{D}[L_k](\rho), \tag{4.3}$$

is the Lindbladian operator describing the overall dissipation of the system (also called the *dissipator* of the system). The fixed point of the Lindblad Master equation is the quantum state ρ_{fixed} for which $\mathcal{L}(\rho_{\text{fixed}}) = 0$. At this point we will introduce some notation that will make our analysis more convenient. Let us express the state ρ in the n-qubit Pauli basis as

$$\rho = \sum_{j=0}^{2^{2n}-1} a_j P_j, \tag{4.4}$$

where $\text{Tr}(P_i P_j) = 2^n \delta_{i,j}$. For each j we have a Pauli string $P_j = P_{j_1} \otimes P_{j_2} \otimes \cdots \otimes P_{j_n}$, with $P_{j_i} \in \{\mathbb{I}_i, X_i, Y_i, Z_i\}$ for every qubit $i \in \{1, 2, ..., n\}$, where $\mathbb{I}$ is the identity matrix and X, Y, Z are the Pauli matrices. The two different signs $+1$, and -1 that appear in front of every Pauli string P_j have been absorbed by the coefficients a_j. The numbering j of the Pauli strings in Eq. (4.4) mimics the standard binary numbering system, with $P_0 = \mathbb{I}_1 \otimes \mathbb{I}_2 \otimes \cdots \otimes \mathbb{I}_n$ being the identity Pauli string, $P_1 = \mathbb{I}_1 \otimes \mathbb{I}_2 \otimes \cdots \otimes X_n$, $P_4 = \mathbb{I}_1 \otimes \mathbb{I}_2 \otimes \cdots \otimes X_{n-1} \otimes \mathbb{I}_n$, $P_5 = \mathbb{I}_1 \otimes \mathbb{I}_2 \otimes \cdots \otimes X_{n-1} \otimes X_n$, etc. For a normalized quantum state ρ, $\text{Tr}(\rho) = 1$ and so $a_0 = 1/2^n$. By plugging Eq. (4.4) into Eq. (4.1), we get

$$\sum_{j=0}^{2^{2n}-1} P_j \frac{\partial a_j}{\partial t} = -i \sum_{j=0}^{2^{2n}-1} [\mathcal{H}, P_j] a_j + \sum_{j=0}^{2^{2n}-1} \sum_k \mathcal{D}[L_k](P_j) a_j \Rightarrow \tag{4.5}$$

$$\sum_{j=0}^{2^{2n}-1} P_i P_j \frac{\partial a_j}{\partial t} = -i \sum_{j=0}^{2^{2n}-1} P_i [\mathcal{H}, P_j] a_j + \sum_{j=0}^{2^{2n}-1} \sum_k P_i \mathcal{D}[L_k](P_j) a_j \Rightarrow \tag{4.6}$$

$$\frac{\partial a_i}{\partial t} = \sum_{j=0}^{2^{2n}-1} \left(-\frac{i}{2^n} \text{Tr}(P_i [\mathcal{H}, P_j]) \right) a_j + \sum_{j=0}^{2^{2n}-1} \sum_k \frac{1}{2^n} \text{Tr}(P_i \mathcal{D}[L_k](P_j)) a_j, \tag{4.7}$$

where in step (4.6) we multiplied both sides with a Pauli string P_i and in step (4.7) we took the trace of both sides and used $\text{Tr}(P_i P_j) = 2^n \delta_{i,j}$.

Let $|P_i\rangle \equiv |P_{i_1} \otimes P_{i_2} \otimes \cdots \otimes P_{i_n}\rangle$ be a complete and orthonormal basis of 2^{2n} dimensions for a Pauli string P_i of n qubits, with $P_{i_j} \in \{\mathbb{I}_j, X_j, Y_j, Z_j\}$ for every qubit $j \in \{1, 2, ..., n\}$.

Let us now define the following real matrices,

$$H_{i,j} \equiv -\frac{i}{2^n}\mathrm{Tr}(P_i[\mathcal{H}, P_j]), \tag{4.8}$$

and

$$D^k_{i,j} \equiv \frac{1}{2^n}\mathrm{Tr}(P_i\mathcal{D}[L_k](P_j)), \tag{4.9}$$

where $H_{i,j} = -H_{j,i}$ is an antisymmetric matrix, and $H_{0,j} = 0$ as well as $D^k_{0,j} = 0$ for all j. We will now express the above matrices in the $|P_i\rangle$ basis,

$$H = \sum_{i=0}^{2^{2n}-1}\sum_{j=0}^{2^{2n}-1} H_{i,j}|P_i\rangle\langle P_j|, \tag{4.10}$$

and

$$D^k = \sum_{i=0}^{2^{2n}-1}\sum_{j=0}^{2^{2n}-1} D^k_{i,j}|P_i\rangle\langle P_j|. \tag{4.11}$$

For a general state ρ given by Eq. (4.4), if we define the vector $|a\rangle$ as

$$|a\rangle = \sum_{i=0}^{2^{2n}-1} a_i|P_i\rangle, \tag{4.12}$$

then by using all of the above definitions, Eq. (4.5) becomes

$$\frac{\partial|a\rangle}{\partial t} = M|a\rangle, \tag{4.13}$$

where M is the *Pauli transfer matrix* [58] given by

$$M \equiv H + \sum_k D^k. \tag{4.14}$$

Because of the above definitions, matrix M is going to have the following entries,

$$M = \begin{pmatrix} 0 & 0 & 0 & \cdots & 0 \\ \sum_k D^k_{1,0} & M_{1,1} & M_{1,2} & \cdots & M_{1,2^{2n}-1} \\ \sum_k D^k_{2,0} & M_{2,1} & M_{2,2} & \cdots & M_{2,2^{2n}-1} \\ \vdots & \vdots & \vdots & \ddots & \vdots \\ \sum_k D^k_{2^{2n}-1,0} & M_{2^{2n}-1,1} & M_{2^{2n}-1,2} & \cdots & M_{2^{2n}-1,2^{2n}-1} \end{pmatrix}. \tag{4.15}$$

Through definition (4.12), we now express a general quantum state ρ as a 2^{2n} dimensional vector $|a\rangle$, where $|a\rangle$ is also often written as $|\rho\rangle\rangle$, and is a vector that lives in the Fock-Liouville space [59]. Also, through Eq. (4.10) we express the Hamiltonian $\mathcal{H}$ of the system as the Liouvillian superoperator H of 2^{2n} dimensions [59], with entries given by Eq. (4.8). Moreover, through Eq. (4.11) we express the operator $D[L_k]$ which acts on a quantum state

ρ as the Liouvillian superoperator D^k of 2^{2n} dimensions, with entries given by Eq. (4.9) for all k.

By defining the *dissipation vector* $|\upsilon\rangle$ of $2^{2n}-1$ dimensions as the first column of M by excluding the first row entry, i.e.

$$|\upsilon\rangle \equiv \sum_{i=1}^{2^{2n}-1}\left(\sum_k D^k_{i,0}\right)|P_i\rangle = \sum_{i=1}^{2^{2n}-1}\langle P_i|M|P_0\rangle|P_i\rangle, \tag{4.16}$$

and we define the *reduced Pauli transfer matrix* $\tilde{M}$ of dimensions $2^{2n}-1$ as matrix M when we remove its first row and first column, i.e.

$$\tilde{M} \equiv \sum_{i=1}^{2^{2n}-1}\sum_{j=1}^{2^{2n}-1}\left(H_{i,j}+\sum_k D^k_{i,j}\right)|P_i\rangle\langle P_j|, \tag{4.17}$$

then for the reduced vector $|\tilde{a}\rangle \equiv \sum_{i=1}^{2^{2n}-1} a_i|P_i\rangle$, Eq. (4.13) becomes

$$\frac{\partial|\tilde{a}\rangle}{\partial t} = \tilde{M}|\tilde{a}\rangle + a_0|\upsilon\rangle, \tag{4.18}$$

with $a_0 = 1/2^n$.

By setting Eq. (4.18) equal to zero, we obtain the fixed point of the Lindblad Master Equation, where the *fixed vector* $|\tilde{a}_{\text{fixed}}\rangle$ satisfies,

$$\tilde{M}|\tilde{a}_{\text{fixed}}\rangle = -a_0|\upsilon\rangle. \tag{4.19}$$

When $\tilde{M}$ is full-rank, and thus *invertible*, the fixed vector $|\tilde{a}_{\text{fixed}}\rangle$ is unique and is given by

$$|\tilde{a}_{\text{fixed}}\rangle = -a_0\tilde{M}^{-1}|\upsilon\rangle. \tag{4.20}$$

The invertability of matrix $\tilde{M}$ depends on the set of quantum jump operators L_k of the dissipator $\mathcal{L}_{\text{dissip}}$. In general, for any finite system Evans' theorem [60] guarantees the existence of at least one fixed point of the Lindblad Master Equation [59]. One can use Evans' theorem to prove the uniqueness of $|\tilde{a}_{\text{fixed}}\rangle$, and thus, the invertability of $\tilde{M}$. The uniqueness of the fixed point as well as the invertability of $\tilde{M}$ will be further discussed in a later section.

For the fixed point ρ_{fixed} of the Lindblad Master Equation (4.1) and a state $|P_i\rangle$, by Eq. (4.4) we have that

$$a_{\text{fixed},i} = \langle P_i|a_{\text{fixed}}\rangle = \frac{1}{2^n}\text{Tr}(P_i\rho_{\text{fixed}}), \tag{4.21}$$

and so, upon solving Eq. (4.20) we will be able to obtain the fixed point ρ_{fixed} of the evolution.

Finally, by Eq. (4.21), for a Pauli string $P_i = P_{i_1}\otimes P_{i_2}\otimes\cdots\otimes P_{i_n}$ represented by the state $|P_i\rangle$, the expectation value $\langle P_i\rangle$ is defined as

$$\langle P_{i_1}\otimes P_{i_2}\otimes\cdots\otimes P_{i_n}\rangle_{|a_{\text{fixed}}\rangle} = 2^n\langle P_i|a_{\text{fixed}}\rangle. \tag{4.22}$$

4.3. PROPERTIES OF THE STEADY STATE FOR A NATIVE SUPERCONDUCTING INTERACTION

For the rest of this thesis, it will be in our interest to study the long-time dynamics of a one-dimensional dissipative system of n qubits coupled via a chain of two-body drives with the addition of a local transverse field, described by the following Hamiltonian

$$\mathcal{H} = \gamma \sum_{i=1}^{n} Z_i X_{i+1} + c \sum_{i=1}^{n} X_i, \tag{4.23}$$

where the periodic boundary condition $X_{n+1} = X_1$ applies, for γ and c being the interaction strengths. One can also have an additional term $a \sum_{i=1}^{n} Z_i Z_{i+1}$ in practice [57], which we ignore in our analysis. Such a drive, as it will be proven for small systems, is able to create correlations between all qubits, and is of great interest since it also serves as our experimental proposal for studying steady-state correlations on an actual superconducting device. In our proposal, one would want to use an array of transmon qubits (see Section 1.6.1) where the Hamiltonian drive given by Eq. (4.23) describes a chain of cross-resonance interactions, where qubit i and $i+1$ are the control and target qubits respectively. The above setup is illustrated below in a simple fashion:

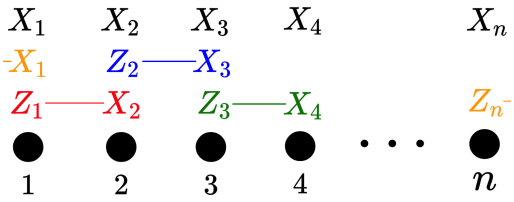

Figure 4.1: A one dimensional array of n qubits, coupled together by cross-resonance drives $Z_i X_{i+1}$ with a periodic boundary condition $X_{n+1} = X_1$. Every drive $Z_i X_{i+1}$ is indicated by a different color and a line in between so as to distinguish them on the figure. On every qubit a transverse field X is being applied (in black).

Obtaining an exact solution for the steady state of the above driven-dissipative n-qubit system comes with a great number of difficulties which will be addressed later in Chapter 5. For now, we will study some of the properties of this system by solving it exactly for two and three qubits.

4.3.1. EXACT-SOLUTION FOR TWO QUBITS

For a system of two transmon qubits, we wish to solve Eq. (4.20) and obtain the steady state for the following Hamiltonian

$$\mathcal{H} = \gamma(Z_1 X_2 + X_1 Z_2) + c(X_1 + X_2). \tag{4.24}$$

The dissipator of the system $\mathcal{L}_{\text{dissip}}$ is chosen in such a way that it describes the main dissipative processes that superconducting transmon qubits undergo during an evolution: relaxation and pure dephasing (see Section 1.6.2).

We solve this system for the steady state by using *Wolfram Mathematica* (see Appendix B.1). Below we present the color plots of the purity $\text{Tr}(\rho^2_{\text{fixed}})$ of the steady state as well

as the quantity $\langle Z_1 Z_2 \rangle - \langle Z_1 \rangle \langle Z_2 \rangle$ for two cases: when we disregard pure dephasing, i.e. $\chi = 0$, and when the pure dephasing rate is set to $\chi = 0.5$.

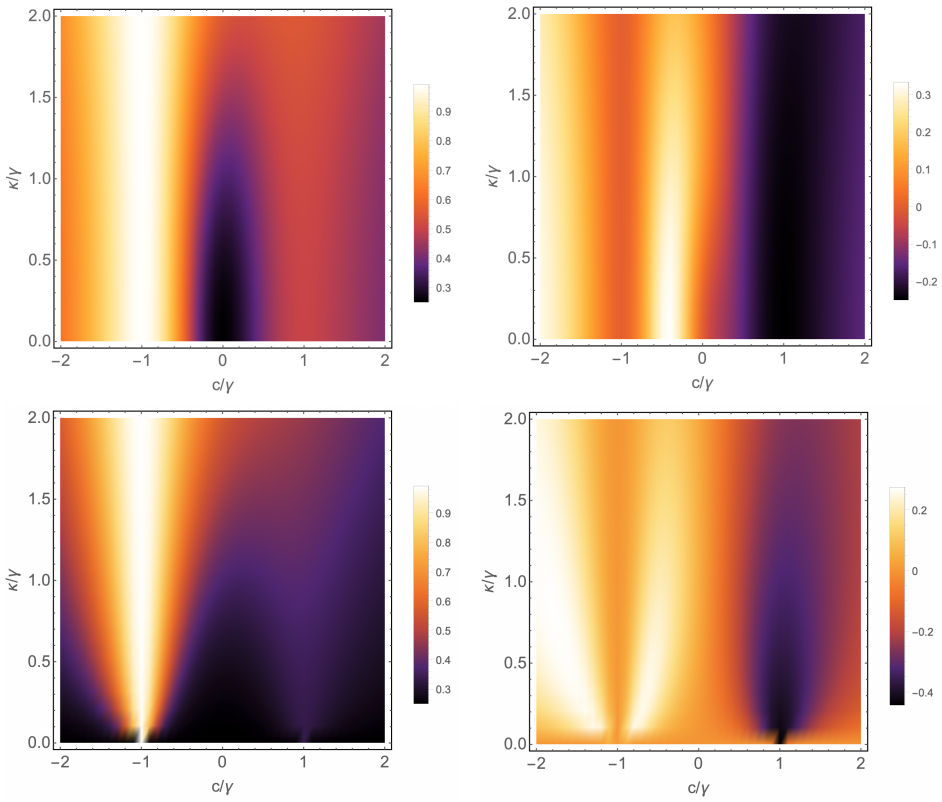

Figure 4.2: Left column: Color plots of the purity $\mathrm{Tr}(\rho^2_{\mathrm{fixed}})$ of the steady state of two qubits as a function of κ/γ and c/γ. On the top plot we set $\gamma = 1$, $\chi = 0$, while on the bottom plot we set $\gamma = 1$ and $\chi = 0.5$. For both plots we set $p = 0.9985$ which is the relaxation probability.
Right column: Color plot of the quantity $\langle Z_1 Z_2 \rangle - \langle Z_1 \rangle \langle Z_2 \rangle$ for the steady state ρ_{fixed} of two qubits as function of κ/γ and c/γ. On the top plot we set $\gamma = 1$, $\chi = 0$, while on the bottom plot we set $\gamma = 1$ and $\chi = 0.5$. For both plots we set $p = 0.9985$ which is the relaxation probability.

We are also interested in calculating the concurrence [61] of ρ_{fixed}, which is a measure of two-qubit entanglement. We present below in a color plot the numerical solution for the concurrence of ρ_{fixed} (see Appendix B.2):

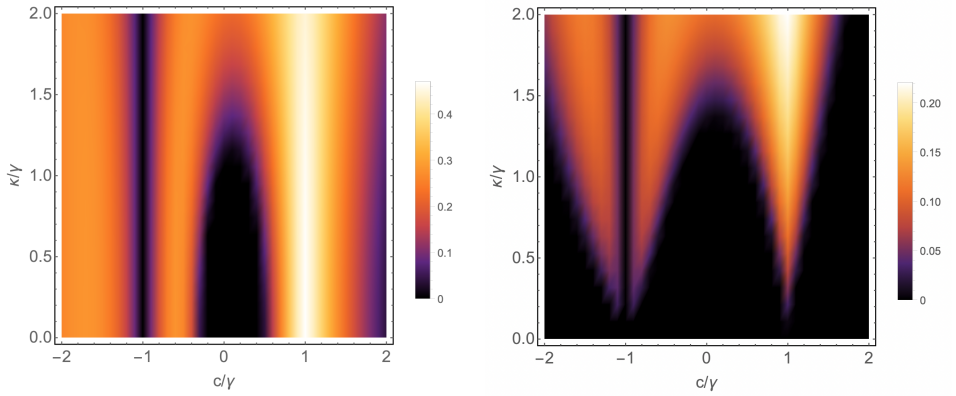

Figure 4.3: Left: Color plot of the concurrence of the steady state ρ_{fixed} as a function of κ/γ and c/γ. For this plot we set $\gamma = 1$, $\chi = 0$ and $p = 0.9985$ which is the relaxation probability.
Right: Color plot of the concurrence of the steady state ρ_{fixed} as a function of κ/γ and c/γ. For this plot we set $\gamma = 1$, $\chi = 0.5$ and $p = 0.9985$ which is the relaxation probability.

From the above figures, we can see that the steady state is a product state for the values $c/\gamma = -1$, and $c/\gamma = 0$ for small values of κ. It seems that an increasing dissipator strength κ promotes the formation of correlations between the two qubits. Also, the addition of pure dephasing did not change the quality of our results, but it reduced significantly the correlations between the two qubits, as we would expect. Furthermore, for the value $c/\gamma = 1$ the two qubits are the most correlated.

For the values $\kappa = c = \gamma = 1$ and $\chi = 0$, by solving Eq. (4.20) we obtain the fixed point

$$\rho_{\text{fixed}} = \begin{pmatrix} 0.506934 & 0.0613046i & 0.0613046i & 0.0000387248 \\ -0.0613046i & 0.246348 & 0.245218 & 9.6812 \cdot 10^{-6}i \\ -0.0613046i & 0.245218 & 0.246348 & 9.6812 \cdot 10^{-6}i \\ 0.0000387248 & -9.6812 \cdot 10^{-6}i & -9.6812 \cdot 10^{-6}i & 0.000370077 \end{pmatrix}. \quad (4.25)$$

We can identify that we approximately have a mixture $\rho_{\text{fixed}} = p|00\rangle\langle 00| + (1-p)\frac{1}{2}(|01\rangle + |10\rangle)(\langle 01| + \langle 10|)$ with $p \approx 0.5$.

Finally, we would like to examine if the entanglement between the two qubits is robust upon changing the parameter value $\gamma = 1$. Below, for the values $\kappa = c = 1$ and $\chi = 0$, we compute the fixed state ρ_{fixed} for the values $\gamma = 0.7$ and $\gamma = 1.3$:

$$\rho_{\text{fixed}}(\gamma = 0.7) = \begin{pmatrix} 0.47874 & 0.0736667i & 0.0736667i & 0.056279 \\ -0.0736667i & 0.251562 & 0.232735 & 0.0295526i \\ -0.0736667i & 0.232735 & 0.251562 & 0.0295526i \\ 0.056279 & -0.0295526i & -0.0295526i & 0.0181361 \end{pmatrix}, \quad (4.26)$$

and

$$\rho_{\text{fixed}}(\gamma = 1.3) = \begin{pmatrix} 0.495012 & 0.0534451i & 0.0534451i & -0.0498111 \\ -0.0534451i & 0.246961 & 0.235168 & -0.0177996i \\ -0.0534451i & 0.235168 & 0.246961 & -0.0177996i \\ -0.0498111 & 0.0177996i & 0.0177996i & 0.0110668 \end{pmatrix}. \quad (4.27)$$

From the above equations, we can see that even for a 30% change of the value of γ, the entanglement between the two qubits is still being preserved, with the state $\frac{1}{\sqrt{2}}(|01\rangle + |10\rangle)$ having a nearly $p = 0.46$ probability into both mixtures $\rho_{\text{fixed}}(\gamma = 0.7)$ and $\rho_{\text{fixed}}(\gamma = 1.3)$. Therefore, the entanglement that arises for $c/\gamma = 1$ in the system is robust against slight deviations from the ratio $c/\gamma = 1$.

4.3.2. Exact-solution for three qubits

For a system of three transmon qubits, we wish to solve Eq. (4.20) and obtain the steady state for the following Hamiltonian

$$\mathcal{H} = \gamma(Z_1X_2 + Z_2X_3 + X_1Z_3) + c(X_1 + X_2 + X_3). \tag{4.28}$$

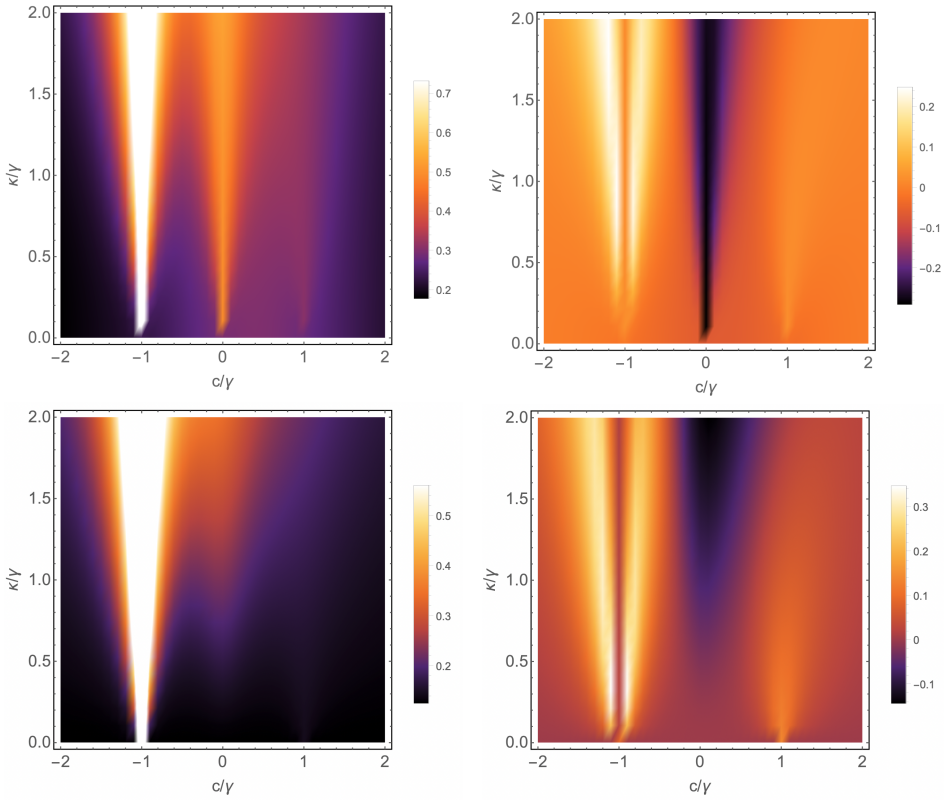

Figure 4.4: Left column: Color plots of the purity $\text{Tr}(\rho^2_{\text{fixed}})$ of the steady state of three qubits as a function of κ/γ and c/γ. On the top plot we set $\gamma = 1$, $\chi = 0$, while on the bottom plot we set $\gamma = 1$ and $\chi = 0.5$. For both plots we set $p = 0.9985$ which is the relaxation probability.
Right column: Color plot of the quantity $\langle Z_1Z_2Z_3\rangle - \langle Z_1\rangle\langle Z_2\rangle\langle Z_3\rangle$ for the steady state ρ_{fixed} of three qubits as function of κ/γ and c/γ. On the top plot we set $\gamma = 1$, $\chi = 0$, while on the bottom plot we set $\gamma = 1$ and $\chi = 0.5$. For both plots we set $p = 0.9985$ which is the relaxation probability.

Here we use the same dissipator $\mathcal{L}_{\text{dissip}}$ as the one that we used for the solution of the

two transmon qubit system. We solve the above system for the steady state by using *Wolfram Mathematica* (see Appendix B.3). Same as before, we present above the color plots of the purity $\mathrm{Tr}(\rho^2_{\mathrm{fixed}})$ of the steady state as well as the quantity $\langle Z_1 Z_2 Z_3\rangle - \langle Z_1\rangle\langle Z_2\rangle\langle Z_3\rangle$ for two cases: when we disregard pure dephasing, i.e. $\chi = 0$, and when the pure dephasing rate is set to $\chi = 0.5$.

Since the concurrence measures the entanglement between two qubits, what we can do to get an estimate of the steady state's entanglement is to take the partial trace with respect to one qubit and compute the concurrence of the other two. This of course is an approximation because we are cutting out one of the three qubits, to which the other two might already be correlated. Nevertheless, it is a necessity that still is able to give some valuable information about the system.

Below we present the color plot of the numerical solution for the concurrence of the state $\mathrm{Tr}_3(\rho_{\mathrm{fixed}})$, that is, the concurrence of qubits 1 and 2 when we trace out qubit 3. Due to symmetry, the concurrences of the states $\mathrm{Tr}_1(\rho_{\mathrm{fixed}})$ and $\mathrm{Tr}_2(\rho_{\mathrm{fixed}})$ are identical:

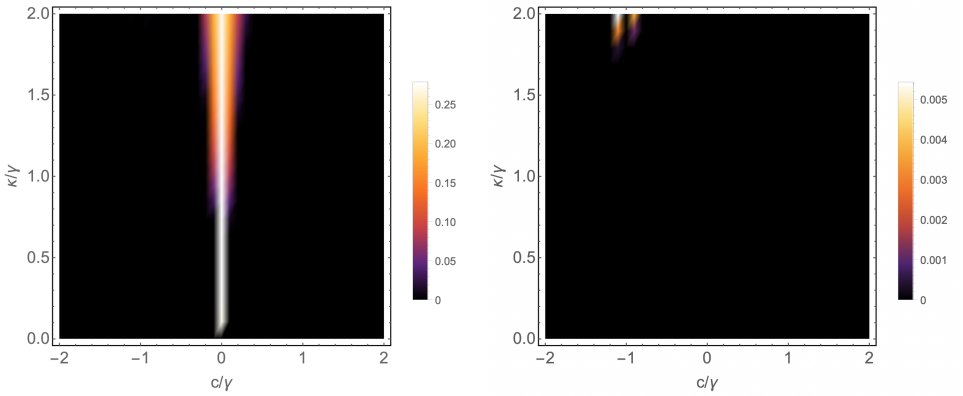

Figure 4.5: Left: Color plot of the concurrence of the state $\mathrm{Tr}_3(\rho_{\mathrm{fixed}})$ as a function of κ/γ and c/γ. For this plot we set $\gamma = 1$, $\chi = 0$ and $p = 0.9985$ which is the relaxation probability.
Right: Color plot of the concurrence of the state $\mathrm{Tr}_3(\rho_{\mathrm{fixed}})$ as a function of κ/γ and c/γ. For this plot we set $\gamma = 1$, $\chi = 0.5$ and $p = 0.9985$ which is the relaxation probability. We can see that the addition of pure dephasing erases the entanglement between qubits 1 and 2 at $c/\gamma = 0$.
General comment: The color plots of the concurrences of the states $\mathrm{Tr}_1(\rho_{\mathrm{fixed}})$ and $\mathrm{Tr}_2(\rho_{\mathrm{fixed}})$ are identical.

From the above plots we can see that for the value $c/\gamma = -1$ the system has no correlations, while for the value of $c = 0$ the system is the most correlated when $\chi = 0$. When we set dephasing to $\chi = 0.5$, it erases all correlations in the system at $c/\gamma = 0$. Therefore, the entanglement at $c = 0$ is not robust against pure dephasing, and *in practice it would always get erased*.

5

Approximate Methods for Estimating the Fixed Point

5.1. Introduction

As has already been said in the previous chapter, if we are able to solve Eq. (4.20) then we will be able to obtain the fixed point ρ_{fixed} of the evolution of the system, as described by the Lindblad Master Equation (4.1). In order to solve Eq. (4.20), one needs to compute the inverse matrix $\tilde{M}^{-1}$ of a full-rank matrix $\tilde{M}$, which in general is impossible: even though the reduced Pauli transfer matrix $\tilde{M}$ is sparse, it still grows exponentially with the system size n and there exist no classical algorithm that can *efficiently* invert it for a general system.

That being said, there exists a quantum algorithm, namely the HHL [62], which can in principle efficiently invert the reduced Pauli transfer matrix $\tilde{M}$ only if its' condition number is sufficiently small. This does not help much though, since estimating the condition number of $\tilde{M}$ is an open problem and even bounding it seems to be a formidable task.

Our only hope for now is to make approximations if we want to solve Eq. (4.20) for the steady state for a system of n qubits. What we are interested in is studying correlations between a small number of qubits in a larger system when all qubits are coupled via an interaction of the form of Eq. (4.23). Under these considerations, we want to know: can we estimate efficiently the expectation values of Pauli operators which act on $O(1)$ qubits for a system of n coupled qubits?

We will follow two approaches here; first, we will treat the driving Hamiltonian $\mathcal{H}$ as a small perturbation in the system and expand the reduced Pauli transfer matrix $\tilde{M}$ accordingly. As we will see, this makes it possible to estimate the expectation values of small Pauli strings efficiently. The second approach is to use the mean-field method, where one treats the density matrix ρ as a product state. This method has already been used for driven-dissipative systems [53–56, 63] for Ising-type Hamiltonians. Here, we will derive the mean-field equations for n qubits and solve them for a Hamiltonian given by Eq. (4.23). At the end, we will compare the results of the approximation methods with those of the exact solution for two qubits.

5.2. Perturbative method

5.2.1. Perturbative expansion of the matrix $\tilde{M}$

We begin by splitting Eq. (4.17) into two parts,

$$\tilde{M} = \underbrace{\sum_{i=1}^{2^{2n}-1}\sum_{j=1}^{2^{2n}-1} H_{i,j}|P_i\rangle\langle P_j|}_{\tilde{M}_{\mathcal{H}}} + \underbrace{\sum_{i=1}^{2^{2n}-1}\sum_{j=1}^{2^{2n}-1}\sum_{k} D_{i,j}^{k}|P_i\rangle\langle P_j|}_{\tilde{M}_{\text{dissip}}} = \tilde{M}_{\mathcal{H}} + \tilde{M}_{\text{dissip}}, \tag{5.1}$$

where $\tilde{M}_{\mathcal{H}}$ includes only contributions from the Hamiltonian $\mathcal{H}$ of the system and $\tilde{M}_{\text{dissip}}$ is the *dissipator matrix* which includes only contributions from the dissipation of the system. We will now expand $\tilde{M}$ by considering matrix $\tilde{M}_{\mathcal{H}}$ as a small perturbation of the system. Assuming that $\tilde{M}_{\text{dissip}}$ is invertible (to be proven in Section 5.2.2), by Eq. (4.20), the fixed vector $|\tilde{a}_{\text{dissip}}\rangle$ of the dissipator matrix $\tilde{M}_{\text{dissip}}$ is

$$|\tilde{a}_{\text{dissip}}\rangle = -a_0\tilde{M}_{\text{dissip}}^{-1}|\upsilon\rangle. \tag{5.2}$$

In general,

$$\tilde{M} = \tilde{M}_{\mathcal{H}} + \tilde{M}_{\text{dissip}} = (\mathbb{I} + \tilde{M}_{\mathcal{H}}\tilde{M}_{\text{dissip}}^{-1})\tilde{M}_{\text{dissip}}, \tag{5.3}$$

and since

$$(\mathbb{I} + \tilde{M}_{\mathcal{H}}\tilde{M}_{\text{dissip}}^{-1})^{-1} = \sum_{k=0}^{\infty}(-1)^k(\tilde{M}_{\mathcal{H}}\tilde{M}_{\text{dissip}}^{-1})^k, \tag{5.4}$$

we can write

$$\tilde{M}^{-1} = \tilde{M}_{\text{dissip}}^{-1} - \tilde{M}_{\text{dissip}}^{-1}\tilde{M}_{\mathcal{H}}\tilde{M}_{\text{dissip}}^{-1} + (\tilde{M}_{\text{dissip}}^{-1}\tilde{M}_{\mathcal{H}})^2\tilde{M}_{\text{dissip}}^{-1} + O(\tilde{M}_{\mathcal{H}}^3). \tag{5.5}$$

We can insert the above expansion of the inverse matrix $\tilde{M}^{-1}$ in Eq. (4.20) to get

$$|\tilde{a}_{\text{fixed}}\rangle = \sum_{k=0}^{\infty}(-1)^k\left(\tilde{M}_{\text{dissip}}^{-1}\tilde{M}_{\mathcal{H}}\right)^k|\tilde{a}_{\text{dissip}}\rangle. \tag{5.6}$$

Through the perturbative expansion of the inverse of the reduced Pauli transfer matrix $\tilde{M}^{-1}$ (Eq. (5.5)), we can see that the uniqueness of the fixed vector $|\tilde{a}_{\text{fixed}}\rangle$ depends now on the invertability of matrix $\tilde{M}_{\text{dissip}}$.

5.2.2. The inverse of the dissipator matrix $\tilde{M}_{\text{DISSIP}}^{-1}$

In order to use the expansion of $|\tilde{a}\rangle$ given by Eq. (5.6), one first needs to prove the invertability of $\tilde{M}_{\text{dissip}}$ and define the inverse of the dissipator matrix $\tilde{M}_{\text{dissip}}^{-1}$.

It is instructive to consider a one-qubit quantum state ρ whose time evolution is governed by the Lindblad Master Equation (4.1) and is undergoing depolarizing noise which can be described by the quantum jump operators given by $L_x = \sqrt{r_x}X$, $L_y = \sqrt{r_y}Y$ and $L_z = \sqrt{r_z}Z$, with r_x, r_y and r_z being the corresponding depolarizing rates [64].

For the above quantum jump operators, by using Eqs. (4.2) and (4.9), one can easily find that the first column of the Pauli transfer matrix M given by Eq. (4.15) will only have

zero entries. Therefore, matrix M will have a zero eigenvalue $\lambda_0 = 0$ with corresponding eigenstate $\rho_0 = \mathbb{I}/2$, which is the maximally mixed state. Note that because of the structure of the Pauli transfer matrix M (see Eq. (4.14)), depolarizing noise always drives any one-qubit (or multi-qubit) quantum state ρ to the maximally mixed state independently of what the Hamiltonian $\mathcal{H}$ of the system is, therefore the fixed point is trivial. *This is the main reason why the analysis done in* [32] *worked well for depolarizing noise*.

Now, for a one-qubit state ρ let $\mathcal{H} = 0$ in the rotating frame, and let $\mathcal{L}_{\text{dissip}}$ be the dissipator of the system with quantum jump operators $L_1 = \sqrt{\kappa p}\sigma_-$, $L_2 = \sqrt{\kappa(1-p)}\sigma_+$ and $L_3 = \sqrt{\chi}Z$ (see Section 1.6.2).

For the above system, the Pauli Transfer matrix $M^{(1)}$ given by Eq. (4.14) is

$$M^{(1)} = \begin{pmatrix} 0 & 0 & 0 & 0 \\ 0 & -2\chi - \kappa/2 & 0 & 0 \\ 0 & 0 & -2\chi - \kappa/2 & 0 \\ (2p-1)\kappa & 0 & 0 & -\kappa \end{pmatrix}. \tag{5.7}$$

The above matrix is sparse and lower triangular. One can always split it into two parts, a diagonal matrix $D^{(1)}$ and a strictly lower triangular matrix $N^{(1)}$,

$$M^{(1)} = \underbrace{\begin{pmatrix} 0 & 0 & 0 & 0 \\ 0 & -2\chi - \kappa/2 & 0 & 0 \\ 0 & 0 & -2\chi - \kappa/2 & 0 \\ 0 & 0 & 0 & -\kappa \end{pmatrix}}_{D^{(1)}} + \underbrace{\begin{pmatrix} 0 & 0 & 0 & 0 \\ 0 & 0 & 0 & 0 \\ 0 & 0 & 0 & 0 \\ (2p-1)\kappa & 0 & 0 & 0 \end{pmatrix}}_{N^{(1)}}. \tag{5.8}$$

By using the $|P_i\rangle$ basis which we introduced in Section 4.2, we can express matrices $D^{(1)}$ and $N^{(1)}$ as

$$D^{(1)} = -(2\chi + \kappa/2)|X_1\rangle\langle X_1| - (2\chi + \kappa/2)|Y_1\rangle\langle Y_1| - \kappa|Z_1\rangle\langle Z_1|, \tag{5.9}$$

and

$$N^{(1)} = (2p-1)\kappa|Z_1\rangle\langle\mathbb{I}_1| = \langle Z_1|M_1|\mathbb{I}_1\rangle|Z_1\rangle\langle\mathbb{I}_1|. \tag{5.10}$$

For n qubits, for the aforementioned quantum jump operators and $\mathcal{H} = 0$ in the rotating frame, the Pauli Transfer matrix of 2^{2n} dimensions is

$$\begin{aligned} M &= \sum_{i=1}^{n} \mathbb{I}_{4\times4}^{(1)} \otimes \mathbb{I}_{4\times4}^{(2)} \otimes \cdots \otimes M^{(i)} \otimes \cdots \otimes \mathbb{I}_{4\times4}^{(n)} \\ &= (M^{(1)} \otimes \mathbb{I}_{4\times4}^{(2)} \otimes \cdots \otimes \mathbb{I}_{4\times4}^{(n)}) + (\mathbb{I}_{4\times4}^{(1)} \otimes M^{(2)} \otimes \cdots \otimes \mathbb{I}_{4\times4}^{(n)}) + \ldots + (\mathbb{I}_{4\times4}^{(1)} \otimes \mathbb{I}_{4\times4}^{(2)} \otimes \cdots \otimes M^{(n)}), \end{aligned} \tag{5.11}$$

where all $M^{(i)}$ for all i are given by Eq. (5.7). Since matrix M is a sum of tensor products of matrices which are all lower-triangular, then M is lower triangular itself. It is useful to mention at this point that the fixed point of the above Pauli Transfer Matrix is

$$\sigma = \begin{pmatrix} p & 0 \\ 0 & 1-p \end{pmatrix}^{\otimes n} \tag{5.12}$$

Considering that we have assumed $\mathcal{H} = 0$, the reduced Pauli Transfer matrix $\tilde{M}$ as defined by Eq. (4.17) will be the dissipator matrix $\tilde{M}_{\text{dissip}}$ which we introduced in Section 5.2.1. For M being lower triangular, that means that matrix $\tilde{M}_{\text{dissip}}$ is also lower triangular, and therefore, we can split it into two parts similarly as with matrix $M^{(1)}$ on Eq. (5.8). The algebra of the aforementioned quantum jump operators L_1, L_2 and L_3 which describe relaxation with pure dephasing noise, spans the full matrix algebra, and thus by Evans' theorem [60] the fixed vector $|\tilde{a}_{\text{fixed}}\rangle$ of Eq. (5.6) is unique, and so $\tilde{M}_{\text{dissip}}$ *is invertible*.

Therefore, we split the dissipator matrix $\tilde{M}_{\text{dissip}}$ into a sum of a diagonal matrix D and a strictly lower triangular matrix N,

$$\tilde{M}_{\text{dissip}} = D + N, \tag{5.13}$$

with D and N being matrices of $2^{2n} - 1$ dimensions. We can define matrix D on the $|P_i\rangle$ basis as follows,

$$D = \sum_{i=1}^{2^{2n}-1} \sum_{k} D_{i,i}^{k} |P_i\rangle\langle P_i|, \tag{5.14}$$

5

where the coefficients $D_{i,i}^{k}$ are given by Eq. (4.9) for $j = i$.

By Eq. (5.11), we can write matrix N as

$$N = \sum_{l=1}^{n} N_l, \tag{5.15}$$

where N_l are strictly lower triangular matrices corresponding to the decoherence of each individual qubit l. Similarly to how we defined matrix $N^{(1)}$ for the case of one qubit on Eq. (5.10), we will now define N_l for every qubit l. For every l, each N_l will have a structure similar to that of $N^{(1)}$, which means that every N_l will map the identity $\mathbb{I}_l$ to the Pauli Z_l for all l.

Let $|P_i^{(l)}\rangle = |P_{i_1} \otimes P_{i_2} \otimes \cdots \otimes \mathbb{I}_l \otimes \cdots \otimes P_{i_n}\rangle$ and $|P_j^{(l)}\rangle = |P_{i_1} \otimes P_{i_2} \otimes \cdots \otimes Z_l \otimes \cdots \otimes P_{i_n}\rangle$ be two different states of n qubits in the $|P_i\rangle$ basis. Then for every qubit l, we define

$$N_l = \langle P_j^{(l)}|\tilde{M}_{\text{dissip}}|P_i^{(l)}\rangle |P_j^{(l)}\rangle\langle P_i^{(l)}|. \tag{5.16}$$

By definition, it is clear that $N_l^m = 0$ for $m > 1$ for all l. Now that we have a complete description of the dissipator matrix $\tilde{M}_{\text{dissip}}$, we can proceed with inverting it. For this, we can rewrite Eq. (5.13) as follows,

$$\tilde{M}_{\text{dissip}} = D(\mathbb{I} + D^{-1}N), \tag{5.17}$$

where

$$D^{-1} = \sum_{i=1}^{2^{2n}-1} \frac{1}{\sum_k D_{i,i}^{k}} |P_i\rangle\langle P_i|. \tag{5.18}$$

For two different states $|P_i^{(l)}\rangle$ and $|P_j^{(l)}\rangle$ of n qubits, we now define

$$\tilde{N}_l \equiv D^{-1}N_l = \sum_{i=1}^{2^{2n}-1} \frac{\langle P_j^{(l)}|\tilde{M}_{\text{dissip}}|P_i^{(l)}\rangle}{\sum_k D_{i,i}^{k}} |P_j^{(l)}\rangle\langle P_i^{(l)}|, \tag{5.19}$$

where $\tilde{N}_l^m = 0$ for $m > 1$, and therefore it follows that

$$\tilde{N} \equiv D^{-1}N = \sum_{l=1}^{n} \tilde{N}_l. \tag{5.20}$$

By inverting the dissipator matrix as it is given on Eq. (5.17), we obtain

$$\tilde{M}_{\text{dissip}}^{-1} = (\mathbb{I} + \tilde{N})^{-1} D^{-1} = \left(\mathbb{I} + \sum_{k=1}^{2^{2n}-1} (-1)^k \tilde{N}^k \right) D^{-1}. \tag{5.21}$$

Notice that for any state $|P_i\rangle$ of n qubits, $\langle P_i|\tilde{N}^{n+1} = 0$, and so, Eq. (5.21) simplifies to

$$\tilde{M}_{\text{dissip}}^{-1} = \left(\mathbb{I} + \sum_{k=1}^{n} (-1)^k \tilde{N}^k \right) D^{-1}. \tag{5.22}$$

The above equation gives us the inverse of the dissipator matrix $\tilde{M}_{\text{dissip}}$. As we can see, in general it is not efficiently computable since the sum scales with the system size n. Although this is true, we must take into consideration the following: if we are interested in calculating the expectation values of p-body Pauli strings of n qubits with $p < n$, such as the $Z_i \otimes Z_j$ terms for $i \neq j$ in Ising Hamiltonians, then the sum in Eq. (5.22) may stop earlier before reaching $k = n$. More specifically, for two-body terms like $P_{i,j} = Z_i \otimes Z_j$, the sum can stop at $k = 2$, since $\langle P_{i,j}|\tilde{N}^k = 0$ for $k > 2$.

Therefore, for Pauli strings P_i of n qubits that represent correlations of size $O(1)$, the inverse of the dissipator matrix $\tilde{M}_{\text{dissip}}$ can be *efficiently computed*.

5.2.3. PERTURBATION METHOD FOR A SYSTEM OF TWO QUBITS

We will use the perturbation method for the Hamiltonian given by Eq. (4.24) with $c = 0$, i.e.

$$\mathcal{H} = \gamma(Z_1X_2 + X_1Z_2), \tag{5.23}$$

where the driving strength γ takes strictly small values in the framework of perturbation theory. "Small" here means small driving values γ compared to the dissipator strength, i.e. $\gamma \ll 1$. As the dissipator of the system $\mathcal{L}_{\text{dissip}}$ we choose the quantum jump operators $L_1 = \sqrt{\kappa p}\sigma_-$, $L_2 = \sqrt{\kappa(1-p)}\sigma_+$ and $L_3 = \sqrt{\chi}Z$ for the processes of relaxation, excitation and pure dephasing respectively (see Section 1.6.2). Even though pure dephasing was left out in sections 4.3.1 and 4.3.2, it is included here for generality. When comparing results with the exact solution, we will set $\chi = 0$.

For the above system, we find that (see Appendix A.3)

$$\tilde{M}_{\mathcal{H}} = 2\gamma \begin{pmatrix} 0 & 0 & 1 & 0 & 0 & 0 & 0 & -1 \\ 0 & 0 & 0 & 0 & 0 & 0 & 1 & 0 \\ -1 & 0 & 0 & -1 & 0 & 0 & 0 & 0 \\ 0 & 0 & 1 & 0 & 0 & 0 & 0 & -1 \\ 0 & 0 & 0 & 0 & 0 & -1 & 0 & 0 \\ 0 & 0 & 0 & 0 & 1 & 0 & 0 & 0 \\ 0 & -1 & 0 & 0 & 0 & 0 & 0 & 0 \\ 1 & 0 & 0 & 1 & 0 & 0 & 0 & 0 \end{pmatrix} \tag{5.24}$$

and

$$\tilde{M}^{-1}_{\text{dissip}} = \begin{pmatrix} -\frac{2}{\kappa+4\chi} & 0 & 0 & 0 & 0 & 0 & 0 & 0 \\ 0 & -\frac{1}{\kappa} & 0 & 0 & 0 & 0 & 0 & 0 \\ 0 & 0 & -\frac{1}{\kappa+4\chi} & 0 & 0 & 0 & 0 & 0 \\ 0 & 0 & 0 & -\frac{2}{\kappa+4\chi} & 0 & 0 & 0 & 0 \\ 0 & 0 & 0 & \frac{4\kappa(1-2p)}{(\kappa+4\chi)(3\kappa+4\chi)} & -\frac{2}{3\kappa+4\chi} & 0 & 0 & 0 \\ 0 & 0 & 0 & 0 & 0 & -\frac{1}{\kappa} & 0 & 0 \\ \frac{4\kappa(1-2p)}{(\kappa+4\chi)(3\kappa+4\chi)} & 0 & 0 & 0 & 0 & 0 & -\frac{2}{3\kappa+4\chi} & 0 \\ 0 & \frac{1-2p}{2\kappa} & 0 & 0 & 0 & \frac{1-2p}{2\kappa} & 0 & -\frac{1}{2\kappa} \end{pmatrix} \tag{5.25}$$

in the Pauli basis $|Y_2\rangle = (1,0,0,0,0,0,0,0)^{\mathrm{T}}$, $|Z_2\rangle = (0,1,0,0,0,0,0,0)^{\mathrm{T}}$, $|X_1X_2\rangle = (0,0,1,0,0,0,0,0)^{\mathrm{T}}$, $|Y_1\rangle = (0,0,0,1,0,0,0,0)^{\mathrm{T}}$, $|Y_1Z_2\rangle = (0,0,0,0,1,0,0,0)^{\mathrm{T}}$, $|Z_1\rangle = (0,0,0,0,0,1,0,0)^{\mathrm{T}}$, $|Z_1Y_2\rangle = (0,0,0,0,0,0,1,0)^{\mathrm{T}}$ and $|Z_1Z_2\rangle = (0,0,0,0,0,0,0,1)^{\mathrm{T}}$. Notice that $\tilde{M}^{\mathrm{T}}_{\mathcal{H}} = -\tilde{M}_{\mathcal{H}}$, which follows directly from Eq. (4.8).

By using the above expressions for $\tilde{M}_{\mathcal{H}}$ and $\tilde{M}^{-1}_{\text{dissip}}$, we can compute the expectation values of all the Pauli strings that make up the basis for the above matrices, by using Eq. (5.6). For example, the expectation value $\langle Z_1Z_2\rangle$ can be computed as

$$\langle Z_1Z_2\rangle = 4\langle Z_1Z_2|\tilde{a}_{\text{fixed}}\rangle = 4\sum_{k=0}^{\infty}(-1)^k\langle Z_1Z_2|\left(\tilde{M}^{-1}_{\text{dissip}}\tilde{M}_{\mathcal{H}}\right)^k|\tilde{a}_{\text{dissip}}\rangle. \tag{5.26}$$

By expanding the expectation values of the exact solution for the steady state for two qubits (see Section 4.3.1), one can verify that the two power series are identical.

5.3. Mean-field method

The mean-field method is an approximation tool used for computing the expectation values of large systems. The method dictates that we treat the density matrix ρ of a system of n qubits as a product state of n single-qubit states $\rho^{(i)}$ [63],

$$\rho = \bigotimes_{i=1}^{n}\rho^{(i)}, \tag{5.27}$$

where each state $\rho^{(i)}$ is given by

$$\rho^{(i)} = \frac{1}{2}(\mathbb{I} + r_x^{(i)}X + r_y^{(i)}Y + r_z^{(i)}Z), \tag{5.28}$$

where $\vec{r}^{(i)} = (r_x^{(i)}, r_y^{(i)}, r_z^{(i)}) \in \mathbb{R}^3$ is a real vector and $|\vec{r}^{(i)}| \leq 1$ for every $i \in \{1,2,...,n\}$.

For a system of two qubits with a Hamiltonian given by Eq. (5.23), and for a dissipator $\mathcal{L}_{\text{dissip}}$ with quantum jump operators $L_1 = \sqrt{\kappa p}\sigma_-$, $L_2 = \sqrt{\kappa(1-p)}\sigma_+$ and $L_3 = \sqrt{\chi}Z$ describing the processes of relaxation, excitation and pure dephasing respectively, we find the mean field equations for the steady state to be (see Appendix B.4)

$$X(4\gamma Y + \kappa + 4\chi) = 0 \tag{5.29}$$

$$4\gamma(X^2 - Z^2) - (\kappa + 4\chi)Y = 0 \tag{5.30}$$

$$2\gamma YZ - \kappa(1 - 2p + Z) = 0, \tag{5.31}$$

where $X = \mathrm{Tr}(X\rho)$, $Y = \mathrm{Tr}(Y\rho)$ and $Z = \mathrm{Tr}(Z\rho)$ are the expectation values of the three Pauli matrices. Notice how because of the symmetry of Eq. (5.23), we obtain the same set of mean field equations for $i = 1, 2$, i.e. the expectation values of all $\rho^{(i)}$ are the same. As a matter of fact, this is also true for the more general Hamiltonian of Eq. (4.23) with a boundary condition $X_{i+1} = X_1$ for a system of n qubits.

5.4. Results and Discussion

A good measure for the success of our approximation methods is to compare them with the exact solution for a small system of two qubits that we already possess. Here, for a driven-dissipative system of two qubits with Hamiltonian

$$\mathcal{H} = \gamma(Z_1X_2 + X_1Z_2), \tag{5.32}$$

we will plot and compare the expectation values $\langle X\rangle$, $\langle Y\rangle$ and $\langle Z\rangle$ acquired using three methods: solving exactly the Lindblad Master Equation (Section 4.3.1), perturbatively expanding the reduced Pauli Transfer matrix (Section 5.2.3) and solving the mean field equations (Section 5.3).

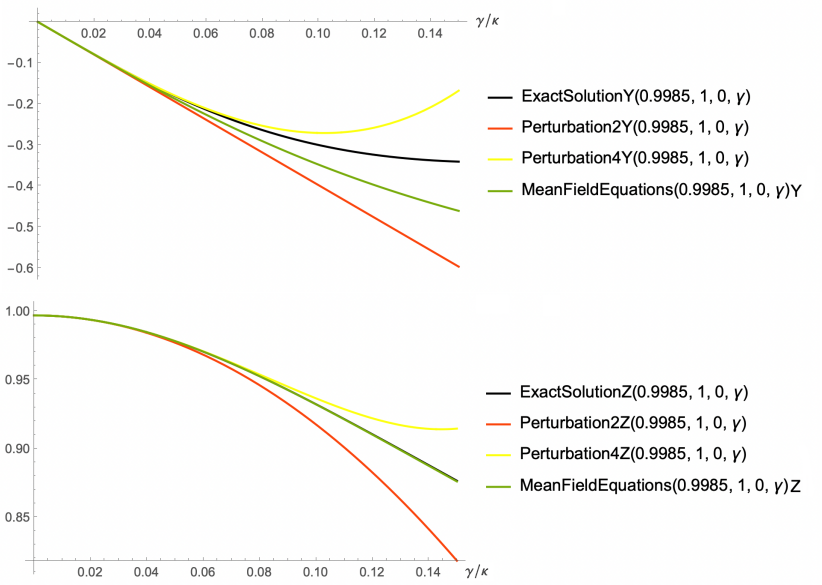

Figure 5.1: Top: Plots of the expectation value $\langle Y\rangle$ as a function of γ/κ, where γ is the driving strength and κ is the strength of the dissipator. For these plots we set $\kappa = 1$. The number in the perturbation labels indicate the perturbation order of the expansion k.
Bottom: Plots of the expectation value $\langle Z\rangle$ as a function of γ/κ, where γ is the driving strength and κ is the strength of the dissipator. For these plots we set $\kappa = 1$. The number in the perturbation labels indicate the perturbation order of the expansion k.
General comment: The exact solution as well as the approximation methods give $\langle X\rangle = 0$ for all γ.

In Fig. 5.1 we see the results for a small range of γ/κ, so that the perturbation method is valid. Every method gives the exact value $\langle X\rangle = 0$, while $\langle Z\rangle > 0$ and $\langle Y\rangle < 0$ for

small γ. We see that both approximate methods are close to the exact solution of $\langle Y \rangle$ and $\langle Z \rangle$, while the mean field method produces slightly better results. We believe though that for higher orders of the perturbative expansion, the perturbation method can significantly outperform the mean field method (in the small range of γ/κ where the perturbation theory is still applicable).

Even though the mean field method gave relatively good results for the expectation values of single Paulis, it fails to do so for two-body Pauli strings. For example, mean field theory predicts that $\langle X_1 X_2 \rangle = \langle X_1 \rangle \langle X_2 \rangle$, and based on the above results where $\langle X \rangle = 0$, the mean field method gives us $\langle X_1 X_2 \rangle = 0$. This is in stark contrast with the results of the perturbation method, as can be seen on the figure below:

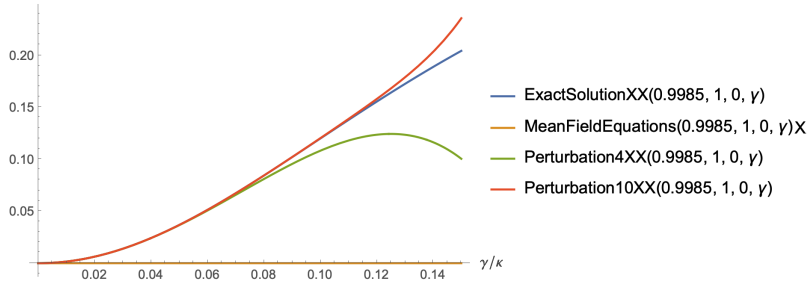

Figure 5.2: Plots of the expectation value $\langle X_1 X_2 \rangle$ as a function of γ/κ, where γ is the driving strength and κ is the strength of the dissipator. For these plots we set $\kappa = 1$. The mean field method gives $\langle X_1 X_2 \rangle = 0$ for all γ, while the exact solution gives a monotonal increase of $\langle X_1 X_2 \rangle$ as a function of γ. We can see that the expectation value of $X_1 X_2$ as has been estimated by the perturbation method approximates well the exact solution. The solution from the mean field equations corresponds to the value of $\langle X_1 \rangle \langle X_2 \rangle$, while the number in the perturbation labels indicate the perturbation order of the expansion k. We can see that the perturbation theory is a better approximation tool for the estimation of $\langle X_1 X_2 \rangle$.

In Fig. 5.2 we can see that the perturbation theory is able to capture richer dynamics by predicting a non-zero expectation value $\langle X_1 X_2 \rangle$, which is close to that of the exact solution for higher perturbation orders.

That being said, the reader should keep in mind that the mean field method is supposed to be used for large systems, where it gives more accurate results [63]. Also, the perturbation theory becomes harder for larger systems, since the matrices $\tilde{M}_{\mathcal{H}}$ and $\tilde{M}_{\text{dissip}}^{-1}$ should naturally grow with the size of the Pauli strings that we want to measure. Still, this growth has a dependency poly(n) on the system size, while the inversion of the Pauli transfer matrix is not efficient. There still exists the difficulty of obtaining those matrices in an efficient way, and the process needs to be automated. One would also need to bound and estimate the error for when we stop the perturbative expansion at an order k. Therefore, this analysis only serves as an exposure to some of the available approximation tools for computing expectation values, and not as a final assessment to which method is better.

6

Conclusion

6.1. Summary and Discussion

In Chapter 2 we proved that the dissipative Lindbladian operator $\mathcal{L}_{\text{dissip}}$ describing relaxation noise along with pure dephasing noise, satisfies a MLSI with constant κ, where κ is the relaxation rate. The absence of the pure dephasing rate χ indicates that the convergence rate of the relative entropy between two states ρ and σ for a Lindbladian operator which includes relaxation and pure dephasing is optimal only for $\chi \ll 1$. Our results hint that perhaps the effects of pure dephasing are severely underestimated in [32], since by using only relaxation noise none of the upper bounds for the relative entropy in Section 3.6 converged to the values reported in [32], where the later only used depolarizing noise.

In Chapter 3 we showed that the convergence rate of the relative entropy is too low for us to assess if the QAOA is inferior to a classical optimization algorithm, even for high-connectivity planar graph problems, such as instances of the MaxCut or the SK model. Thus, the methods developed by França and Raul-Garcia [32] seem to be used in a very simplistic and one-sided fashion by them, since they only focus on using the symmetric depolarizing channel for their analysis and results. We argue here that there should be no reason (as per existing experimental evidence) as to why one should use the depolarizing noise versus a different noise model, such as relaxation and pure dephasing, which make a more realistic model of noise for superconducting qubits. For the later type of noise, the bounds converge at a very slow rate, which puts into question the universality of the methods developed in [32].

In Chapter 4, we reformulated the Lindblad Master equation and solved it for the steady state of the system, in order to study long-time dynamics. We analysed an array of n transmon qubits coupled by a nearest-neighbor interaction, and solved the system exactly for two and three transmons. For the two transmons, we showed that the system preserves its main characteristics when we increase the pure dephasing rate χ. Furthermore, for specific driving strengths, we have a near 50% chance of creating an entangled state (for $\chi = 0$) which is robust against slight deviations between the two driving strengths in the entanglement regime. The characteristics of the three transmon system were quite different,

for which entanglement cannot be preserved when we introduce pure dephasing into the system.

In Chapter 5 we perturbatively expanded the Pauli Transfer matrix and demonstrated how the method works for a system of two qubits (see Appendix A.3). We then obtained the mean field equations and compared the two approximation methods with the exact solution which was previously obtained in Section 4.3.1.

6.2. Outlook

Here we will address some parts of the *perturbation theory* which stand out in the thesis, and for which further research needs to be done.

One issue that arises when using perturbation theory to approximate the expectation value of some Pauli string, is *how* could one determine efficiently the subspace of all the Pauli strings that are involved in the computations of matrices $\tilde{M}_{\mathcal{H}}$ and $\tilde{M}^{-1}_{\text{dissip}}$? The computations on Appendix A.3 were done by hand, and the simplistic method used was to just apply $\tilde{M}_{\mathcal{H}}$ and $\tilde{M}^{-1}_{\text{dissip}}$ to every new Pauli string that came up, with the hope that at some point the subspace would stop growing. Obviously there is the need to automate this process intelligently. If for larger Pauli strings the computer would need to learn the subspace by trial and error application of $\tilde{M}_{\mathcal{H}}$ and $\tilde{M}^{-1}_{\text{dissip}}$ on successive Pauli strings, this could easily overwhelm the memory and would defeat the purpose of applying the perturbation method in the first place.

Another aspect of the perturbation theory that needs to be explored is the error that one makes when they stop the perturbative expansion at any order k. Perhaps it would be easier to bound the error, and several techniques already exist for doing that. Finally, it would be interesting to study the regime γ/κ at which perturbation theory breaks down. From the calculations that were done on Section 5.4, it turns out that for most cases the perturbation theory still holds for $\gamma/\kappa < 0.18$. That being said, an analytical estimation of the range of γ/κ for which the method still works is very much needed.

References

1. Preskill, J. Quantum computing and the entanglement frontier. Preprint at https://doi.org/10.48550/arXiv.1203.5813 (2012).
2. Sharma, A. Google plans to build commercial-grade quantum computer by 2029. *The National News*. https://www.thenationalnews.com/business/technology/google-plans-to-build-commercial-grade-quantum-computer-by-2029-1.1225463 (May 19, 2021).
3. Gambetta, J. IBM's roadmap for scaling quantum technology. *IBM Research Blog*. https://research.ibm.com/blog/ibm-quantum-roadmap (Sep. 15, 2020).
4. Farhi, E., Goldstone, J. & Gutmann, S. A quantum approximate optimization algorithm. Preprint at https://doi.org/10.48550/arXiv.1411.4028 (2014).
5. Harrigan, M. *et al.* Quantum approximate optimization of non-planar graph problems on a planar superconducting processor. *Nature Physics* **17,** 332–336. https://doi.org/10.1038/s41567-020-01105-y (2021).
6. Zhou, L., Wang, S.-T., Choi, S., Pichler, H. & Lukin, M. Quantum Approximate Optimization Algorithm: Performance, Mechanism, and Implementation on Near-Term Devices. *Phys. Rev. X* **10,** 021067. https://doi.org/10.1103/PhysRevX.10.021067 (2020).
7. Lacroix, N. *et al.* Improving the Performance of Deep Quantum Optimization Algorithms with Continuous Gate Sets. *PRX Quantum* **1,** 110304. https://doi.org/10.1103/PRXQuantum.1.020304 (2020).
8. Landau, L. D. & Lifshitz, E. M. *Quantum mechanics: non-relativistic theory* (Elsevier, 2013).
9. Sakurai, J. J. & Commins, E. D. *Modern quantum mechanics, revised edition* 1995.
10. Nazarov, Y. V. & Danon, J. *Advanced Quantum Mechanics: A Practical Guide* (Cambridge University Press, 2013).
11. Landau, L. & Lifshitz, E. *Mechanics (Course of Theoretical Physics, Volume 1)* 2002.
12. Blais, A., Grimsmo, A. L., Girvin, S. & Wallraff, A. Circuit quantum electrodynamics. *Reviews of Modern Physics* **93,** 025005. https://doi.org/10.1103/RevModPhys.93.025005 (2021).
13. Bruzewicz, C. D., Chiaverini, J., McConnell, R. & Sage, J. M. Trapped-ion quantum computing: Progress and challenges. *Applied Physics Reviews* **6,** 021314. https://doi.org/10.1063/1.5088164 (2019).
14. Kok, P. *et al.* Linear optical quantum computing with photonic qubits. *Reviews of modern physics* **79,** 135. https://doi.org/10.1103/RevModPhys.79.135 (2007).

15. Pezzagna, S. & Meijer, J. Quantum computer based on color centers in diamond. *Applied Physics Reviews* **8,** 011308. https://doi.org/10.1063/5.0007444 (2021).

16. Vandersypen, L. *et al.* Interfacing spin qubits in quantum dots and donors—hot, dense, and coherent. *npj Quantum Information* **3,** 1–10. https://doi.org/10.1038/s41534-017-0038-y (2017).

17. Bloch, F. Generalized theory of relaxation. *Physical Review* **105,** 1206. https://doi.org/10.1103/PhysRev.105.1206 (1957).

18. Redfield, A. G. On the theory of relaxation processes. *IBM Journal of Research and Development* **1,** 19–31. 10.1147/rd.11.0019 (1957).

19. Krantz, P. *et al.* A quantum engineer's guide to superconducting qubits. *Applied Physics Reviews* **6,** 021318. https://doi.org/10.1063/1.5089550 (2019).

20. Shannon, C. E. A mathematical theory of communication. *The Bell system technical journal* **27,** 379–423. 10.1002/j.1538-7305.1948.tb01338.x (1948).

21. Kullback, S. & Leibler, R. A. On information and sufficiency. *The annals of mathematical statistics* **22,** 79–86 (1951).

22. Petz, D. A variational expression for the relative entropy. *Communications in Mathematical Physics* **114,** 345–349 (1988).

23. Berta, M., Fawzi, O. & Tomamichel, M. On variational expressions for quantum relative entropies. *Letters in Mathematical Physics* **107,** 2239–2265. https://doi.org/10.1007/s11005-017-0990-7 (2017).

24. Lindblad, G. On the generators of quantum dynamical semigroups. *Communications in Mathematical Physics* **48,** 119–130. https://doi.org/10.1007/BF01608499 (1976).

25. Diaconis, P. & Saloff-Coste, L. Logarithmic Sobolev inequalities for finite Markov chains. *The Annals of Applied Probability* **6,** 695–750. 10.1214/aoap/1034968224 (1996).

26. Kastoryano, M. J. & Temme, K. Quantum logarithmic Sobolev inequalities and rapid mixing. *Journal of Mathematical Physics* **54,** 052202. https://doi.org/10.1063/1.4804995 (2013).

27. Gross, L. Logarithmic sobolev inequalities. *American Journal of Mathematics* **97,** 1061–1083. https://doi.org/10.2307/2373688 (1975).

28. Gross, L. Logarithmic Sobolev inequalities and contractivity properties of semigroups. *Dirichlet forms,* 54–88. https://doi.org/10.1007/BFb0074091 (1993).

29. Bardet, I., Capel, A. & Rouzé, C. *Approximate tensorization of the relative entropy for noncommuting conditional expectations* in *Annales Henri Poincaré* **23** (2022), 101–140. https://doi.org/10.1007/s00023-021-01088-3.

30. Capel, Á., Lucia, A. & Pérez-Garcıa, D. Quantum conditional relative entropy and quasi-factorization of the relative entropy. *Journal of Physics A: Mathematical and Theoretical* **51,** 484001. https://doi.org/10.1088/1751-8121/aae4cf (2018).

31. Capel, Á., Rouzé, C. & França, D. S. The modified logarithmic Sobolev inequality for quantum spin systems: classical and commuting nearest neighbour interactions. *arXiv preprint arXiv:2009.11817*. https://doi.org/10.48550/arXiv.2009.11817 (2020).

32. Stilck França, D. & García-Patrón, R. Limitations of optimization algorithms on noisy quantum devices. *Nature Physics* **17,** 1221–1227. https://doi.org/10.1038/s41567-021-01356-3 (2021).

33. Christandl, M. & Müller-Hermes, A. Relative entropy bounds on quantum, private and repeater capacities. *Communications in Mathematical Physics* **353,** 821–852. https://doi.org/10.1007/s00220-017-2885-y (2017).

34. Müller-Lennert, M., Dupuis, F., Szehr, O., Fehr, S. & Tomamichel, M. On quantum Rényi entropies: A new generalization and some properties. *Journal of Mathematical Physics* **54,** 122203. https://doi.org/10.1063/1.4838856 (2013).

35. Müller-Hermes, A., Stilck França, D. & Wolf, M. M. Relative entropy convergence for depolarizing channels. *Journal of Mathematical Physics* **57,** 022202. https://doi.org/10.1063/1.4939560 (2016).

36. Beigi, S., Datta, N. & Rouzé, C. Quantum Reverse Hypercontractivity: Its Tensorization and Application to Strong Converses. *Communications in Mathematical Physics* **376,** 753–794. https://doi.org/10.1007/s00220-020-03750-z (2020).

37. Arute, F. *et al.* Quantum supremacy using a programmable superconducting processor. *Nature* **574,** 505–510. https://doi.org/10.1038/s41586-019-1666-5 (2019).

38. Pednault, E., Gunnels, J. A., Nannicini, G., Horesh, L. & Wisnieff, R. Leveraging secondary storage to simulate deep 54-qubit sycamore circuits. *arXiv preprint arXiv:1910.09534*. https://doi.org/10.48550/arXiv.1910.09534 (2019).

39. Pednault, E., Gunnels, J., Maslov, D. & Gambetta, J. On "Quantum Supremacy". *IBM Research Blog*. ibm.com/blogs/research/2019/10/on-quantum-supremacy/ (Oct. 21, 2019).

40. Zhong, H.-S. *et al.* Quantum computational advantage using photons. *Science* **370,** 1460–1463. 10.1126/science.abe8770 (2020).

41. Wu, Y. *et al.* Strong quantum computational advantage using a superconducting quantum processor. *Physical review letters* **127,** 180501. https://doi.org/10.1103/PhysRevLett.127.180501 (2021).

42. Brandao, F. G. L., Kueng, R. & França, D. S. Faster quantum and classical SDP approximations for quadratic binary optimization. *Quantum* **6,** 625. https://doi.org/10.22331/q-2022-01-20-625 (2022).

43. Wang, S. *et al.* Noise-induced barren plateaus in variational quantum algorithms. *Nature communications* **12,** 1–11. https://doi.org/10.1038/s41467-021-27045-6 (2021).

44. Barkoutsos, P. K., Nannicini, G., Robert, A., Tavernelli, I. & Woerner, S. Improving Variational Quantum Optimization Using CVaR. *Quantum* **4,** 256. https://doi.org/10.22331/q-2020-04-20-256 (2020).

45. Farhi, E., Goldstone, J., Gutmann, S. & Zhou, L. The Quantum Approximate Optimization Algorithm and the Sherrington-Kirkpatrick Model at Infinite Size. Preprint at https://doi.org/10.48550/arXiv.1910.08187 (2019).

46. Crooks, G. E. Performance of the quantum approximate optimization algorithm on the maximum cut problem. Preprint at https://doi.org/10.48550/arXiv.1811.08419 (2018).

47. Khatri, S., Sharma, K. & Wilde, M. M. Information-theoretic aspects of the generalized amplitude-damping channel. *Physical Review A* **102,** 012401. https://doi.org/10.1103/PhysRevA.102.012401 (2020).

48. Wilde, M. M. From Classical to Quantum Shannon Theory. Preprint at https://doi.org/10.48550/arXiv.1106.1445 (2011).

49. Simakov, I., Besedin, I. & Ustinov, A. Simulation of the five-qubit quantum error correction code on superconducting qubits. *Physical Review A* **105,** 032409. https://doi.org/10.1103/PhysRevA.105.032409 (2022).

50. Eldan, R., Koehler, F. & Zeitouni, O. A spectral condition for spectral gap: fast mixing in high-temperature Ising models. *Probability Theory and Related Fields,* 1–17. https://doi.org/10.1007/s00440-021-01085-x (2021).

51. Friis, N., Melnikov, A. A., Kirchmair, G. & Briegel, H. J. Coherent controlization using superconducting qubits. *Scientific reports* **5,** 1–11. https://doi.org/10.1038/srep18036 (2015).

52. Paz, D. A. & Maghrebi, M. F. Driven-dissipative Ising model: An exact field-theoretical analysis. *Physical Review A* **104,** 023713. https://doi.org/10.1103/PhysRevA.104.023713 (2021).

53. Sierant, P. *et al.* Dissipative Floquet dynamics: from steady state to measurement induced criticality in trapped-ion chains. *Quantum* **6,** 638. https://doi.org/10.22331/q-2022-02-02-638 (2022).

54. Maghrebi, M. F. & Gorshkov, A. V. Nonequilibrium many-body steady states via Keldysh formalism. *Physical Review B* **93,** 014307. https://doi.org/10.1103/PhysRevB.93.014307 (2016).

55. Overbeck, V. R., Maghrebi, M. F., Gorshkov, A. V. & Weimer, H. Multicritical behavior in dissipative Ising models. *Physical Review A* **95,** 042133. https://doi.org/10.1103/PhysRevA.95.042133 (2017).

56. Fitzpatrick, M., Sundaresan, N. M., Li, A. C., Koch, J. & Houck, A. A. Observation of a dissipative phase transition in a one-dimensional circuit QED lattice. *Physical Review X* **7,** 011016. https://doi.org/10.1103/PhysRevX.7.011016 (2017).

57. Malekakhlagh, M., Magesan, E. & McKay, D. C. First-principles analysis of cross-resonance gate operation. *Physical Review A* **102,** 042605. https://doi.org/10.1103/PhysRevA.102.042605 (2020).

58. Helsen, J., Battistel, F. & Terhal, B. M. Spectral quantum tomography. *npj Quantum Information* **5,** 1–11. https://doi.org/10.1038/s41534-019-0189-0 (2019).

59. Manzano, D. A short introduction to the Lindblad master equation. *AIP Advances* **10,** 025106. https://doi.org/10.1063/1.5115323 (2020).

60. Evans, D. E. Irreducible quantum dynamical semigroups. *Communications in Mathematical Physics* **54,** 293–297. https://doi.org/10.1007/BF01614091 (1977).

61. Wootters, W. K. Entanglement of formation and concurrence. *Quantum Inf. Comput.* **1,** 27–44 (2001).

62. Harrow, A. W., Hassidim, A. & Lloyd, S. Quantum algorithm for linear systems of equations. *Physical review letters* **103,** 150502. https://doi.org/10.1103/PhysRevLett.103.150502 (2009).

63. Krämer, S. & Ritsch, H. Generalized mean-field approach to simulate the dynamics of large open spin ensembles with long range interactions. *The European Physical Journal D* **69,** 1–11. https://doi.org/10.1140/epjd/e2015-60266-5 (2015).

64. Ma, J., Jiang, L.-N., Yu, S.-Y., Ran, Q.-W. & Tan, L.-Y. Entanglement dynamics of the mixed two-qubit system in different noisy channels. *International Journal of Theoretical Physics* **53,** 3843–3855. https://doi.org/10.1007/s10773-014-2137-2 (2014).

65. Schäcke, K. On the Kronecker Product. Preprint at https://www.math.uwaterloo.ca/~hwolkowi/henry/reports/kronthesisschaecke04.pdf (2013).

A

Appendix: Mathematical Derivations

A.1. Discrete bound calculations

We will begin by evaluating the relative entropy $D(\rho_0\|\sigma)$ which appears in the first term of the r.h.s. of Eq. (3.21). Because of the additivity property of the quantum relative entropy (Eq. (11.136), [48]),

$$D(\rho_0\|\sigma) = D\left(|+\rangle\langle+|^{\otimes n}\|\sigma_0^{\otimes n}\right) = nD\left(|+\rangle\langle+|\|\sigma_0\right). \tag{A.1}$$

We proceed to calculate the following quantities,

$$\log(|+\rangle\langle+|) = \log(1)|+\rangle\langle+| = 0, \tag{A.2}$$

$$\log(\sigma_0) = \log(p)|0\rangle\langle 0| + \log(1-p)|1\rangle\langle 1| = \begin{pmatrix}\log(p) & 0\\ 0 & \log(1-p)\end{pmatrix}, \tag{A.3}$$

$$|+\rangle\langle+|\log(\sigma_0) = \frac{1}{2}\begin{pmatrix}1 & 1\\ 1 & 1\end{pmatrix}\begin{pmatrix}\log(p) & 0\\ 0 & \log(1-p)\end{pmatrix} = \frac{1}{2}\begin{pmatrix}\log(p) & \log(1-p)\\ \log(p) & \log(1-p)\end{pmatrix}. \tag{A.4}$$

Consequently,

$$D\left(|+\rangle\langle+|\|\sigma_0\right) = \mathrm{Tr}[|+\rangle\langle+|(\log(|+\rangle\langle+|) - \log(\sigma_0))] = -\mathrm{Tr}[|+\rangle\langle+|\log(\sigma_0)] \Rightarrow$$

$$\Rightarrow D\left(|+\rangle\langle+|\|\sigma_0\right) = -\frac{1}{2}(\log(p) + \log(1-p)), \tag{A.5}$$

and therefore

$$D(\rho_0\|\sigma) = -\frac{n}{2}(\log(p) + \log(1-p)). \tag{A.6}$$

A

Let us now calculate the max-relative entropy term of Eq. (3.21). First, note that

$$\mathcal{U}_B(\beta_j)(\sigma) = U_B(\beta_j)\sigma U_B^\dagger(\beta_j) = (R_X(2\beta_j)\sigma_0 R_X(-2\beta_j))^{\otimes n}. \tag{A.7}$$

This gives us

$$\begin{aligned} D_\infty(\mathcal{U}_B(\beta_j)(\sigma)\|\sigma) &= D_\infty\left((R_X(2\beta_j)\sigma_0 R_X(-2\beta_j))^{\otimes n}\|\sigma_0^{\otimes n}\right) \\ &= \log(\|\sigma^{-\frac{1}{2}}(R_X(2\beta_j)\sigma_0 R_X(-2\beta_j))^{\otimes n}\sigma^{-\frac{1}{2}}\|) \\ &= n\log(\|\sigma_0^{-\frac{1}{2}}(R_X(2\beta_j)\sigma_0 R_X(-2\beta_j))\sigma_0^{-\frac{1}{2}}\|). \end{aligned}$$

For a rotation $R_X(2\beta_j)$ which is given by

$$R_X(2\beta_j) = \begin{pmatrix} \cos(\beta_j) & i\sin(\beta_j) \\ i\sin(\beta_j) & \cos(\beta_j) \end{pmatrix}, \tag{A.8}$$

we compute the following:

$$R_X(2\beta_j)\sigma_0 R_X(-2\beta_j) = \begin{pmatrix} \sin^2(\beta_j) + p(\cos^2(\beta_j) - \sin^2(\beta_j)) & i(1-2p)\cos(\beta_j)\sin(\beta_j) \\ i(1-2p)\cos(\beta_j)\sin(\beta_j) & \cos^2(\beta_j) + p(\sin^2(\beta_j) - \cos^2(\beta_j)) \end{pmatrix}, \tag{A.9}$$

$$\sigma_0^{-\frac{1}{2}}(R_X(2\beta_j)\sigma_0 R_X(-2\beta_j))\sigma_0^{-\frac{1}{2}} = \begin{pmatrix} \cos^2(\beta_j) + \frac{1-p}{p}\sin^2(\beta_j) & i\sin(\beta_j)\cos(\beta_j)\frac{1-2p}{\sqrt{p(1-p)}} \\ i\sin(\beta_j)\cos(\beta_j)\frac{2p-1}{\sqrt{p(1-p)}} & \cos^2(\beta_j) - \frac{p}{1-p}\sin^2(\beta_j) \end{pmatrix}. \tag{A.10}$$

By defining $A(j)$ as

$$A(j) \equiv \begin{pmatrix} \cos^2(\beta_j) + \frac{1-p}{p}\sin^2(\beta_j) & i\sin(\beta_j)\cos(\beta_j)\frac{1-2p}{\sqrt{p(1-p)}} \\ i\sin(\beta_j)\cos(\beta_j)\frac{2p-1}{\sqrt{p(1-p)}} & \cos^2(\beta_j) - \frac{p}{1-p}\sin^2(\beta_j) \end{pmatrix}, \tag{A.11}$$

Eq. (3.21) finally becomes

$$D(\rho\|\sigma) \leq n\left[-\frac{(1-\alpha)^{(m+1)P}}{2}(\log(p) + \log(1-p)) + \sum_{j=1}^{P}(1-\alpha)^{(m+1)(P-j)}\log(\|A(j)\|)\right]. \tag{A.12}$$

A.2. Computing the norm $\|\sigma^{-\frac{1}{2}}[X_i, \sigma]\sigma^{-\frac{1}{2}}\|$

In order to compute $[X_i, \sigma]$, we will first start by computing $[X, \sigma_0]$, where σ_0 is given by Eq. (3.17):

$$X\sigma_0 = \begin{pmatrix} 0 & 1 \\ 1 & 0 \end{pmatrix}\begin{pmatrix} p & 0 \\ 0 & 1-p \end{pmatrix} = \begin{pmatrix} 0 & 1-p \\ p & 0 \end{pmatrix},$$

$$\sigma_0 X = \begin{pmatrix} p & 0 \\ 0 & 1-p \end{pmatrix}\begin{pmatrix} 0 & 1 \\ 1 & 0 \end{pmatrix} = \begin{pmatrix} 0 & p \\ 1-p & 0 \end{pmatrix},$$

and so

$$[X,\sigma_0] = X\sigma_0 - \sigma_0 X = \begin{pmatrix} 0 & 1-2p \\ 2p-1 & 0 \end{pmatrix}. \tag{A.13}$$

Since σ_0 is diagonal in the computational basis, it holds that

$$\sigma_0 = \begin{pmatrix} p & 0 \\ 0 & 1-p \end{pmatrix} \Rightarrow \sigma_0^{-\frac{1}{2}} = \begin{pmatrix} p^{-1/2} & 0 \\ 0 & (1-p)^{-1/2} \end{pmatrix}. \tag{A.14}$$

Using equations (A.13) and (A.14) we compute

$$\sigma_0^{-\frac{1}{2}}[X,\sigma_0]\sigma_0^{-\frac{1}{2}} = \begin{pmatrix} p^{-1/2} & 0 \\ 0 & (1-p)^{-1/2} \end{pmatrix}\begin{pmatrix} 0 & 1-2p \\ 2p-1 & 0 \end{pmatrix}\begin{pmatrix} p^{-1/2} & 0 \\ 0 & (1-p)^{-1/2} \end{pmatrix} \Rightarrow$$

$$\Rightarrow \sigma_0^{-\frac{1}{2}}[X,\sigma_0]\sigma_0^{-\frac{1}{2}} = \begin{pmatrix} 0 & p^{-1/2}(1-p)^{-1/2}(1-2p) \\ p^{-1/2}(1-p)^{-1/2}(2p-1) & 0 \end{pmatrix}. \tag{A.15}$$

For reasons that will become clear later, we now define

$$C := \sigma_0^{-\frac{1}{2}}[X,\sigma_0]\sigma_0^{-\frac{1}{2}}, \tag{A.16}$$

and so taking the Hermitian conjugate of C, we find that

$$C^\dagger = \begin{pmatrix} 0 & p^{-1/2}(1-p)^{-1/2}(2p-1) \\ p^{-1/2}(1-p)^{-1/2}(1-2p) & 0 \end{pmatrix}, \tag{A.17}$$

and so

$$C^\dagger C = \begin{pmatrix} p^{-1}(1-p)^{-1}(2p-1)^2 & 0 \\ 0 & p^{-1}(1-p)^{-1}(1-2p)^2 \end{pmatrix}. \tag{A.18}$$

We now proceed with computing $[X_i,\sigma]$ for a Pauli-X matrix acting on the i^{th} qubit and $\sigma = \sigma_0^{\otimes n}$:

$$\begin{aligned}
[X_i,\sigma] &= [\mathbb{I}_1 \otimes \cdots \otimes X_i \otimes \cdots \otimes \mathbb{I}_n, \sigma_0^{\otimes n}] \\
&= (\mathbb{I}_1 \otimes \cdots \otimes X_i \otimes \cdots \otimes \mathbb{I}_n)\sigma_0^{\otimes n} - \sigma_0^{\otimes n}(\mathbb{I}_1 \otimes \cdots \otimes X_i \otimes \cdots \otimes \mathbb{I}_n) \\
&= (\mathbb{I}_1\sigma_0) \otimes \cdots \otimes (X_i\sigma_0) \otimes \cdots \otimes (\mathbb{I}_n\sigma_0) - (\sigma_0\mathbb{I}_1) \otimes \cdots \otimes (\sigma_0 X_i) \otimes \cdots \otimes (\sigma_0\mathbb{I}_n) \\
&= \sigma_0 \otimes \cdots \otimes (X_i\sigma_0) \otimes \cdots \otimes \sigma_0 - \sigma_0 \otimes \cdots \otimes (\sigma_0 X_i) \otimes \cdots \otimes \sigma_0 \\
&= \sigma_0 \otimes \cdots \otimes (X_i\sigma_0 - \sigma_0 X_i) \otimes \cdots \otimes \sigma_0 \Rightarrow
\end{aligned}$$

$$\Rightarrow [X_i,\sigma] = \sigma_0 \otimes \cdots \otimes [X_i,\sigma_0] \otimes \cdots \otimes \sigma_0. \tag{A.19}$$

Using the fact that

$$\sigma^{-\frac{1}{2}} = (\sigma_0^{\otimes n})^{-\frac{1}{2}} = (\sigma_0 \otimes \sigma_0 \otimes \cdots \otimes \sigma_0)^{-\frac{1}{2}} = \sigma_0^{-\frac{1}{2}} \otimes \sigma_0^{-\frac{1}{2}} \otimes \cdots \otimes \sigma_0^{-\frac{1}{2}}, \tag{A.20}$$

A

we can show that

$$\begin{aligned}\sigma^{-\frac{1}{2}}[X_i,\sigma] &= (\sigma_0^{-\frac{1}{2}}\otimes\sigma_0^{-\frac{1}{2}}\otimes\cdots\otimes\sigma_0^{-\frac{1}{2}})(\sigma_0\otimes\cdots\otimes[X_i,\sigma_0]\otimes\cdots\otimes\sigma_0)\\ &= (\sigma_0^{-\frac{1}{2}}\sigma_0)\otimes\cdots\otimes(\sigma_0^{-\frac{1}{2}}[X_i,\sigma_0])\otimes\cdots\otimes(\sigma_0^{-\frac{1}{2}}\sigma_0)\\ &= \sigma_0^{\frac{1}{2}}\otimes\cdots\otimes(\sigma_0^{-\frac{1}{2}}[X_i,\sigma_0])\otimes\cdots\otimes\sigma_0^{\frac{1}{2}},\end{aligned}$$

hence

$$\sigma^{-\frac{1}{2}}[X_i,\sigma]\sigma^{-\frac{1}{2}} = \mathbb{I}_1\otimes\cdots\otimes\sigma_0^{-\frac{1}{2}}[X_i,\sigma_0]\sigma_0^{-\frac{1}{2}}\otimes\cdots\otimes\mathbb{I}_n = \mathbb{I}_1\otimes\cdots\otimes C_i\otimes\cdots\otimes\mathbb{I}_n, \quad (A.21)$$

where on the last equality we make use of Eq. (A.16).

We will now define B as

$$B := \sigma^{-\frac{1}{2}}[X_i,\sigma]\sigma^{-\frac{1}{2}} = \mathbb{I}_1\otimes\cdots\otimes C_i\otimes\cdots\otimes\mathbb{I}_n, \quad (A.22)$$

where

$$B^\dagger = \mathbb{I}_1\otimes\cdots\otimes C_i^\dagger\otimes\cdots\otimes\mathbb{I}_n. \quad (A.23)$$

As a final step, we want to compute $B^\dagger B$:

$$\begin{aligned}B^\dagger B &= (\mathbb{I}_1\otimes\cdots\otimes C^\dagger\otimes\cdots\mathbb{I}_n)(\mathbb{I}_1\otimes\cdots\otimes C\otimes\cdots\mathbb{I}_n)\\ &= (\mathbb{I}_1\mathbb{I}_1)\otimes\cdots\otimes(C^\dagger C)\otimes\cdots\otimes(\mathbb{I}_n\mathbb{I}_n)\Rightarrow\end{aligned}$$

$$\Rightarrow B^\dagger B = \mathbb{I}_1\otimes\cdots\otimes(C^\dagger C)\otimes\cdots\otimes\mathbb{I}_n. \quad (A.24)$$

It is known that $\|B\|_2 = (\text{maximum eigenvalue of } B^\dagger B)^{1/2}$. Theorem 2.3 of [65] states that the eigenvalues of $B^\dagger B$, with $B^\dagger B$ given by Eq. (A.24), are all the possible products of the eigenvalues of the individual matrices that appear in the tensor product of Eq. (A.24). Each identity matrix for every $n\in\mathbb{N}$ has the degenerate eigenvalue $\lambda = 1$, while the eigenvalues of $C^\dagger C$ are the diagonal elements of Eq. (A.18). Putting all these together, we get the following result,

$$\|\sigma^{-\frac{1}{2}}[X_i,\sigma]\sigma^{-\frac{1}{2}}\| = \frac{|2p-1|}{\sqrt{p(1-p)}}, \text{ for all } i\in\{1,2,...,n\}. \quad (A.25)$$

Using the above result, Eq. (3.33) finally becomes

$$X(T,H,\sigma) \le n\frac{|2p-1|}{\sqrt{p(1-p)}}\frac{\left(1-e^{-\tau_1/T_1}\right)T_1}{\tau_1}\sum_{j=1}^{P} e^{-(P-j)(\tau_1+n\tau_2)/T_1}|\beta_j|, \quad (A.26)$$

and therefore, the upper bound of the relative entropy given by Eq. (3.26) is computed to be

$$\begin{aligned}D(\rho(t)\|\sigma) \le n\Bigg[&-e^{-P\Delta t/T_1}\frac{\log(p)+\log(1-p)}{2}+\\ &+\frac{|2p-1|}{\sqrt{p(1-p)}}\frac{\left(1-e^{\tau_1/T_1}\right)T_1}{\tau_1}\sum_{j=1}^{P} e^{-(P-j)\Delta t/T_1}|\beta_j|\Bigg].\end{aligned} \quad (A.27)$$

A.3. COMPUTING THE PERTURBATIVE EXPANSION

We wish to compute the expectation values for the fixed point $|\tilde{a}_{\text{fixed}}\rangle$ as it is given by the perturbative expansion of Eq. (5.6), for a general Hamiltonian

$$\mathcal{H} = \gamma(Z_\alpha X_\beta + X_\alpha Z_\beta) = \underbrace{\gamma Z_\alpha X_\beta}_{\mathcal{H}_A} + \underbrace{\gamma X_\alpha Z_\beta}_{\mathcal{H}_B}, \tag{A.28}$$

on qubits α and β with $\alpha \neq \beta$. For this, we need to compute matrices $\tilde{M}^{-1}_{\text{dissip}}$ and $\tilde{M}_{\mathcal{H}}$. The computation depends on which expectation values we want to calculate, since those will determine the size of the Hilbert subspace of Pauli states $|P_q\rangle$. Here, we will demonstrate how the perturbation method works for a system of n qubits and for two general qubits α and β where $\alpha \neq \beta$. At the end, we will map the results to $\alpha = 1$ and $\beta = 2$ for a nearest-neighbor interaction.

Let $\langle P_q| = \langle Z_\alpha \otimes Z_\beta|$ be a two-body n-qubit state for a Pauli string of $n-2$ identities and two Pauli-Z terms on qubits α and β, i.e. $P_q = \mathbb{I}_1 \otimes \cdots \otimes Z_\alpha \otimes \cdots \otimes Z_\beta \otimes \cdots \otimes \mathbb{I}_n$. By acting on this state with the inverse of the dissipator matrix $\tilde{M}^{-1}_{\text{dissip}}$ (Eq. (5.22)), we get

$$\langle P_q|\tilde{M}^{-1}_{\text{dissip}} = \langle P_q|D^{-1} + \sum_{k=1}^{n}(-1)^k \langle P_q|\tilde{N}^k D^{-1}. \tag{A.29}$$

By Eq. (5.18),

$$\langle P_q|D^{-1} = \frac{1}{\sum_k D^k_{q,q}}\langle Z_\alpha \otimes Z_\beta|, \tag{A.30}$$

while for the initial state $\langle P_q|$, by Eqs. (5.19) and (5.20) the second term of Eq. (A.29) gives

$$\begin{aligned}\sum_{k=1}^{n}(-1)^k \langle P_q|\tilde{N}^k D^{-1} =& \langle Z_\alpha \otimes Z_\beta|(-N_\alpha - N_\beta + N_\alpha N_\beta + N_\beta N_\alpha + O(\tilde{N}^3))D^{-1} \\ =& (-\langle Z_\alpha \otimes Z_\beta|\tilde{M}_{\text{dissip}}|Z_\beta\rangle\langle Z_\beta| - \langle Z_\alpha \otimes Z_\beta|\tilde{M}_{\text{dissip}}|Z_\alpha\rangle\langle Z_\alpha| \\ &+ 2\langle Z_\alpha \otimes Z_\beta|\tilde{M}_{\text{dissip}}|Z_\alpha\rangle\langle Z_\alpha \otimes Z_\beta|\tilde{M}_{\text{dissip}}|Z_\beta\rangle\langle \mathbb{I}|)D^{-1},\end{aligned} \tag{A.31}$$

where $\langle P_q|\tilde{N}^k = 0$ for $k > 2$, and so, the sum needs to be expanded only up to $k = 2$. Since matrix D^{-1} does not contain the map $|\mathbb{I}\rangle\langle\mathbb{I}|$, and therefore $\langle\mathbb{I}|D^{-1} = 0$, for the states $\langle P_s| \equiv \langle Z_\alpha|$ and $\langle P_f| \equiv \langle Z_\beta|$ we get

$$\langle P_q|\tilde{M}^{-1}_{\text{dissip}} = \frac{1}{\sum_k D^k_{q,q}}\langle Z_\alpha \otimes Z_\beta| - \frac{\langle Z_\alpha \otimes Z_\beta|\tilde{M}_{\text{dissip}}|Z_\alpha\rangle}{\sum_k D^k_{s,s}}\langle Z_\alpha| - \frac{\langle Z_\alpha \otimes Z_\beta|\tilde{M}_{\text{dissip}}|Z_\beta\rangle}{\sum_k D^k_{f,f}}\langle Z_\beta|. \tag{A.32}$$

Let a small perturbation in the system be caused by a Hamiltonian of the form

$$\mathcal{H}_A = \gamma Z_\alpha X_\beta, \tag{A.33}$$

where γ is the interaction-strength and $Z_\alpha X_\beta = \mathbb{I}_1 \otimes \cdots \otimes Z_\alpha \otimes \cdots \otimes X_\beta \otimes \cdots \otimes \mathbb{I}_n$. Constant γ takes strictly small values in the framework of perturbation theory. By Eq. (5.1) we have

that

$$\tilde{M}_{\mathcal{H}_A} = \frac{i}{2^n} \sum_{i=1}^{2^{2n-1}} \sum_{j=1}^{2^{2n-1}} \mathrm{Tr}([P_i, P_j]\mathcal{H}_A)|P_i\rangle\langle P_j|, \tag{A.34}$$

and so, in order to compute $\langle Z_\alpha \otimes Z_\beta|\tilde{M}_{\mathcal{H}_A}$ we need to find those Pauli strings P_j for which the trace $\mathrm{Tr}([Z_\alpha \otimes Z_\beta, P_j]\mathcal{H}_Y)$ is not zero. At this stage it is necessary to introduce the following identity:

Identity A.3.1. *Let A, B, C, D and E be general finite-dimensional operators. It holds that*

$$A \otimes B \otimes C - D \otimes B \otimes E = \frac{1}{2}\Big((A - D) \otimes B \otimes (C + E) + (A + D) \otimes B \otimes (C - E)\Big). \tag{A.35}$$

Proof. One can prove the above statement by expanding the right-hand side of Eq. (A.35). □

Let $P_j = P_{j_1} \otimes P_{j_2} \otimes \cdots \otimes P_{j_n}$ be a general Pauli string of n qubits, with $P_{j_i} \in \{\mathbb{I}_i, X_i, Y_i, Z_i\}$ for every qubit $i \in \{1, 2, ..., n\}$. Then,

$$\begin{aligned}[Z_\alpha \otimes Z_\beta, P_j] = (\mathbb{I}_1 \otimes \cdots \otimes Z_\alpha \otimes \cdots \otimes Z_\beta \otimes \cdots \otimes \mathbb{I}_n)P_j \\ - P_j(\mathbb{I}_1 \otimes \cdots \otimes Z_\alpha \otimes \cdots \otimes Z_\beta \otimes \cdots \otimes \mathbb{I}_n)\end{aligned} \tag{A.36}$$

$$\begin{aligned}[Z_\alpha \otimes Z_\beta, P_j] = &\underbrace{P_{j_1} \otimes \cdots \otimes Z_\alpha P_{j_\alpha}}_{A} \otimes \underbrace{\cdots}_{B} \otimes \underbrace{Z_\beta P_{j_\beta} \otimes \cdots \otimes P_{j_n}}_{C} \\ &- \underbrace{P_{j_1} \otimes \cdots \otimes P_{j_\alpha} Z_\alpha}_{D} \otimes \underbrace{\cdots}_{B} \otimes \underbrace{P_{j_\beta} Z_\beta \otimes \cdots \otimes P_{j_n}}_{E}\end{aligned} \tag{A.37}$$

$$\begin{aligned}\Rightarrow [Z_\alpha \otimes Z_\beta, P_j] = \frac{1}{2}\Big(&P_{j_1} \otimes \cdots \otimes [Z_\alpha, P_{j_\alpha}] \otimes \cdots \otimes \{Z_\beta, P_{j_\beta}\} \otimes \cdots \otimes P_{j_n} \\ &+ P_{j_1} \otimes \cdots \otimes \{Z_\alpha, P_{j_\alpha}\} \otimes \cdots \otimes [Z_\beta, P_{j_\beta}] \otimes \cdots \otimes P_{j_n}\Big),\end{aligned} \tag{A.38}$$

where during the derivation of Eq. (A.38) we made use of Eq. (A.35). We then calculate,

$$\begin{aligned}\mathrm{Tr}([Z_\alpha \otimes Z_\beta, P_j]\mathcal{H}_A) = \frac{\gamma}{2}\Big(&\mathrm{Tr}(P_{j_1}) \cdots \mathrm{Tr}([Z_\alpha, P_{j_\alpha}]Z_\alpha) \cdots \mathrm{Tr}(\{Z_\beta, P_{j_\beta}\}X_\beta) \cdots \mathrm{Tr}(P_{j_n}) \\ &+ \mathrm{Tr}(P_{j_1}) \cdots \mathrm{Tr}(\{Z_\alpha, P_{j_\alpha}\}Z_\alpha) \cdots \mathrm{Tr}([Z_\beta, P_{j_\beta}]X_\beta) \cdots \mathrm{Tr}(P_{j_n})\Big).\end{aligned} \tag{A.39}$$

From the above equation, we see that $\mathrm{Tr}([Z_\alpha \otimes Z_\beta, P_j]\mathcal{H}_A) \neq 0$ only for the Pauli string $P_j = \mathbb{I}_1 \otimes \cdots \otimes Y_\beta \otimes \cdots \otimes \mathbb{I}_n$. This gives the result

$$\langle Z_\alpha \otimes Z_\beta|\tilde{M}_{\mathcal{H}_A} = 2\gamma\langle Y_\beta|. \tag{A.40}$$

By beginning with the state $\langle P_q| = \langle Z_\alpha \otimes Z_\beta|$, we see that by applying $\tilde{M}^{-1}_{\text{dissip}}$ on $\langle P_q|$ we also mapped to the states $\langle Z_\alpha|$ and $\langle Z_\beta|$, while by applying $\tilde{M}_{\mathcal{H}_A}$ on $\langle P_q|$ we obtained the state $\langle Y_\beta|$. In order to compute the matrices $\tilde{M}^{-1}_{\text{dissip}}$ and $\tilde{M}_{\mathcal{H}}$, we need to keep applying $\tilde{M}^{-1}_{\text{dissip}}$, $\tilde{M}_{\mathcal{H}_A}$ and $\tilde{M}_{\mathcal{H}_B}$ on every new state that comes up, and hopefully the subspace of all the states that are involved in these mappings does not increase much in size.

By doing this process for the Hamiltonian given by Eq. (A.28) and for the quantum jump operators $L_1 = \sqrt{\kappa p}\sigma_-$, $L_2 = \sqrt{\kappa(1-p)}\sigma_+$ and $L_3 = \sqrt{\chi}Z$ (see Section 1.6.2), we end up with

$$\tilde{M}_{\mathcal{H}_A} + \tilde{M}_{\mathcal{H}_B} = \tilde{M}_{\mathcal{H}} = 2\gamma \begin{pmatrix} 0 & 0 & 1 & 0 & 0 & 0 & 0 & -1 \\ 0 & 0 & 0 & 0 & 0 & 0 & 1 & 0 \\ -1 & 0 & 0 & -1 & 0 & 0 & 0 & 0 \\ 0 & 0 & 1 & 0 & 0 & 0 & 0 & -1 \\ 0 & 0 & 0 & 0 & 0 & -1 & 0 & 0 \\ 0 & 0 & 0 & 0 & 1 & 0 & 0 & 0 \\ 0 & -1 & 0 & 0 & 0 & 0 & 0 & 0 \\ 1 & 0 & 0 & 1 & 0 & 0 & 0 & 0 \end{pmatrix} \tag{A.41}$$

and

$$\tilde{M}^{-1}_{\text{dissip}} = \begin{pmatrix} -\frac{2}{\kappa+4\chi} & 0 & 0 & 0 & 0 & 0 & 0 & 0 \\ 0 & -\frac{1}{\kappa} & 0 & 0 & 0 & 0 & 0 & 0 \\ 0 & 0 & -\frac{1}{\kappa+4\chi} & 0 & 0 & 0 & 0 & 0 \\ 0 & 0 & 0 & -\frac{2}{\kappa+4\chi} & 0 & 0 & 0 & 0 \\ 0 & 0 & 0 & \frac{4\kappa(1-2p)}{(\kappa+4\chi)(3\kappa+4\chi)} & -\frac{2}{3\kappa+4\chi} & 0 & 0 & 0 \\ 0 & 0 & 0 & 0 & 0 & -\frac{1}{\kappa} & 0 & 0 \\ \frac{4\kappa(1-2p)}{(\kappa+4\chi)(3\kappa+4\chi)} & 0 & 0 & 0 & 0 & 0 & -\frac{2}{3\kappa+4\chi} & 0 \\ 0 & \frac{1-2p}{2\kappa} & 0 & 0 & 0 & \frac{1-2p}{2\kappa} & 0 & -\frac{1}{2\kappa} \end{pmatrix} \tag{A.42}$$

in the Pauli subspace $|Y_\beta\rangle = (1,0,0,0,0,0,0,0)^{\mathrm{T}}$, $|Z_\beta\rangle = (0,1,0,0,0,0,0,0)^{\mathrm{T}}$, $|X_\alpha X_\beta\rangle = (0,0,1,0,0,0,0,0)^{\mathrm{T}}$, $|Y_\alpha\rangle = (0,0,0,1,0,0,0,0)^{\mathrm{T}}$, $|Y_\alpha Z_\beta\rangle = (0,0,0,0,1,0,0,0)^{\mathrm{T}}$, $|Z_\alpha\rangle = (0,0,0,0,0,1,0,0)^{\mathrm{T}}$, $|Z_\alpha Y_\beta\rangle = (0,0,0,0,0,0,1,0)^{\mathrm{T}}$ and $|Z_\alpha Z_\beta\rangle = (0,0,0,0,0,0,0,1)^{\mathrm{T}}$.

By Eqs. (A.41) and (A.42), we can calculate the expectation values of those Pauli strings that are part of the subspace of the maps $\tilde{M}^{-1}_{\text{dissip}}$ and $\tilde{M}_{\mathcal{H}}$. For example,

$$\langle Z_\alpha Z_\beta\rangle = 2^n \langle Z_\alpha Z_\beta|\tilde{a}_{\text{fixed}}\rangle = 2^n \sum_{k=0}^{\infty} (-1)^k \langle Z_\alpha Z_\beta| \left(\tilde{M}^{-1}_{\text{dissip}}\tilde{M}_{\mathcal{H}}\right)^k |\tilde{a}_{\text{dissip}}\rangle, \tag{A.43}$$

for a system of n qubits.

All the calculations for Eqs. (A.41) and (A.42) were done by hand, in lack of a better method. Consequently, there is the need to automate this process for larger Pauli strings. Also, there is the need to estimate the size of the subspace in which the mappings $\tilde{M}^{-1}_{\text{dissip}}$ and $\tilde{M}_{\mathcal{H}}$ act. What can already be said is that for a Hamiltonian $\mathcal{H}$ which acts on m number of different qubits, the subspace of Pauli states should contain at most 2^{2m} states.

For the practical purposes of Section 5.2.3, $\alpha = 1$, $\beta = 2$ and $n = 2$. Therefore, Eq. (A.44) becomes

$$\langle Z_1 Z_2 \rangle = 4\langle Z_1 Z_2 | \tilde{a}_{\text{fixed}} \rangle = 4 \sum_{k=0}^{\infty} (-1)^k \langle Z_1 Z_2 | \left(\tilde{M}_{\text{dissip}}^{-1} \tilde{M}_{\mathcal{H}} \right)^k | \tilde{a}_{\text{dissip}} \rangle, \tag{A.44}$$

By expanding the expectation values of the exact solution for the steady state for two qubits (see Section 4.3.1), one can verify that the two power series are identical.

B

Appendix: Wolfram Mathematica Codes

B.1. LindbladME - 2qubits.nb

```
In[•]:= Clear[p] && Clear[κ] && Clear[χ] && Clear[γ] && Clear[c];
        Commutator[A_, B_] := A.B - B.A;
        AntiCommutator[A_, B_] := A.B + B.A;
        sigmaminus = {{0, 1}, {0, 0}};
        sigmaplus = {{0, 0}, {1, 0}};
        Paulis = ConstantArray[0, 16];
        constant = 0;
        Hamiltonian = ConstantArray[0, {4, 4}]; (*initialization, IGNORE*)
        For[i = 1, i < 5, i++, For[j = 1, j < 5, j++,  Paulis[[j + constant]] =
            KroneckerProduct[PauliMatrix[i - 1], PauliMatrix[j - 1]]] &&
          If[j == 5, constant = constant + 4]]
        Hamiltonian = γ * (Paulis[[14]] + Paulis[[8]]) + c * (Paulis[[5]] + Paulis[[2]])
         (*INPUT HAMILTONIAN*);

In[•]:= H = ConstantArray[0, {16, 16}];
        Dmatrix1 =  ConstantArray[0, {4, 4}];
        Dmatrix2 =  ConstantArray[0, {4, 4}];
        Dmatrix3 =  ConstantArray[0, {4, 4}];
        Dmatrix = ConstantArray[0, {4, 4}];
        Ddissip = ConstantArray[0, {16, 16}];
        A = ConstantArray[0, {15, 15}];
        u = ConstantArray[0, 15];
        a0 = 1 / 4;
```

B

```
beta = ConstantArray[0, 15];

Dissip[L_, rho_] := L.rho.ConjugateTranspose[L] -
   (1 / 2) * AntiCommutator[ConjugateTranspose[L].L, rho];
L1 = Sqrt[κ] * Sqrt[p] * sigmaminus;
L2 = Sqrt[κ] * Sqrt[1 - p] * sigmaplus;
L3 = Sqrt[χ] * PauliMatrix[3];
(*Dissipator*)
```

```
In[•]:= For[i = 1, i < 17, i++, For[j = 1, j < 17, j++,
  H[[i, j]] = (I / 4) * Tr[Commutator[Paulis[[i]], Paulis[[j]]].Hamiltonian]]]
For[i = 1, i < 5, i++, For[j = 1, j < 5, j++, Dmatrix1[[i, j]] =
   (1 / 2) * Tr[PauliMatrix[i - 1].Dissip[L1, PauliMatrix[j - 1]]]]]
For[i = 1, i < 5, i++, For[j = 1, j < 5, j++, Dmatrix2[[i, j]] =
   (1 / 2) * Tr[PauliMatrix[i - 1].Dissip[L2, PauliMatrix[j - 1]]]]]
For[i = 1, i < 5, i++, For[j = 1, j < 5, j++, Dmatrix3[[i, j]] =
   (1 / 2) * Tr[PauliMatrix[i - 1].Dissip[L3, PauliMatrix[j - 1]]]]]
```

```
In[•]:= Dmatrix = Dmatrix1 + Dmatrix2 + Dmatrix3;
```

```
In[•]:= Ddissip = KroneckerProduct[Dmatrix, Paulis[[1]]] +
   KroneckerProduct[Paulis[[1]], Dmatrix];
M = H + Ddissip;
Ddissip = Assuming[p ∈ Reals && κ ∈ Reals && χ ∈ Reals && 0 < p < 1 && κ > 0 && χ > 0,
   FullSimplify[ComplexExpand[Ddissip]]];
 M = Assuming[p ∈ Reals && κ ∈ Reals && χ ∈ Reals && 0 < p < 1 && κ > 0 && χ > 0,
    FullSimplify[ComplexExpand[M]]];
MatrixForm[M](*Pauli Transfer Matrix*)
```

```
In[•]:= For[i = 1, i < 16, i++, For[j = 1, j < 16, j++, A[[i, j]] = M[[i + 1, j + 1]]]]
```

```
In[•]:= For[i = 1, i < 16, i++, u[[i]] = M[[i + 1, 1]]]
```

```
In[•]:= beta = LinearSolve[A, -a0 * u];
beta // MatrixForm
```

```
alpha = Insert[ beta, 1 / 4, 1];
alpha // MatrixForm
rhofixed = Sum[alpha[[i]] * Paulis[[i]], {i, 16}];
(*Fixed point of the evolution*)

alpha[[13]] (*<Z_1> / 4*)

alpha[[4]] (*<Z_2> / 4*)

alpha[[16]] (*<Z_1 Z_2> / 4*)

z1plot[p_, κ_, χ_, γ_, c_] := (*put here 4*alpha[[13]]*)

z2plot[p_, κ_, χ_, γ_, c_] := (*put here 4*alpha[[4]]*)
```

```
z1z2plot[p_, κ_, χ_, γ_, c_] := (*put here 4*alpha[[16]]*)

In[•]:= data = Table[z1z2plot[0.9985, κ, 0, 1, c] - z1plot[0.9985, κ, 0, 1, c] *
      z2plot[0.9985, κ, 0, 1, c], {κ, 0.001, 2, 0.1}, {c, -2.001, 2, 0.1}];

ListDensityPlot[data, DataRange → {{-2.001, 2}, {0.001, 2}},
 ColorFunction → "SunsetColors", PlotLegends → Automatic,
 FrameLabel → {"c/γ", "κ/γ"}, FrameStyle → 15]
 (*<Z_1 Z_2> - <Z_1> <Z_2> color plot*)

rhofixedsquared = MatrixPower[rhofixed, 2];
Tr[rhofixedsquared] (*Purity of the fixed point*)

rho2function[p_, κ_, χ_, γ_, c_] := (*put here Tr[rhofixedsquare]*)

In[•]:= data2 =
  Table[rho2function[0.9985, κ, 0, 1, c], {κ, 0.001, 2, 0.1}, {c, -2.001, 2, 0.1}];

ListDensityPlot[data2, DataRange → {{-2.001, 2}, {0.001, 2}},
 ColorFunction → "SunsetColors", PlotLegends → Automatic,
 FrameLabel → {"c/γ", "κ/γ"}, FrameStyle → 15](*Purity plot*)
```

B.2. Concurrence - 2qubits.nb

```
In[•]:= Clear[p] && Clear[κ] && Clear[χ] && Clear[γ] && Clear[c];

In[•]:= Paulis = ConstantArray[0, 16];
constant = 0;
For[i = 1, i < 5, i++,
 For[j = 1, j < 5, j++, Paulis[[j + constant]] = KroneckerProduct[
     PauliMatrix[i - 1], PauliMatrix[j - 1]]] && If[j == 5, constant = constant + 4]]

rhofixedfunction[p_, κ_, χ_, γ_, c_] :=
 (*put fixed point of Lindblad Equation here*)

p = SetPrecision[0.9985, 25]; (*relaxation probability*)
χ = SetPrecision[0, 25];
(*pure dephasing rate*)
```

B

```
ConcurrenceFunction[p_, κ_, χ_, γ_, c_] :=
 (rhofixedfunction[p, κ, χ, γ, c]; rhotilde = Assuming[p ∈ Reals && κ ∈ Reals &&
     χ ∈ Reals && 0 < p < 1 && κ >= 0 && χ >= 0, Paulis[[11]].ComplexExpand[
      Conjugate[rhofixedfunction[p, κ, χ, γ, c]].Paulis[[11]]]]; eigenvalues =
   Re[ComplexExpand[Eigenvalues[rhofixedfunction[p, κ, χ, γ, c].rhotilde]]];
  eigenvalues2 = NumericalSort[Sqrt[eigenvalues]];
  Concurrence = Max[0, eigenvalues2[[4]] - eigenvalues2[[3]] -
     eigenvalues2[[2]] - eigenvalues2[[1]]])(*Concurrence*)

In[•]:= data = Table[ConcurrenceFunction[p, κ, χ, 1, c],
    {κ, 0.001, 2, 0.1}, {c, -2.001, 2, 0.1}];

ListDensityPlot[data, DataRange → {{-2.001, 2}, {0.001, 2}},
 ColorFunction → "SunsetColors", PlotLegends → Automatic,
 FrameLabel → {"c/γ", "κ/γ"}, FrameStyle → 15](*Concurrence color plot*)
```

B.3. LindbladME - 3qubits.nb

```
SwapParts[expr_, pos1_, pos2_] :=
 ReplacePart[#, #, {pos1, pos2}, {pos2, pos1}] &[expr]
TraceSystem[D_, s_] := (

  Qubits = Reverse[Sort[s]];
  TrkM = D;

  z = (Dimensions[Qubits][[1]] + 1);

  For[q = 1, q < z, q++,
   n = Log[2, (Dimensions[TrkM][[1]])];
   M = TrkM;
   k = Qubits[[q]];
   If[k == n,
    TrkM = {};
    For[p = 1, p < 2^n + 1, p = p + 2,
     TrkM = Append[TrkM,
       Take[M[[p, All]], {1, 2^n, 2}] + Take[M[[p + 1, All]], {2, 2^n, 2}]];
     ],
    For[j = 0, j < (n - k), j++,
     b = {0};
     For[i = 1, i < 2^n + 1, i++,
      If[(Mod[(IntegerDigits[i - 1, 2, n][[n]] +
```

```
                IntegerDigits[i - 1, 2, n][[n - j - 1]]], 2]) == 1 &&
          Count[b, i] == 0, Permut = {i, (FromDigits[SwapParts[
                (IntegerDigits[i - 1, 2, n]), {n}, {n - j - 1}], 2] + 1)};
         b = Append[b, (FromDigits[SwapParts[(IntegerDigits[i - 1, 2, n]),
                {n}, {n - j - 1}], 2] + 1)];
         c = Range[2^n];
         perm = SwapParts[c, {i}, {(FromDigits[
                SwapParts[(IntegerDigits[i - 1, 2, n]), {n}, {n - j - 1}], 2] + 1)}];

         M = M[[perm, perm]];

          ]
       ]    ;
       TrkM = {};
       For[p = 1, p < 2^n + 1, p = p + 2,
        TrkM = Append[TrkM,
           Take[M[[p, All]], {1, 2^n, 2}] + Take[M[[p + 1, All]], {2, 2^n, 2}]];
       ]
        ];
  ]



 ]

 ;
 Return[TrkM])(*original author of this script is Mark S. Tame,
 script title: DensityTrace.nb, Found online: https://
    library.wolfram.com/infocenter/MathSource/5571/https://library.wolfram.
        com/infocenter/MathSource/5571/DensityTrace.nb?file_id=5299*)

In[•]:= Clear[p] && Clear[κ] && Clear[χ] && Clear[γ] && Clear[c];
Commutator[A_, B_] := A.B - B.A;
AntiCommutator[A_, B_] := A.B + B.A;
sigmaminus = {{0, 1}, {0, 0}};
sigmaplus = {{0, 0}, {1, 0}};
Paulis = ConstantArray[0, 64];
constant = 0;
Hamiltonian = ConstantArray[0, {8, 8}]; (*initialization, IGNORE*)
For[l = 1, l < 5, l++,
 For[i = 1, i < 5, i++, For[j = 1, j < 5, j++, Paulis[[j + constant]] =
    KroneckerProduct[PauliMatrix[l - 1], PauliMatrix[i - 1], PauliMatrix[j - 1]]];
  If[j == 5, constant = constant + 4]]]
constant = 0; (*reset of constant*)
Hamiltonian = γ * (Paulis[[53]] + Paulis[[14]] + Paulis[[20]]) +
   c * (Paulis[[2]] + Paulis[[5]] + Paulis[[17]])(*INPUT HAMILTONIAN*);
```

B

```
H = ConstantArray[0, {64, 64}];
Dmatrix1 = ConstantArray[0, {4, 4}];
Dmatrix2 = ConstantArray[0, {4, 4}];
Dmatrix3 = ConstantArray[0, {4, 4}];
Dmatrix = ConstantArray[0, {4, 4}];
Ddissip = ConstantArray[0, {64, 64}];
A = ConstantArray[0, {63, 63}];
u = ConstantArray[0, 63];
a0 = 1 / 8;
beta = ConstantArray[0, 63];

Dissip[L_, rho_] := L.rho.ConjugateTranspose[L] -
    (1 / 2) * AntiCommutator[ConjugateTranspose[L].L, rho];
L1 = Sqrt[κ] * Sqrt[p] * sigmaminus;
L2 = Sqrt[κ] * Sqrt[1 - p] * sigmaplus;
L3 = Sqrt[χ] * PauliMatrix[3];
(*Dissipator*)
```

```
For[i = 1, i < 65, i++, For[j = 1, j < 65, j++,
  H[[i, j]] = (I / 4) * Tr[Commutator[Paulis[[i]], Paulis[[j]]].Hamiltonian]]]
For[i = 1, i < 5, i++, For[j = 1, j < 5, j++, Dmatrix1[[i, j]] =
   (1 / 2) * Tr[PauliMatrix[i - 1].Dissip[L1, PauliMatrix[j - 1]]]]]
For[i = 1, i < 5, i++, For[j = 1, j < 5, j++, Dmatrix2[[i, j]] =
   (1 / 2) * Tr[PauliMatrix[i - 1].Dissip[L2, PauliMatrix[j - 1]]]]]
For[i = 1, i < 5, i++, For[j = 1, j < 5, j++, Dmatrix3[[i, j]] =
   (1 / 2) * Tr[PauliMatrix[i - 1].Dissip[L3, PauliMatrix[j - 1]]]]]
```

```
Dmatrix = Dmatrix1 + Dmatrix2 + Dmatrix3;
```

```
Ddissip =
  KroneckerProduct[Dmatrix, PauliMatrix[0], PauliMatrix[0], PauliMatrix[0],
    PauliMatrix[0]] + KroneckerProduct[PauliMatrix[0], PauliMatrix[0],
    Dmatrix, PauliMatrix[0], PauliMatrix[0]] + KroneckerProduct[PauliMatrix[0],
    PauliMatrix[0], PauliMatrix[0], PauliMatrix[0], Dmatrix];
M = H + Ddissip;
Ddissip = Assuming[p ∈ Reals && κ ∈ Reals && χ ∈ Reals && 0 < p < 1 && κ > 0 && χ > 0,
   FullSimplify[ComplexExpand[Ddissip]]];

M = Assuming[p ∈ Reals && κ ∈ Reals && χ ∈ Reals && 0 < p < 1 && κ > 0 && χ > 0,
   FullSimplify[ComplexExpand[M]]];
MatrixForm[M](*Pauli Transfer Matrix*)
```

```
For[i = 1, i < 64, i++, For[j = 1, j < 64, j++, A[[i, j]] = M[[i + 1, j + 1]]]]
```

```
For[i = 1, i < 64, i++, u[[i]] = M[[i + 1, 1]]]
```

```
Alphafunction[p_, κ_, χ_, γ_, c_] :=
 (*Put here reduced Pauli Transfer Matrix here*)

ufunction[p_, κ_, χ_, γ_, c_] := (*Put here dissipation vector*)

In[•]:= SolveSystem[p_, κ_, χ_, γ_, c_] := (beta = LinearSolve[Alphafunction[p, κ, χ, γ, c],
      -a0 * ufunction[p, κ, χ, γ, c]]; alpha = Insert[beta, 1 / 8, 1];
   8 * alpha[[64]] - 512 * alpha[[49]] * alpha[[13]] * alpha[[4]]);

In[•]:= data = Table[SolveSystem[SetPrecision[0.9985, 25], κ, SetPrecision[0, 25], 1, c],
   {κ, 0.001, 2, 0.1}, {c, -2.001, 2, 0.1}];

ListDensityPlot[data, DataRange → {{-2.001, 2}, {0.001, 2}},
 ColorFunction → "SunsetColors", PlotLegends → Automatic,
 FrameLabel → {"c/γ", "κ/γ"}, FrameStyle → 15]
 (*<Z_1 Z_2 Z_3> - <Z_1> <Z_2> <Z_3> color plot*)

In[•]:= SolveSystem2[p_, κ_, χ_, γ_, c_] :=
  (beta = LinearSolve[Alphafunction[p, κ, χ, γ, c],
     -a0 * ufunction[p, κ, χ, γ, c]]; alpha = Insert[beta, 1 / 8, 1];
   rhofixed = Sum[alpha[[i]] * Paulis[[i]], {i, 64}];
   rhofixedsquared = MatrixPower[rhofixed, 2]; Tr[rhofixedsquared]);

In[•]:= data2 = Table[SolveSystem2[SetPrecision[0.9985, 25], κ,
    SetPrecision[0, 25], 1, c], {κ, 0.001, 2, 0.1}, {c, -2.001, 2, 0.1}];

ListDensityPlot[data2, DataRange → {{-2.001, 2}, {0.001, 2}},
 ColorFunction → "SunsetColors", PlotLegends → Automatic,
 FrameLabel → {"c/γ", "κ/γ"}, FrameStyle → 15](*Purity color plot*)

ConcurrenceAB[p_, κ_, χ_, γ_, c_] := (constant = 0;
  Clear[Paulis];
  Paulis = ConstantArray[0, 64];
  For[l = 1, l < 5, l++, For[i = 1, i < 5, i++, For[j = 1, j < 5, j++,
     Paulis[[j + constant]] = KroneckerProduct[PauliMatrix[l - 1], PauliMatrix[
        i - 1], PauliMatrix[j - 1]]]; If[j == 5, constant = constant + 4]]];
  beta = LinearSolve[Alphafunction[p, κ, χ, γ, c], -a0 * ufunction[p, κ, χ, γ, c]];
  alpha = Insert[beta, 1 / 8, 1];
  rhofixedfull = Sum[alpha[[i]] * Paulis[[i]], {i, 64}];
  rhofixed = TraceSystem[rhofixedfull, {3}];
  constant = 0; Clear[Paulis]; Paulis = ConstantArray[0, 16];
  For[i = 1, i < 5, i++, For[j = 1, j < 5, j++, Paulis[[j + constant]] =
      KroneckerProduct[PauliMatrix[i - 1], PauliMatrix[j - 1]]] && If[j == 5,
     constant = constant + 4]]; rhotilde = Assuming[p ∈ Reals && κ ∈ Reals && χ ∈
      Reals && 0 < p < 1 && κ >= 0 && χ >= 0, Paulis[[11]].ComplexExpand[Conjugate[
        rhofixed].Paulis[[11]]]]; eigenvalues = Re[ComplexExpand[Eigenvalues[
      rhofixed.rhotilde]]]; eigenvalues2 = NumericalSort[Sqrt[eigenvalues]];
  Concurrence = Max[0, eigenvalues2[[4]] - eigenvalues2[[3]] - eigenvalues2[[
      2]] - eigenvalues2[[1]]])(*Calculates concurrence for qubits 1,
 2 when we trace out qubit 3, similar for the case of 2,3 and 1,3 qubits*)
```

B

```
dataAB = Table[ConcurrenceAB[SetPrecision[0.9985, 25], κ,
    SetPrecision[0, 25], 1, c], {κ, 0.001, 2, 0.1}, {c, -2.001, 2, 0.1}];

ListDensityPlot[dataAB, DataRange → {{-2.001, 2}, {0.001, 2}},
 ColorFunction → "SunsetColors", PlotLegends → Automatic,
 FrameLabel → {"c/γ", "κ/γ"}, FrameStyle → 15](*Concurrence color plot*)
```

B.4. Mean-Field Equations.nb

```
Clear[p] && Clear[κ] && Clear[χ] && Clear[γ] &&
  Clear[c] && Clear[rx] && Clear[ry] && Clear[rz];
Commutator[A_, B_] := A.B - B.A;
AntiCommutator[A_, B_] := A.B + B.A;
sigmaminus = {{0, 1}, {0, 0}};
sigmaplus = {{0, 0}, {1, 0}};
Paulis = ConstantArray[0, 16];
constant = 0;
Hamiltonian = ConstantArray[0, {4, 4}]; (*initialization, IGNORE*)
For[i = 1, i < 5, i++, For[j = 1, j < 5, j++,  Paulis[[j + constant]] =
    KroneckerProduct[PauliMatrix[i - 1], PauliMatrix[j - 1]]] &&
  If[j == 5, constant = constant + 4]]
Hamiltonian = γ * (Paulis[[14]] + Paulis[[8]]) (*INPUT HAMILTONIAN*);
```

```
Diss[L_, rho_] := L.rho.ConjugateTranspose[L] -
   (1 / 2) * AntiCommutator[ConjugateTranspose[L].L, rho];
L[1] = Sqrt[κ] * Sqrt[p] * KroneckerProduct[sigmaminus, PauliMatrix[0]];
L[2] = Sqrt[κ] * Sqrt[1 - p] * KroneckerProduct[sigmaplus, PauliMatrix[0]];
L[3] = Sqrt[χ] * KroneckerProduct[PauliMatrix[3], PauliMatrix[0]];
L[4] = Sqrt[κ] * Sqrt[p] * KroneckerProduct[PauliMatrix[0], sigmaminus];
L[5] = Sqrt[κ] * Sqrt[1 - p] * KroneckerProduct[PauliMatrix[0], sigmaplus];
L[6] = Sqrt[χ] * KroneckerProduct[PauliMatrix[0], PauliMatrix[3]];
Dissipator[rho_] := Sum[Diss[L[i], rho], {i, 6}];
```

```
Lindbladian[rho_] := -I * Commutator[Hamiltonian, rho] + Dissipator[rho];
```

In[•]:=
```
alpha1 = {1 / 2, rx / 2, ry / 2, rz / 2};
alpha = KroneckerProduct[alpha1, alpha1];
alpha = Flatten[alpha];
```

In[•]:=
```
rho = Sum[alpha[[i]] * Paulis[[i]], {i, 16}];
```

In[•]:=
```
rhs = Assuming[p ∈ Reals && κ ∈ Reals && χ ∈ Reals && 0 < p <= 1 && κ >= 0 && χ >= 0,
   FullSimplify[ComplexExpand[Lindbladian[rho]]]];
```

In[•]:=
```
Equation[1] = FullSimplify[Tr[Paulis[[5]].rhs]]
```

Out[•]=
$$-\frac{1}{2}\,rx\,(4\,ry\,\gamma + \kappa + 4\,\chi)$$

In[•]:=
```
Equation[2] = FullSimplify[Tr[Paulis[[9]].rhs]]
```

Out[•]=
$$2\,(rx - rz)\,(rx + rz)\,\gamma - \frac{1}{2}\,ry\,(\kappa + 4\,\chi)$$

In[•]:=
```
Equation[3] = FullSimplify[Tr[Paulis[[13]].rhs]]
```

Out[•]=
$$2\,ry\,rz\,\gamma - (1 - 2\,p + rz)\,\kappa$$

In[•]:=
```
{rx, ry, rz} = {rx, ry, rz} /.
  First@ Solve[{Equation[1] == 0 , Equation[2] == 0 , Equation[3] == 0, 0 ≤ p ≤ 1,
     κ > 0, χ ≥ 0, γ ≥ 0, -1 ≤ rx ≤ 1, -1 ≤ ry ≤ 1, -1 ≤ rz ≤ 1 }, {rx, ry, rz}, Reals]
```

Acknowledgements

During my master studies I faced a number of hardships which helped me grow as a person and strengthened my motivation to further pursue science. That being said, I always had the overwhelming support from friends and family, and along the way I met a lot of new people who helped and inspired me to be a better person. It is all these people who I would like to thank here.

First, I would like to thank my thesis supervisor **Barbara**. I approached you during a very difficult period of my studies and you offered me the opportunity to prove myself and work with you. Working with you for over one year, I learned more than I ever did in any other time while studying physics. I am thankful for your guidance and your attention during the whole part of my thesis, and I appreciate your honesty.

I would also like to thank the study advisor **Alyssa**. You were (accidentally) my very first interaction in the Applied Physics building before I even got accepted in TU Delft to begin my studies. I value our conversations during the earlier parts of my studies and also the help and the assistance that you have provided.

My thanks also goes to the program coordinator **Arno**. You were always friendly to me and open to answer any question that I would throw at you. I appreciate all the support that you have shown to me.

Thanks to the committee members for reading my thesis and being present at my defense.

Thanks also to my good friends **Santi**, **Tanko**, **Ies** and **Helena** that I made during my studies in TUD. I cherish all the hours that we have spent together either trying to solve some challenging problems or just having all-around conversations.

Yang, it was fun TAing with you the mathematical methods course. You are a good colleague and someone that people can rely on.

Also, many thanks to **Maarten**, **Stephan**, **Boris** and **Francesco** for all the conversations and valuable help that I received during the preparation of my thesis.

Thanks to all of my childhood friends from Greece, **Sifis**, **Elvi**, **Michalis**, **Lazaros**, **Stelios** and **Spyros**, for corresponding and staying in touch with me, and for being excited with me pursuing my dreams.

Thanks also goes to you **Aggelos**. You were my first encounter during my journey in physics, and you are a valuable friend who continuous to inspire me a lot.

A big thanks goes to my mother **Elena** and grandmother **Pepi**. You have provided me with unconditional support and love for the whole of my studies, and there are no words to express my gratitude and appreciation for this.

Many thanks also goes to my brother **Petros** and **Francesca**. It is through you **Petros** that in difficult times I am able to see the bigger picture, and multiple times during my studies you have helped alleviate a lot of stress off of me. Also, eating home-cooked Italian food from both of you has helped cheer me up in every possible way!

A special thank you goes to my partner **Jarka**. We met during a tough period, and since then you are actively helping me to become a better person and a better partner. I could not

have asked for a lovelier person in my life, thank you for being so much supportive during my studies and especially during my thesis preparation.